The Effect of Machining Residual Stresses on the Dimensional Stability of Aluminum Alloys used in Optical Systems

by

Timothy W. Spence

A thesis submitted to the faculty of

Worcester Polytechnic Institute

in partial fulfillment of the requirement of

Doctor of Philosophy

in

Materials Science and Engineering

April 2010

_____

Professor Makhlouf M. Makhlouf, Advisor

_____

Professor Richard M. Sisson, Jr., George F. Fuller Professor

Director of the Materials Science and Engineering Program

Abstract

Dimensional stability of materials is of critical importance in the fabrication of precision components used for applications such as optical systems. One source of dimensional instability is residual stress produced on the surfaces of parts due to machining operations. A creep model is proposed in this research that describes how these stressed layers affect the overall geometry of a component as they creep over time and temperature. Depth corrected XRD stress measurements and a bimetallic strip model were utilized to quantify the residual stress layer of two machining operations. The creep model parameters were determined by monitoring curvature over time and temperature. This model can be used for two purposes, the prediction of long term storage effects on part geometry for purposes of reliability assessment, and the design of short term, moderate temperature stress relief treatments. Two alloys were investigated, aluminum 6061-T6, and aluminum 4032-0. A methodology for applying the observed creep strain to complex parts using a finite element analysis is proposed.

Acknowledgements

The author would like to thank the following individuals who contributed to the success of the project:

From BAE Systems; Tom Arsenault and Steve Diorio providing the initial approval for the project; Rich Rossetti, Brian Foley, and Don Hellmers for providing much needed funding for the fabrication of samples; Joe Krasucki for his help developing the Sodium Hydroxide etching procedure, for the use of his lab facilities, and for his continued encouragement; Annette Lamy and Greg Swift for their help developing the inspection program, for their encouragement, and for the use of the equipment during countless evenings; Mike Fisher and Dennis Bergeron for their fine work machining the test samples; and Dan Magarrell for his help performing the initial XRD measurement. A special thanks to Dr. John Dion for his suggestion of this topic as a research area and for his participation on the committee.

From Panalytical; Kathy Macchiarola for help performing the surface only stress measurements

From WPI; Committee members Drs. Diran Apelian, Jianyu Liang and dept Head Dr. Richard Sisson for reviewing the project; Chang Kai “Lance” Wu for tensile testing; Laura Hanlon for her assistance retrieving papers and guidance during the thesis submission process.

Special thanks to Dr. Makhlouf Makhlouf for the patience, encouragement, and thoughtful guidance he provided on this project.

A very special thank you goes to Mrs. Julie Spence for her unwavering support, patience, and encouragement.

This project is dedicated to the late Thomas Evan Spence, whose trade as a welder provided his son with a very early interest in metallurgy and materials.

TABLE OF CONTENTS

TABLE OF FIGURES

TABLE OF TABLES

1 Project Motivation and Objectives

In the design of precision mechanical parts, such as those used in optical systems, control of dimensions and tolerances is critical to the sustained performance of the overall system. Changes in the geometry of these parts over time are unacceptable, particularly if the change causes the parts to no longer meet the required dimensions. Many sources of dimensional instability have been identified and studied over the years, one of which is residual stresses in the material.

Stress relief procedures have been developed for many alloys in order to control stresses induced by the various fabrication processes including rolling, machining, and post-machining operations such as plating. Dimensional instability caused by surface stresses due to machining operations has not been thoroughly characterized. A comprehensive understanding of the magnitude of the geometry changes and the kinetics of the strains that develop in the material over time and temperature ranges does not exist.

Understanding how surface stresses will affect the shape of a part over time and temperature is an extremely useful tool in predicting whether a precision part will maintain its critical dimensions after exposure to temperature. This same understanding will guide development of stress relief procedures that provide the required reduction in stresses without exposing the material to extended temperature soaks that may reduce its strength.

There are two goals for this research effort:

(1) To develop a model that allows prediction of geometry instabilities due to machining residual stresses in high precision components, and

(2) To collect data on the stability of an aluminum alloy that has promise in certain optical applications, but for which only little dimensional stability data is available.

2 Background

2.1 Types of Dimensional Instability

The various types of dimensional stability will be discussed briefly in this section and the reader is directed to the more detailed description by Marschall and Meringer [1]. One category of dimensional instability, namely temporal instability is of prime interest to this project and therefore it will be discussed in more detail.

2.1.1 Temperature-Induced Dimensional Instability

Temperature induced instability is defined as a *reversible* change in the geometry of a material that occurs in a fixed environment and is independent of the path of that environment [2]. These modes of instability can generally be understood rather easily, and their reversible nature allows them to be designed around. The classic example of this type of instability is thermal expansion, which can have an obvious effect on the lengthening of a part with an increase in temperature.

A less obvious effect is the loss of surface smoothness (known as optical or surface figure) on a scale that is equal to the grain structure. Since many mechanical and physical properties, including coefficient of thermal expansion (CTE), will vary according to crystallographic geometry, individual grains within the microstructure having a predominantly uniform crystal orientation will also have slightly anisotropic properties. In a large specimen, with many randomly oriented grains, this effect tends to be cancelled out. But along a surface, the different orientation of each grain can lead to an irregular surface as the grains increase in size with temperature. This causes a loss of smoothness, or a loss of optical figure. An example of this effect in a Beryllium alloy has been summarized by Paquin [3].

2.1.2 Dimensional Instability Caused by Thermo-Mechanical Cycling

Thermo-mechanical cycling is a *permanent* change in the properties of a material that is caused by exposure to a variable environment, such as temperature cycles or vibration. In composite materials, this instability can be caused by the formation of micro-cracks between the phases.

2.1.3 Hysteresis

Hysteresis is a change that is measured in a material at fixed environments but has a magnitude dependant on the particular thermal path. This change can be permanent or reversible. An example of hysteresis instability is the change in the overall length of a

specimen of Zerodur (a low expansion glass) that has been cooled from 300°C to 20°C [4].

2.1.4 Temporal Dimensional Instability

Temporal instability is a *permanent* change that occurs in a material after exposure to an environment. An example of temporal instability was one of the first recorded observations of very small changes in geometry over extended periods of time. The study was performed on the length of gauge blocks used as standards for measuring critical mechanical dimensions on machined parts. Stainless steel, 1-inch, gauge blocks used were repeatedly measured in length over a 25-year period by the National Bureau of Standards. The results are shown in **Fig. 2-1**.

Over 25 years, most of the gauges increased steadily in length, some by as much as 24 μ-in (0.000024"). While this figure may not seem significant, it is in the order of the thickness of many types of useful engineering platings, and it is also totally unacceptable for the purpose for which the gauge blocks were fabricated [5]. The gauge block instability is due to the martensitic transformation that can continue very slowly in steel at room temperature. A slight volume change accompanies this transformation. While temporal instability due to phase transformation is not the intended topic of this research, this phenomenon may be examined in order to explain the experimental behavior of the materials under study.

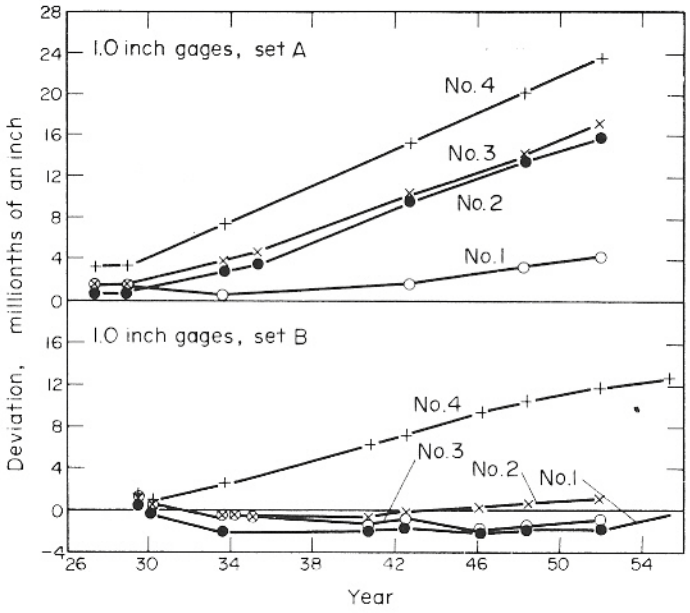

Fig. 2-1 Change in length of stainless steel gauge blocks over 25 years.

A second mode of temporal instability is caused by the relaxation of residual stresses in materials. These residual stresses can come from a variety of sources such as rolling, machining, heat treating, quenching, plating, welding, etc. Marschall and Meringer, who have written the most comprehensive book on the subject of instability, indicate that there are some graphical and mathematical models for the prediction of stress relaxation. These rely on adequate knowledge of the creep strain rate vs. stress [6].

2.2 Residual Stresses Caused by Machining

In a study funded by the French company Aerospatiale, residual stresses induced by milling operations were investigated in an attempt to better understand how surface stresses would affect fatigue life [7]. The alloy under investigation was 7075-T7351, a common precipitation hardenable alloy used in the aerospace industry. The variables tested were "up-milling" vs. "down-milling", cutting speed (m/min), feed speed (mm/tooth), depth of cut (mm), and coolant presence (yes/no). Up-milling refers to the rotation of the tool being opposite the direction of the material feed, and therefore chips are scraped "up" and away from the work piece. Down-milling involves the cutting tool teeth and workpiece traveling in the same direction.

Several findings are noted in the report. First, residual stresses always peaked at the surface of the part. Second, up-milling lowered the residual stress by approximately 100MPa. Third, the depth of cut had no effect on residual stress. Fourth, decreasing the cutting speed in a ratio of 11:1 reduces residual stress by approximately 200 MPa. Fifth, decreasing the feed speed by a ratio of 3:1 produces an approximately 150 MPa reduction in stress. The relationship between residual stress magnitude, XRD peak width, and the depth from the material surface are illustrated in **Fig. 2-2**.

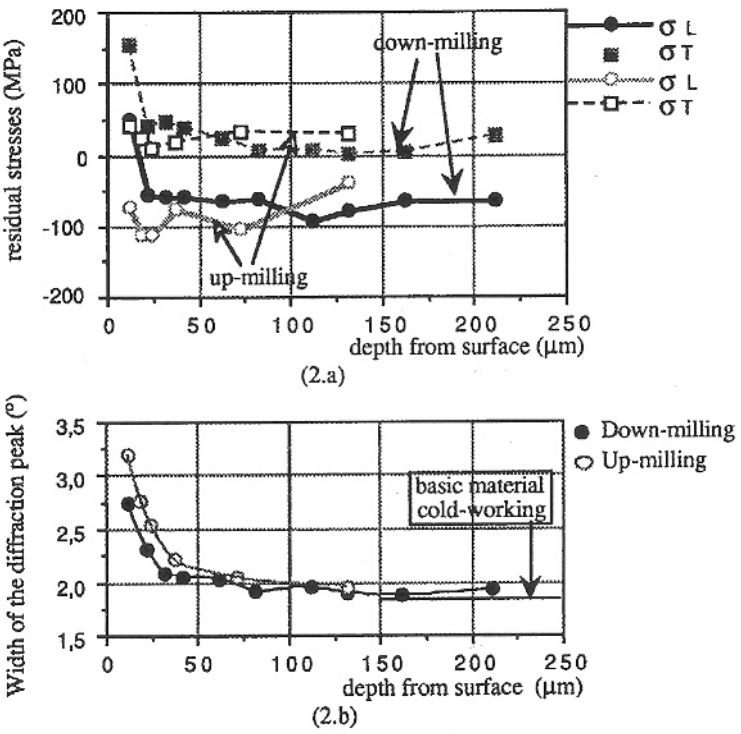

Fig. 2-2 (Top) Up-milling and down-milling and the effect on residual stress as a function of depth. (Dashed lines are transverse to cutting, solid lines are longitudinal) (Bottom) Up-milling vs. down-milling (solid dots) and their effect on XRD peak width.

Another study focused on grinding operations in quenched and tempered 4340 steel [8]. By altering the grinding wheel type, the wheel speed, stock feed (or wheel down feed), and cutting fluid, a "conventional" operation was compared to a "gentle" and an "abusive" grinding operation. Of particular interest is how relative thin stressed layers near the surface, produce longer order stresses of the opposite sign deeper into the parent material. This illustrates how residual stresses must balance one another to be in equilibrium. **Fig. 2-3** illustrates how "gentle" grinding operations will produce small compressive stresses at the surface, and virtually no internal stress, while more abusive grinding operations will produce high tensile stresses at the surface balanced by deeper compressive stresses.

Many other studies have been performed to characterize the level of residual stress imparted by machining operations on various alloys [9, 10].

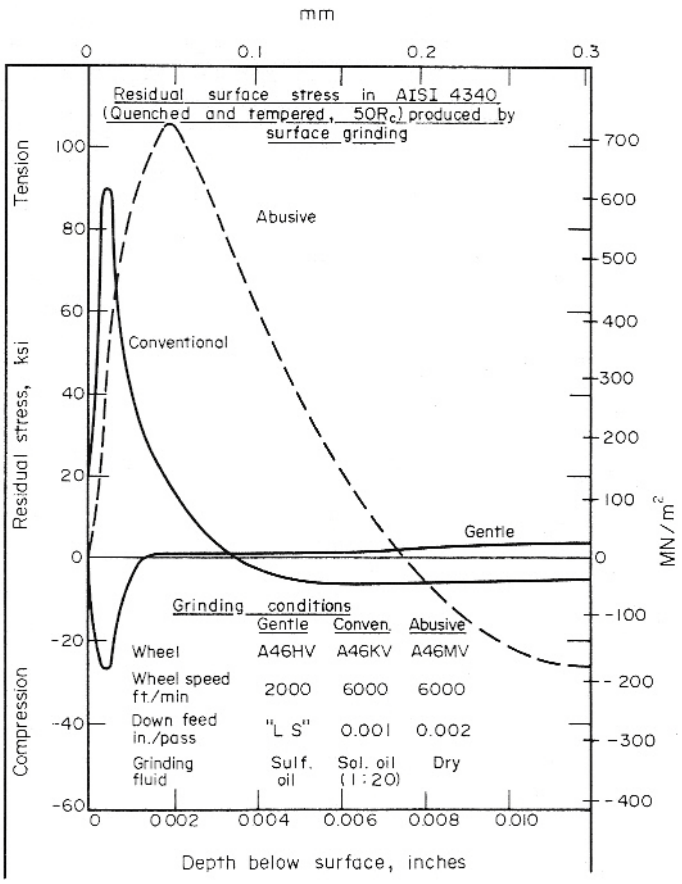

Fig. 2-3 Residual stress vs. depth for 4340 steel parts subjected to conventional, gentle, and abusive grinding operations.

Imgram and others demonstrated the effects of machining residual stresses on Ni-Span-C [11]. Two rods of Ni-Span-C were chemically etched to remove any machining damage caused by previous operations to a final diameter of approximately .625". A controlled machining pass was then performed on the OD of each specimen on a lathe using a single point cutting tool. .001" was removed from one specimen, and .003" was removed the other. A length increase from 3.500" of approximately 110 and 140 u-in respectively was immediately observed upon the lathe machining pass. The test specimen is seen below in **Fig. 2-4**.

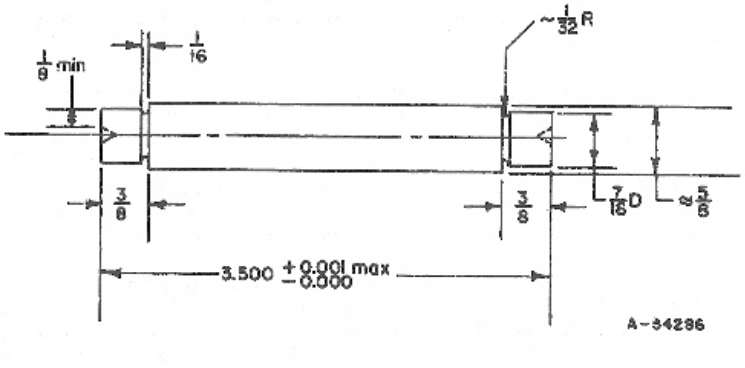

Fig. 2-4 Specimen used for Battelle Labs machining studies related to dimensional stability.

The surfaces of the specimen were then chemically etched in a controlled fashion in increments of .001" to simulate stress relaxation, and the length was recorded. The .001" turned specimen returned to its original length sooner than the .003" cut specimen indicating a steeper stress gradient. Conversely, the .003" machined specimen sustained deeper damage from the machining operation. The length vs. etching depth profiles can be seen below in **Fig. 2-5**. It is easy to see parallels between the removal of the stressed machining layer by chemical etching, and the creeping of the stressed layer over time.

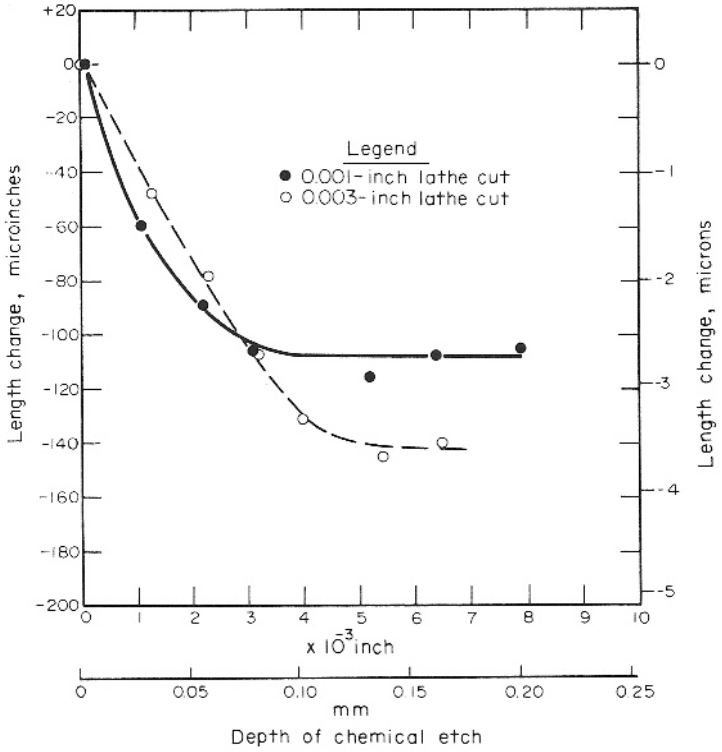

Fig. 2-5 Length change during surface etching of machined Ni-Span-C specimen.

Frommer and Lloyd investigated the residual stresses left behind from various machining operations on two heat treated aluminum alloys" [12]. They also used back reflected X-Rays and a Debye Scherrer camera setup. Among their general findings are the following:

1. No appreciable surface layer stresses were caused by the following operations:
    a. lathe machining with fine a finishing cut,
    b. surface milling with straddling mill,
    c. side milling of external surface with end-mill (tool not enclosed by material of job).
2. Small or moderate surface layer stresses were produced by:
    a. turning with rough cut,
    b. recessing with flat bottom drill,
    c. automatic polishing with a course emery cloth.
3. Very high surface layer stresses were created by:
    a. milling of slots or grooves with a formed cutter (tool enclosed al-around by material of job),
    b. turning under conditions producing conspicuous chatter marks,
    c. heavy shot blasting.

Specifically they made measurements of surface stresses and also estimated the depth of the stressed layer by acid etching. Acid etching was utilized until an X-ray pattern consistent with zero stress was obtained. It is important to note that at this time no correction was being made for the removed material (see Section 2.4). The findings that are relevant to this research are summarized below in **Table 2-1** [13].

Table 2-1 Summary of findings of Frommer and Lloyd related to surface stresses produced by various machining operations.

Type of Operation	Description	Stress (ksi)	Depth (in)
Turning	Flat Surface finished off with a fine finishing cut (0.0015 in/rev., 0.0005" depth of cut)	6.6	0.002
	Cylindrical surface turned with a rough cut (575 RPM, 0.012 in/rev., 0.050" depth of cut)	14.4	0.015
	Surface faced off under conditions producing chatter marks	41.4	0.024
Recessing	Recess made with flat bottom drill (290 RPM, 0.005 in/rev.)	13.8	0.004-0.015
Surface milling (cutter not enclosed by material	Flat surface side milled with 2" long 3/8 diameter end-mill (220 RPM, 0.01 in/rev., 0.125" depth of cut)	Nil	Nil
	Flat surface milled with straddling end mill (220 RPM, 0.01 in/rev., 0.125" depth of cut)	Nil	Nil

2.3 Measurement of Stress Using X-Ray Diffraction

X-Rays were first used for non-destructive material evaluation in the early 1920's by Dr. H. H. Lester of the Watertown Arsenal, working on behalf of the Army. Residual stress was first measured in 1925 by Lester and Dr. R.H. Aborn by measuring the lattice strain of tensile stressed steel using the Debye-Scherrer method of X-Ray Diffraction [14]. Examples of the original diagrams and the shifting in peak position (line shifting) caused by the supplication of stress (and the resulting strain) are seen below in **Fig. 2-6** and **Fig. 2-7**.

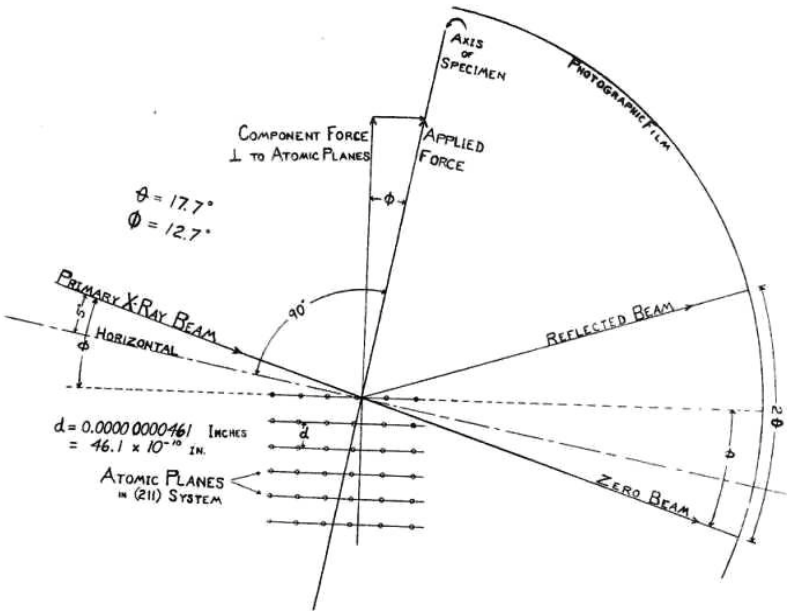

Fig. 2-6 Original schematic diagram from Lester and Aborn's novel use of XRD to measure stress within a bulk material.

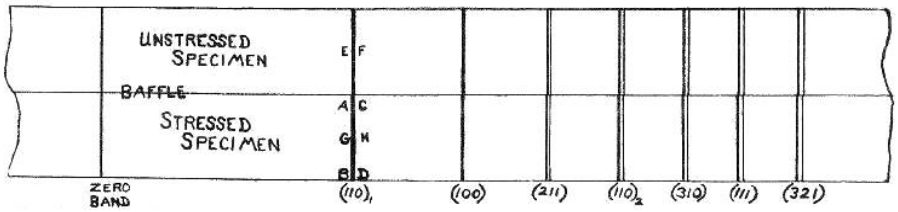

Fig. 2-7 Illustration of peak position shifting due to stress application as observed by Lester and Aborn.

Several conclusions are drawn from their initial experiments among which are; (a) individual crystals within an aggregate experience slightly different stress-strain curves than that of the aggregate as a whole, (b) strain below the proportional limit occurs by a mechanism of small-scale stepped slipping along glide planes which leaves the surrounding lattice in much the same geometric configuration, (c) the stress is taken by the iron crystal structure exclusively below the proportional limit, and to some extend by other structure in the aggregate above the proportional limit, (d) carbon is in solid solution in the iron crystal structure of sorbitic steel as detectable by a distorted lattice, (e) pearlitic steel does not show a distorted lattice and therefore the carbon does not sit in solution. This initial study also yielded the following general deduction which is

included in this text to demonstrate the immediate and broad impact of XRD stress analysis:

"Steel owes its strength to the nature of the atomic bonding, and to influences that tend to prevent slip of atoms along the glide planes. These influences may be the mutual interference between adjacent crystals, the effect of distorted crystal planes due to dissolved carbon, the effect of disorganized material formed during plastic deformation, and possibly other effects not found in these experiments. The proportional point of the crystalline aggregate may be defined as the range of stress values for which the stepped slip begins to merge into blocked slip, and the yield point may be regard as the region of stress values for which there is well defined block slip."

Lester and Aborn relied on the use of Bragg's Law, **Eq. 2-1**, to determine interplanar or lattice spacing. Interplanar spacing of a lattice is measured using X-Rays of a known wavelength.

$$n\lambda = 2d\sin\theta \qquad \textbf{Eq. 2-1}$$

In this relationship, n is a whole integer, λ the wavelength of the incident X-Ray beam, d the interplanar distance or spacing, and θ is the diffraction angle. In very general terms, this relationship states that diffraction occurs will occur when a lattice of spacing d is bombarded by X-Rays of a wavelength λ, and at an angle of θ. If these three parameters are not simultaneously satisfied the X-Rays will be scattered weakly in all directions. When these parameters are satisfied simultaneously the X-Ray energy will be *refracted* strongly in the single direction of 2θ from the original source. In a polycrystalline sample, only those grains of material whose lattice is perpendicular to the X-ray beam will experience refraction and contribute to the lattice spacing measurement. This is illustrated in **Fig. 2-8** [15].

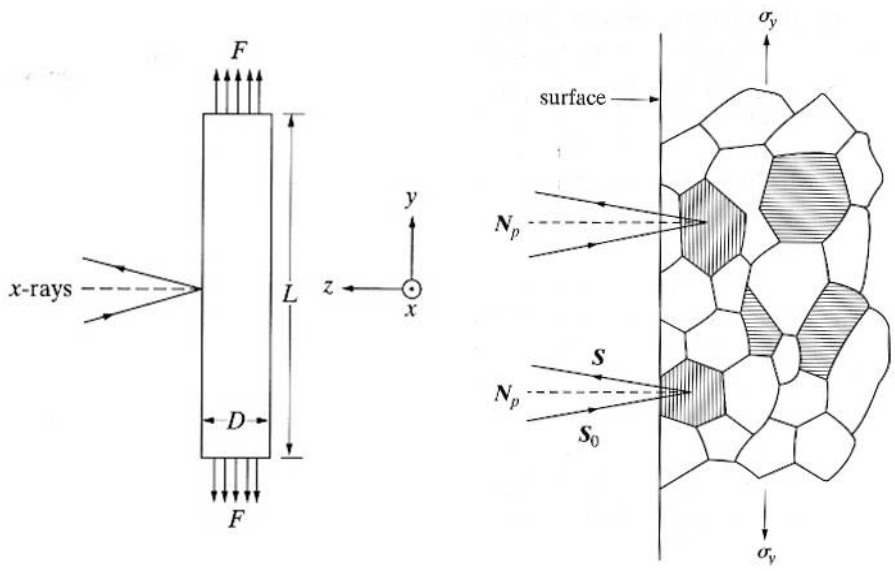

Fig. 2-8 Relationship between stress, X-Ray beam, and grain involvement in a polycrystalline sample.

By establishing the non-stressed, or strain free, value of d for a particular crystal or lattice, generally referred to as d_o, the associated peak position θ is established. A stress to the lattice will result in a proportional change in the lattice spacing, resulting in a corresponding shift in the θ position of the peak. The relationship between the stress and the lattice strain (change in d) is related by Hooke's Law, see **Eq. 2-2**:

$$\sigma_y = -\frac{E}{\nu}\varepsilon_z = -\frac{E}{\nu}\left(\frac{d-d_o}{d_o}\right) \qquad \textbf{Eq. 2-2}$$

For the measurement of stress in a single axis this relationship is sufficient if the value of d_o is precisely known. To account for the variation in d_o from alloy to alloy and sample to sample a method has been developed that precludes the need to know d_o precisely. The sin2 Ψ method involves making a series of measurements of d-spacing about angles that deviate from normal to the samples surface, where Ψ is designated as 0. The coordinate system for measurement of this type is seen in **Fig. 2-9** below.

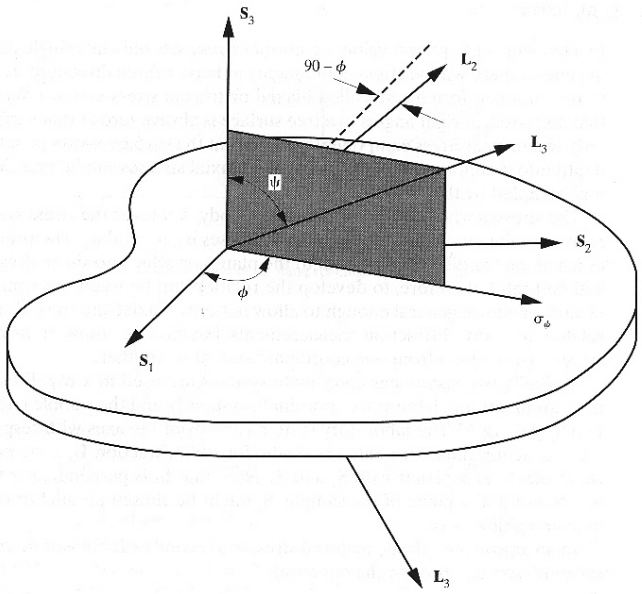

Fig. 2-9 Coordinate system for measuring stress using the sin2 Ψ method.

For performing stress analysis for a single direction, only a single value of ϕ is used for measurement. Biaxial measurements can be made by selected two or more values of ϕ to make a series of Ψ measurements about. The θ range used to capture the diffracting angle is centered about the Ψ angle.

The sin2 Ψ method is effective due to the fact that the outermost lattice layers on a samples surface are virtually stress-free in the normal direction. These are measured most directly by the values of d recorded at Ψ=0, the other values of Ψ are measuring components increasing in-plane with the surface. The following relationship governs biaxial stress measurement using XRD, see **Eq. 2-3** and **Eq. 2-4**:

$$\frac{d_{\phi,\Psi} - d_o}{d_o} = \frac{1+\nu}{E}\sigma_\phi - \frac{\nu}{E}(\sigma_1 + \sigma_2) \qquad \textbf{Eq. 2-3}$$

where:

$$\sigma_\phi = \sigma_1 \cos^2\phi + \sigma_2 \sin^2\phi \qquad \textbf{Eq. 2-4}$$

In this relationship σ_1 and σ_2 are the principal stresses and σ_ϕ is the value of the stress component at the orientation of ϕ on the sample surface.

2.4 Depth Corrected Stress Profiles Using Material Removal

If a stress gradient is present from the surface of a sample to some depth, a more sophisticated means of evaluating the magnitude of the stresses present is required. Removing thin layers of material from the sample's surface and making a series of stress measurements is the most common method. It is important when using this technique to recognize that an effect of removing a layer of material is that it will change the stress on the surface that has become exposed. Moore and Evans put forth a mathematical procedure for correcting for the removed layer of material [16]. Using the Timoshenko's theory of Elasticity as a basis, Moore and Evans developed mathematical corrections for removed layers for 4 cases:

- Solid cylinder with rotationally symmetrical stresses
- Solid cylinder with non-symmetrical stresses
- Hollow cylinder with rotationally symmetrical stresses
- Flat plate with stress as a function of depth from one flat surface

The methodology developed by Moore and Evans has been incorporated into the industry specification SAE HS-784 [17] and has become the standard means of measuring stress by depth profiling and mathematical correction.

A generalized solution effect of layer removal on the measured stress for the case of the Flat Plate is presented below, **Eq. 2-5**:

$$\sigma(z_1) = \sigma_m(z_1) + 2\int_{z_1}^{H} \frac{H\sigma_m(z)}{z} dz - 6z_1\int_{z_1}^{H} \frac{H\sigma_m(z)}{z^2} dz \qquad \textbf{Eq. 2-5}$$

where:

H is the total thickness of the sample

$\sigma(z_1)$ is the true stress in any direction at a measured depth of z_1 before material removal

$\sigma_m(z_1)$ is the measured value of stress at the depth of z_1 after material was removed

The correction in stress, $c(z_1)$, is the difference between the true stress and the measured value of stress after material removal, **Eq. 2-6**.

$$c(z_1) = \sigma(z_1) - \sigma_m(z_1) = 2\int_{z_1}^{H} \frac{H\sigma_m(z)}{z} dz - 6z\int_{z_1}^{H} \frac{H\sigma_m(z)}{z} dz \qquad \textbf{Eq. 2-6}$$

This can be expanded by Taylor series to the following form, **Eq. 2-7**.

$$c(z_1) = -4\sigma_m(H)\left(\frac{H - z_1}{H}\right) + \left[\sigma_m(H) + 2H\sigma'_m(H)\right]\left(\frac{H - z_1}{H}\right)^2 + \frac{1}{3}\left[2\sigma_m(H) + \sigma'_m(H) - 2H^2\sigma''_m(H)\right]\times\left(\frac{H - z_1}{H}\right)^3 + \cdots \qquad \textbf{Eq. 2-7}$$

where:

$\sigma_m(H)$, $\sigma'_m(H)$, etc = the true surface stresses and the successive derivatives with respect to z at the surface

For "shallow" depths of material only the first term in the Taylor Series needs to be considered, and the following approximation can be made, **Eq. 2-8**.

$$c(z_1) = -4\sigma_m(H)\frac{\Delta z_1}{H} \qquad \textbf{Eq. 2-8}$$

where:

$$\Delta z_1 = H - z_1$$

By solving for Δz_1, the appropriate depth of material removal can be calculated, **Eq. 2-9**.

$$\Delta z_1 = -\frac{1}{4}\frac{Hc(z_1)}{\sigma_m(H)} \qquad \textbf{Eq. 2-9}$$

where:

$Hc(z_1)/\sigma_m(H)$ = error in the correction

Specifying a correction error, such as 5% or .005, will allow the appropriate slice depth to be calculated. This slice depth will be a function of both the desired accuracy and the total thickness of the sample.

SAE HS784 does caution that in high stress gradients the second term in the Taylor series needs to be included, and that an estimates of $\sigma'_m(H)$ needs to be made based on

experience. Not including this term would lead to slightly higher errors than calculated by **Eq. 2-9**.

In 1994 Kang, Li, and Wang developed a mathematical procedure for depth correction that does not required the use of Taylor Series integral evaluation, and precludes the need for an estimate of $\sigma'_m(H)$ [18]. This method had not been introduced into the latest version of SAE HS784 and is therefore not the widely accepted industry methodology for depth profiling of stress.

The accuracy of the depth correction technique was validated in a study by R. England at the University of Cincinnati. In this study, a crankshaft and a connecting rod, two diesel engine components, were used to examine the stress profiles near the surface after manufacture. Synchrotron radiation was utilized to characterize the near surface stresses and neutron diffraction was utilized to characterize the subsurface stresses, those below 1mm. The synchrotron strains were corrected for effect of the exponentially weighted average over irradiated area using a numerical linear reversion method. The combined data of these two methods represented a non-destructive method for characterizing the full stress profile of the two parts.

These measurements were compared to the more common method of utilizing a series XRD stress measurements, destructively removing layers of material, and mathematically correcting for the removed material described in Section 2.4. The two methods showed good correlation, as can be seen below in **Fig. 2-10** [19].

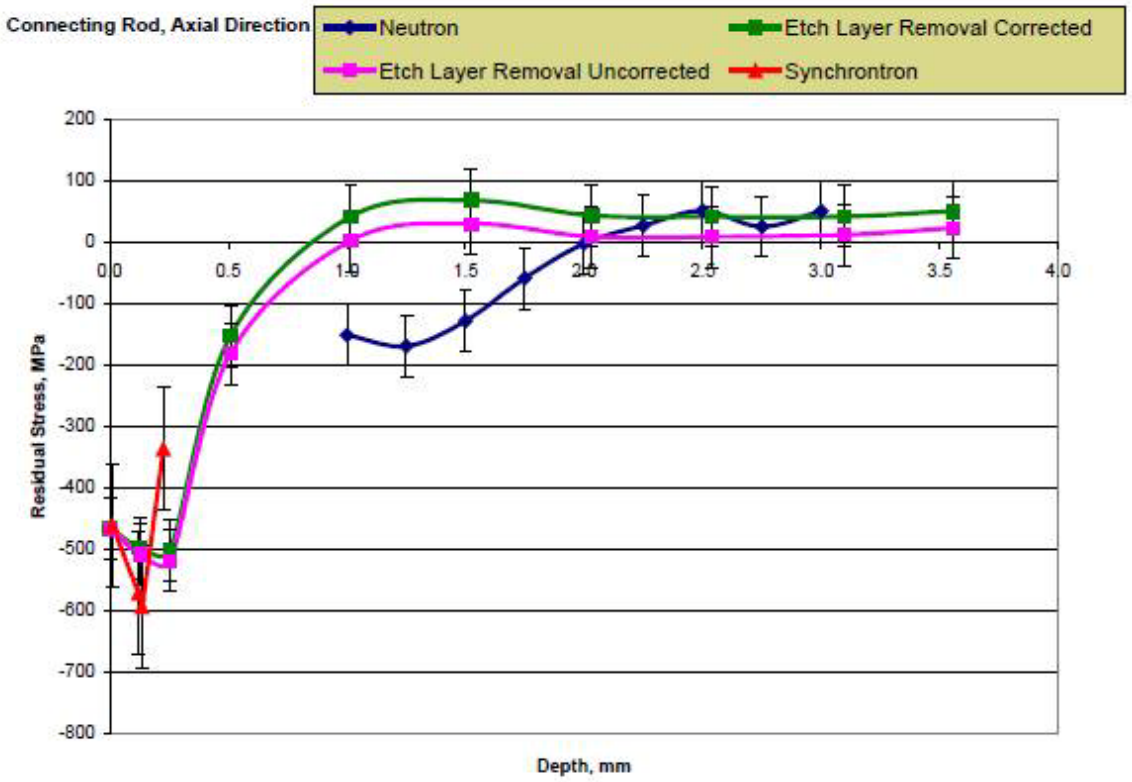

Fig. 2-10 Comparison of depth corrected XRD stress measurements, and the non-destructive techniques of synchrotron radiation and neutron diffraction.

2.5 Materials to Be Studied

Two alloys will be examined in this project. These are:

1. **AL6061-T6** - This alloy is the most widely used and most well understood aluminum alloy in aerospace and optical systems. It is included in this study because, at least in a subjective way, it can serve as a control material since its behavior during testing can be compared to previous experiences with the alloy.
2. **AL4032-0** - This is a high silicon alloy that has similar thermal conductivity and a lower CTE than AL6061. These two properties may make AL4032 a viable alloy for use in certain environments where AL6061 is inadequate. (AL6061 is prone to surface damage caused by rapid heating and expansion of a thin layer at the surface.) This alloy is not typically used in optical systems, so any data collected will be a valuable addition to the knowledge base.

Basic properties of the alloys can be seen below in **Table 2-2**.

Table 2-2 Basic properties of the two aluminum alloys under investigation.

	AL6061-T6[20]	**AL4032-0 [21]**
Description	Wrought	Wrought
Condition	Solutionized, Artificially Aged	Annealed
Major Alloying Elements	Mg: 0.8-1.2 Si: 0.4-0.8 Cu: 0.15-0.4 Cr: 0.04-0.35	Si: 11.0-13.5 Mg: 0.8-1.3 Cu: 0.5-1.3 Ni: 0.5-1.3
Yield Strength	40 ksi	35 ksi
UTS	45 ksi	30 ksi
Elongation	12%	4%
CTE	23.6×10^{-6}/°C	19.4×10^{-6}/°C

3 Theoretical Development

It is well understood that machining operations produce surface stresses in the machined components and that these stress can be of considerable magnitude. Typically, there exists an elastic response to these stresses such that the surface stresses balance out with the stress in the bulk of the material. For example, a thin layer of highly compressed material at the surface will have to balance out with a portion of the material that is in sustained tension. These stresses will be in a state of semi equilibrium. Material that is in a state of sustained stress will be subject to creep. There are two unique characteristics to this situation:

1. Creep models have a stress term that is raised to an exponent which is higher than 1 for metals. Consequently, if a specimen has non-uniform stresses, the more stressed regions will creep at exponentially higher rates than the less stressed regions.
2. As the material strains, the stress level will become proportionally lower.

These two characteristics serve as the basis for the proposed creep model as they relate to dimensional instability in real components.

3.1 Modeling Creep Due to Residual Stresses

The temperature range of interest in this research project is -55°C to +125°C for 6061 alloy. This range was selected because it is used on a wide variety of products that may need to operate over what are generally considered full military temperatures ranges. 4032 is under consideration for a satellite application in which the useful temperature range would be much more limited. Maximum temperatures would be associated with the internally generated heat of the electronics and would likely not exceed 60-80C. The typical residual stress magnitude caused by machining operations found in the literature is 100-200MPa. This puts the creep mode in the range of both the Dislocation Glide and the Dislocation Creep [22] mechanisms as seen in **Fig. 3-1**.

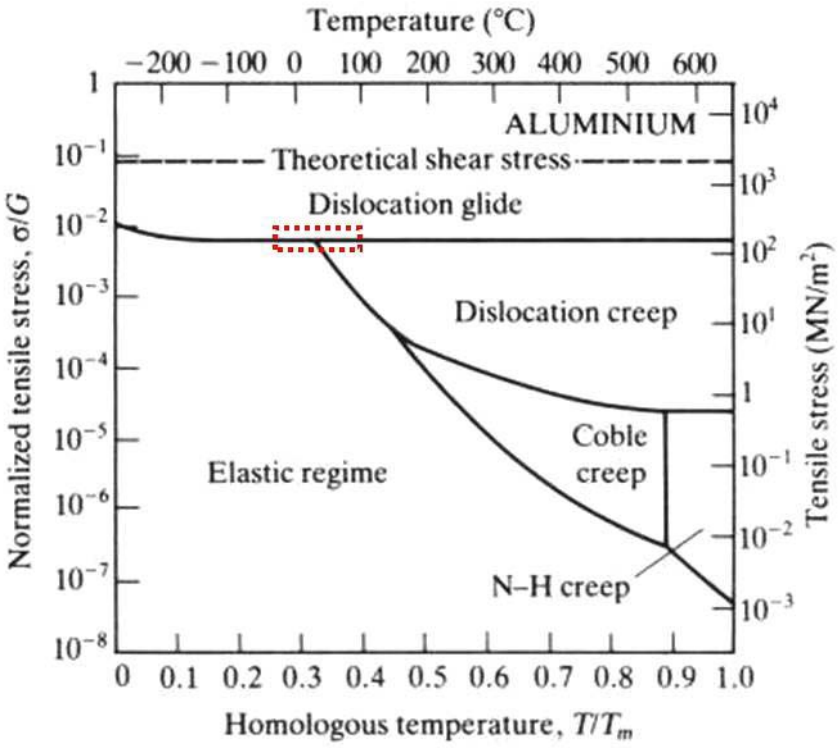

Fig. 3-1 Creep Mechanism Map for Aluminum.

The simplest creep model that is applicable for Dislocation Glide and Dislocation Creep, and also accounts for both stress and temperature is the Power Law [23]. However, the Power Law model best represents the Secondary Creep Mode. In the case described herein, constantly changing stress magnitude (due to creep strain) will keep the creep mode in Primary Creep Mode. Nevertheless, the strains are expected to be small enough that a straight line approximation over the range should hold well. Since the slope is different than that in the Secondary Creep Mode, the Creep Model parameters will differ from those published. Typical creep behavior [24] is shown in **Fig. 3-2**.

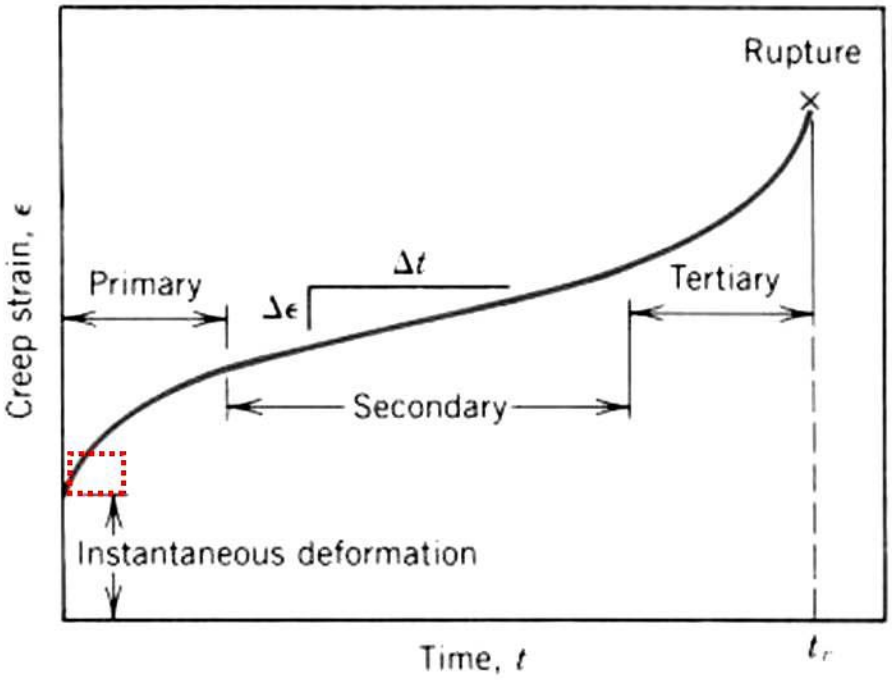

Fig. 3-2 The region of interest of this research is the primary creep zone.

The general expression for Creep is known as the Mukherjee-Bird-Dorn equation and is as follows [25]:

$$\dot{\varepsilon}_{ss} = \frac{d\varepsilon}{dt} = \frac{AGb}{k'T} D \left(\frac{b}{d}\right)^{P} \left(\frac{1}{G}\right)^{m} \sigma^{m} e^{\frac{-Q}{RT}}$$

where:

$\dot{\varepsilon}_{ss}$ = creep strain
t = time
A = material dependant constant
G = Shear Modulus
b = Burger's Vector
k' = Boltzman's Constant
T = temperature
D = Diffusion Constant
σ = stress
d = grain diameter
P = grain size exponent
m = stress exponent
Q = thermal activation energy
R = gas constant

The Power Law Creep equation can be obtained from the general equation for steady state creep rate for crystalline materials [26], namely

$$\dot{\varepsilon}_{ss} = \frac{d\varepsilon}{dt} = \frac{\sigma^m}{d^q}\frac{k}{T}e^{-\frac{Q_c}{RT}} \qquad \textbf{Eq. 3-1}$$

In Eq. (1), the variables that affect the strain rate $\dot{\varepsilon}$ are stress σ, average grain diameter d, and absolute temperature T. The coefficients k, the exponents m and q, and the activation energy Q_c have values that depend on the material and the creep mechanism.

Grain boundaries are not a major factor in Power Law Creep for crystalline materials and so the strain rate is not significantly affected by grain size; hence, for Power Law Creep, therefore q = 0 [27], and **Eq. 3-1** becomes:

$$\dot{\varepsilon}_{ss} = \frac{k}{T}\sigma^m e^{-\frac{Q_c}{RT}} \qquad \textbf{Eq. 3-2}$$

The following steps in the development of the creep strain model are proposed in this research, and are not part of the literature.

A unique condition of creep strain due to residual (and not applied) stresses in an un-restrained material is that stress is not constant but is a function of strain, i.e.,

$$\sigma_{res} \neq \text{constant}$$
$$\sigma_{res} = f(\varepsilon) \qquad \textbf{Eq. 3-3}$$

A simplified stress model considering only one stress demonstrates the linear relationship between stress and strain as given in **Eq. 3-4**.

Given Hooke's Law:

$$\varepsilon_1 = \frac{1}{E}\left[\sigma_1 - \nu(\sigma_2 + \sigma_2)\right]$$

and if,

$$\sigma_2 = \sigma_3 = 0$$

then:

$$\sigma_1 = \sigma = E\varepsilon \qquad \textbf{Eq. 3-4}$$

A stress function is then defined with a linear relationship to strain and where the value of stress is reduced to zero as strain reaches a final value as in **Eq. 3-5**. It is recognized that the value of ε_f is likely a function of temperature.

$$\sigma = \sigma_{in}\left(1 - \frac{\varepsilon}{\varepsilon_f}\right) \qquad \textbf{Eq. 3-5}$$

Substituting Eq. (5) into the Power Law, and integrating from initial strain of zero at an initial time of zero yields an expression that defines strain as a function of initial stress (σ_{in}), final strain (ε_f), the stress exponent (m), an Activation Energy (Q_c), a constant (k), and time (t) as given by **Eq. 3-6**.

$$\int_{\varepsilon=0}^{\varepsilon=\varepsilon}\left(\sigma_{in}-\frac{\sigma_{in}\varepsilon}{\varepsilon_f}\right)^{-m}d\varepsilon=\int_{t=0}^{t=t}ke^{\frac{-Q_c}{RT}}dt$$

$$\varepsilon=\varepsilon_f-\frac{\varepsilon_f}{\sigma_{in}}\left[\frac{(m-1)\sigma_{in}}{\varepsilon_f}kte^{\left(\frac{-Q_c}{RT}\right)}+(\sigma_{in})^{1-m}\right]^{\frac{1}{1-m}} \qquad \textbf{Eq. 3-6}$$

A step by step derivation of **Eq. 3-7** is provided in Appendix A.

As the data in this project will show, the value of final strain, ε_f, is a function of temperature. Within the temperature ranges investigated herein, increasing dwell temperature increases the ε_f value. The theoretical maximum creep strain that would be recovered during isothermal temperature exposures would be if the initial stress were completely converted to strain in accordance with Hooke's Law:

$$\varepsilon_{f,\ \text{theoretical maximum}}=\frac{\sigma_{in}}{E}$$

In actuality, the theoretical maximum is not reached, so an expression has been developed to predict ε_f that includes a material constant, B, and Temperature dependence term, T^n, see **Eq. 3-7**:

$$\varepsilon_f=B\frac{\sigma_{in}}{E}T^n \qquad \textbf{Eq. 3-7}$$

The constants B and n can be found graphically using the slope-intercept method.

The Bimetallic Strip model described in Section 3.2 is aimed at verifying the applicability of the mathematical model described by **Eq. 3-6** to the case of dimensional instability caused by machining residual stresses**.**

3.2 The Bimetallic Strip Model

A convenient method of testing the proposed creep model is by inducing residual stress on one side of a thin strip of material. Strain can be measured by observing the change in curvature. A procedure for performing this test will be discussed in the following Materials, Procedures, and Measurements section. Understanding how stress layers effect curvature can be explained by a bimetallic strip model.

The bimetallic strip model is traditionally used to describe the curvature and stress states of two strips of different metals bonded together and exposed to temperature excursions. As the temperature is changed, the difference in the two values of CTE creates a "misfit strain", and this strain results in a stress which causes the bimetallic strip to curve. In our case, it will be the layer of residually stressed material and the bulk unaffected material that make up the "bimetallic strip".

The bimetallic strip is governed by the following set of equations for thermally induced stresses where curvature (radius^{-1}) is given by **Eq. 3-8**. This set of equations was originally published by Timoshenko for the purpose of describing the behavior of bimetallic thermometers [28].

$$\frac{1}{\rho} = \frac{(\alpha_B - \alpha_A)(T - T_o)}{\frac{h}{2} + \frac{2(E_A l_A + E_B l_B)}{h}\left(\frac{1}{E_A t_A} + \frac{1}{E_B t_B}\right)} \qquad \textbf{Eq. 3-8}$$

where:

t = layer thickness

T = temperature

ρ = radius

$h = t_a + t_b$

$l = \frac{t^3}{12}$

$m = \frac{\alpha_1}{\alpha_2}$

$n = \frac{E_1}{E_2}$

The distribution of stresses is described by **Eq. 3-9** through **Eq. 3-13**:

$$\sigma_{A,Surface} = \frac{P}{h_A} - \frac{h_A E_A}{2\rho} \qquad \textbf{Eq. 3-9}$$

$$\sigma_{A,Interface} = \frac{P}{h_A} + \frac{h_A E_A}{2\rho} \qquad \textbf{Eq. 3-10}$$

$$\sigma_{B,Surface} = -\frac{P}{h_B} + \frac{h_B E_B}{2\rho} \qquad \textbf{Eq. 3-11}$$

$$\sigma_{B,Interface} = -\frac{P}{h_B} - \frac{h_B E_B}{2\rho} \qquad \textbf{Eq. 3-12}$$

where:

$$P = \frac{2\left(E_A l_A + E_B l_B\right)}{h\rho} \qquad \textbf{Eq. 3-13}$$

The following is an alternate formulation that sometimes appears in the literature [29]. The radius of curvature is given by **Eq. 3-14** and the stresses on the surfaces of layer A and layer B are given by **Eq. 3-15** and **Eq. 3-16**. A constant based on geometry is by **Eq. 3-17**. The algebraic equivalence of these expressions to the Timoshenko expressions is established in Appendix B.

$$r = \frac{E_A^2 h_A^4 + 4E_A E_B h_A^3 h_B + 6E_A E_B h_A^2 h_B^2 + 4E_A E_B h_A h_B^3 + E_B^2 h_B^4}{6E_A E_B\left(h_A + h_B\right)h_A h_B \Delta\varepsilon} \qquad \textbf{Eq. 3-14}$$

$$\sigma_A = \frac{\varepsilon_{misfit} E_A}{K_1}\left[3\frac{h_A}{h_B} + 2\left(\frac{h_A}{h_B}\right)^2 - \frac{E_B h_B}{E_A h_A}\right] \qquad \textbf{Eq. 3-15}$$

$$\sigma_B = \frac{\varepsilon_{misfit} E_B}{K_1}\left[3\frac{h_A}{h_B} + 2 - \frac{E_A}{E_B}\left(\frac{h_A}{h_B}\right)^3\right] \qquad \textbf{Eq. 3-16}$$

where:

$$K_1 = 4 + 6\frac{h_A}{h_B} + 4\left(\frac{h_A}{h_B}\right)^2 + \frac{E_A}{E_B}\left(\frac{h_A}{h_B}\right)^3 + \frac{E_B h_B}{E_A h_A} \qquad \textbf{Eq. 3-17}$$

h_A = stressed layer thickness

h_B = non-stressed thickness

E = Elastic Modulus

In the residual stress model, the misfit strain term will be changed from a CTE differential term to a term that describes the stress state in the surface layer. The traditional bi-metallic strip misfit strain term is as follows:

$$\Delta\varepsilon = (\alpha_A - \alpha_B)(T_1 - T_2) \qquad \textbf{Eq. 3-18}$$

Since the following conditions apply to the modified bimetallic strip model,

$$\varepsilon_A = \frac{\sigma_A}{E_A}$$

$$\varepsilon_B = \frac{\sigma_B}{E_B}$$

$$E_B = E_B$$

the following misfit strain term applies to the model:

$$\Delta\varepsilon = \frac{(\sigma_A - \sigma_B)}{E} \qquad \textbf{Eq. 3-19}$$

Given that the substrate is unstressed, misfit strain can be expressed as follows, the σ_{in} term represents the initial stress of the machined surface:

$$\Delta\varepsilon = \frac{\sigma_{in}}{E} \qquad \textbf{Eq. 3-20}$$

The bimetallic strip model can be further simplified for the case of a stressed surface layer caused by machining residual stresses. In this case, $E_a = E_b$, and $h_A << h_B$. The simplified form is seen below in **Eq. 3-21** and the algebraic derivation is contained in Appendix B.

$$\sigma_a = \frac{E}{6}\frac{h_B}{h_B}(3h_A + h_B)\frac{1}{r} \qquad \textbf{Eq. 3-21}$$

This equation can also be used to express the change in curvature due to a change in stress, **Eq. 3-22**, or a change in strain, **Eq. 3-23**.

$$\Delta\sigma_A = \frac{E}{6}\frac{h_B}{h_A}\left(3h_A + h_B\right)\left(\frac{1}{r_2} - \frac{1}{r_1}\right) \qquad \textbf{Eq. 3-22}$$

$$\varepsilon_{r_1 \to r_2} = \frac{h_B}{6h_A}\left(3h_A + h_B\right)\left(\frac{1}{r_2} - \frac{1}{r_1}\right) \qquad \textbf{Eq. 3-23}$$

Another implication both layers in the bimetallic strip having equal Young's Modulus', and of the misfit strain term used to describe the stressed layer, is that the initial stress will not be a function Young's Modulus. This is important as Young's modulus is a function of temperature.

Inserting the misfit strain term, **Eq. 3-20**, into the Timoshenko curvature expression, **Eq. 3-8**, the following is attained.

$$\rho = \frac{E}{\sigma_{in}} K_2 \qquad \textbf{Eq. 3-24}$$

where K_2 is a constant that is a function of geometry only:

$$K_2 = \left[\frac{h}{2} + \frac{1}{6h}\left(h_A^3 + h_B^3\right)\left(\frac{1}{h_A} + \frac{1}{h_B}\right)\right] \qquad \textbf{Eq. 3-25}$$

and **Eq. 3-13** becomes:

$$P = \frac{\sigma_{in}}{K_2} K_3 \qquad \textbf{Eq. 3-26}$$

where K_3 is another constant dependant on geometry only:

$$K_3 = \frac{h_A^3 + h_B^3}{6h} \qquad \textbf{Eq. 3-27}$$

The equations that describe the distribution of stresses, **Eq. 3-9** through **Eq. 3-12**, contain only two terms, and these can now be seen to be independent of Young's Modulus:

$$\frac{P}{h_x} = \frac{\sigma_{in} K_3}{K_2 h_x} \qquad \textbf{Eq. 3-28}$$

$$\frac{h_x E}{2\rho} = \frac{h_x \sigma_{in}}{2K_2} \qquad \textbf{Eq. 3-29}$$

3.3 Testing Methodology

The testing strategy for the project is as follows:

The stressed layer created by two different machining operations will be studied by intentionally creating samples that are dimensionally unstable. A stress free coupon will have a single machined layer produced on one side, causing a curvature. The curvature of these specimens will be monitored over time and multiple temperatures to gain an understanding of the creep behavior of the stressed layer. Curvature is a convenient measurement to make on the samples.

The bimetallic strip model allows conversion of curvature to strain in the machined layer. Two things must be known to employ the bimetallic strip model, the thickness of the affected layer, and the stress magnitude of the affected layer. Stress will be measured directly on a sample of coupons using X-Ray Diffraction. A measurement of the overall coupon thickness and the curvature of the coupon allow the thickness of the stresses layer to be calculated. This thickness is referred to as the equivalent thickness.

By observing curvature changes over time and temperature, and converting these curvature changes to strains, the creep parameters m, Q, and k from **Eq. 3-6** can be obtained using curve fitting software.

A model for predicting the final strain, $\varepsilon_{f,}$ achieved as a function of temperature will be developed empirically.

Knowing m, Q, k, and having a means for predicting ε_f allows for a complete creep model that can be used both for predicting dimensional stability over time and temperature. This model can be used for two purposes (1) to predict long-term storage stability and (2) to design short term isothermal treatments to relieve stress.

4 Procedures

4.1 Coupon Preparation

Coupons were prepared in three steps; 1" by 6" by.060" pieces were machined in accordance with the following procedure. These are referred to as ***Blanks***. A drawing of the Blank can be seen in Appendix B.

1. Equal amounts of material were removed from each side of the raw material using flycutting passes to bring the final thickness to .060"
2. Length and width dimensions were milled
3. Mounting holes were drilled (however not ultimately used)
4. No stress relieving, bending, or straightening operations were allowed per the drawing notes.

Since these blanks were manufactured using machining operations, there would be a stressed layer of material on all surfaces. These stressed layers were removed using a chemical etching process that was developed for this purpose. After etching, the samples were referred to as ***Etched Blanks***. A total thickness removal of .005-.006" was removed. This thickness was selected based on the observations of Frommer and Lloyd [30].

1. Thickness was measured using digital Vernier Calipers. These calipers are controlled by BAE Systems calibration program and are assigned CAL ID 209731 for this purpose.
2. The stressed layer was removed by chemical etching using a solution of 20% Sodium Hydroxide (NaOH) solution [31].
    a. Samples were placed in a large glass dish on a hotplate at approximately 40C.
    b. Two samples were processed at a time.
    c. The samples were periodically removed and the dark layer of aluminum hydroxide was removed by wiping with a cloth.
    d. The thickness was checked using the Vernier calipers.
    e. .0025-.003" (.005-.006" total thickness) was targeted for removal.
    f. Final thickness measurements were recorded.
3. It is noted during this process that after approximately .001" from each surface, the etch removal rate dramatically decreased.

4. The removal of .005” of total thickness took approximately ten minutes of submersion time. This however did increase as the number of coupons processed increased. The bath needed to be periodically replenished.
5. The etched blanks were serialized manually using a scribe to scratch a serial number near the two mounting holes. 6061-T6 alloy etched blanks were assigned “6061-XX” and 4032 etched blanks were assigned “4-XX”.
6. The baseline curvature was measured using the procedure described in Section 4.6.

The Etched Blanks were then machined on one side using one of two controlled machining procedures, Flycutting and Milling.

1. Machining was performed using a Bridgeport milling machine fitted with a CNC control system.
2. A fixture plate was clamped in place and level and the top surface leveled by making a skim pass with the flycutter. The setup can be seen in **Fig. 4-1**.
3. Individual Etched Blanks were secured to this plate using two-sided tape.
4. A single machining pass was performed on each sample.
    a. **Flycutting** was performed using the following parameters, images of the tool can be seen in **Fig. 4-2**, through **Fig. 4-6**
        i. Single cutting point with approximately 7.7° back rake angle and a 4.5° end relief angle.
        ii. Tool diameter of 3.2”
        iii. Spindle speed of 3000 RPM.
        iv. Feed rate of 30 in/min.
        v. Depth of cut of .020”
        vi. Isopropyl Alcohol used as a lubricant.
    b. **Milling** was performed using the following parameters, images can be seen in **Fig. 4-7** through **Fig. 4-10**.
        i. ½”, 3-flute, solid carbide endmill, with approximately 41° rake and a 13.7° edge relief angle and a 9.1° End Cutting Edge Angle. MSC Catalog number 65250193.
        ii. Spindle speed of 3000 RPM.
        iii. Feed rate of 20 in/min.
        iv. Depth of cut of .020”
        v. Isopropyl Alcohol used as a lubricant.

5. Initial curvature of the sample was measured using the procedure described in Section 4.6.

Fig. 4-1 Bridgeport milling machine used for performing controlled machining passes.

Fig. 4-2 Overall image of flycutter.

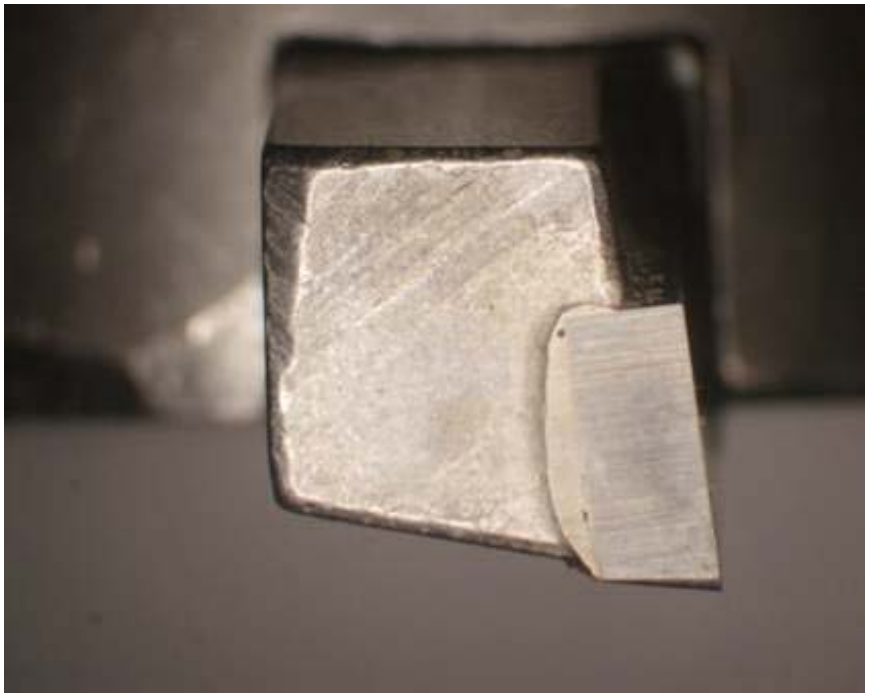

Fig. 4-3 Image of Flycutter showing cutter rake and backangle.

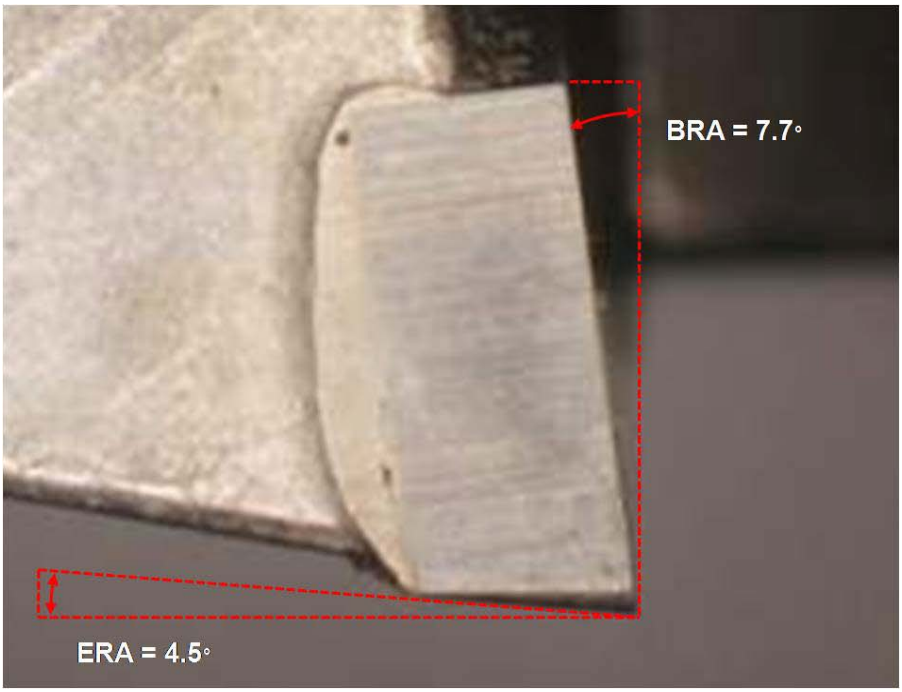

Fig. 4-4 Flycutter showing Back Relief Angle (BRA) and End Relief Angle (ERA).

Fig. 4-5 Image of flycutter face.

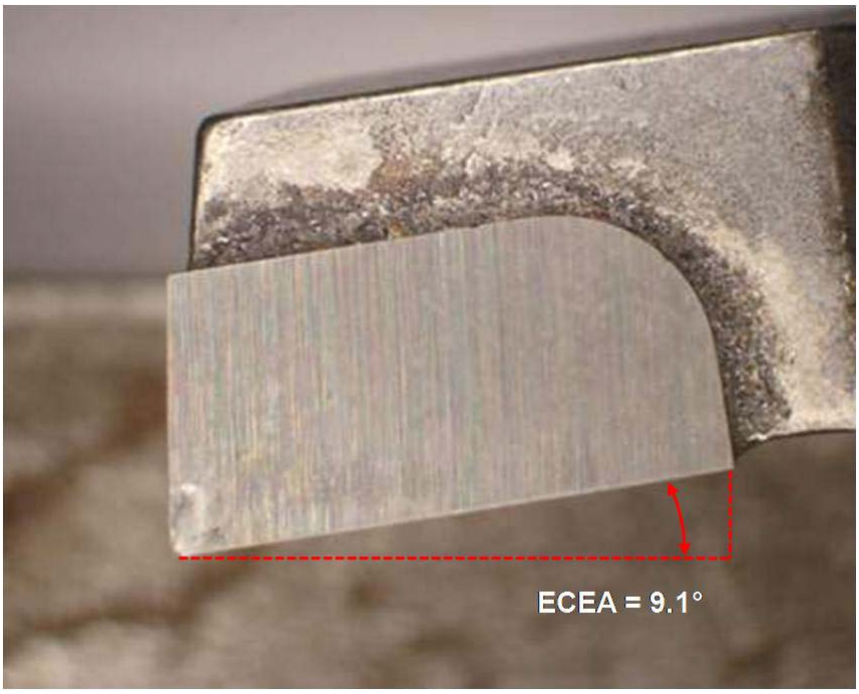

Fig. 4-6 Flycutter face with End Cutting Edge Angle (ECEA).

Fig. 4-7 Overall image of endmill.

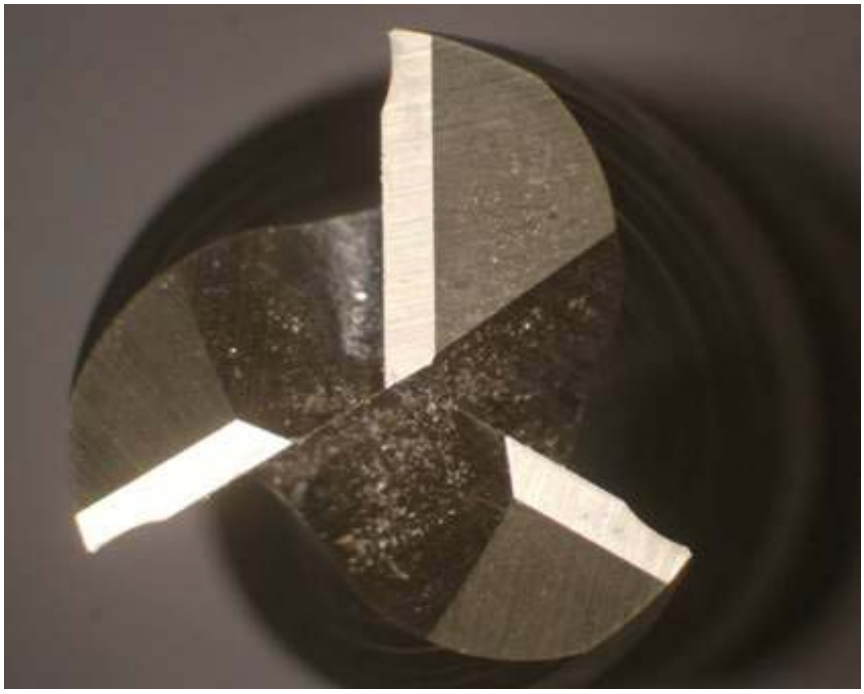

Fig. 4-8 Bottom view of the endmill showing the three cutting tips.

Fig. 4-9 Image showing the endmill rake and backangle.

Fig. 4-10 Endmill showing the Back Relief Angle (BRA) and End Relief Angle (ERA).

Two types of control samples were used for experimentation. ***Control Coupons*** were identical to Etched Blanks described above, and they did not receive any further processing. ***Offset Control Coupons*** were Blanks that had.020" of material removed from one side using a flycutting pass. These were then etched using the NaOH process described above. A diagram showing the sequence of material removal during the fabrication of these Control Coupons is shown below in **Fig. 4-11**.

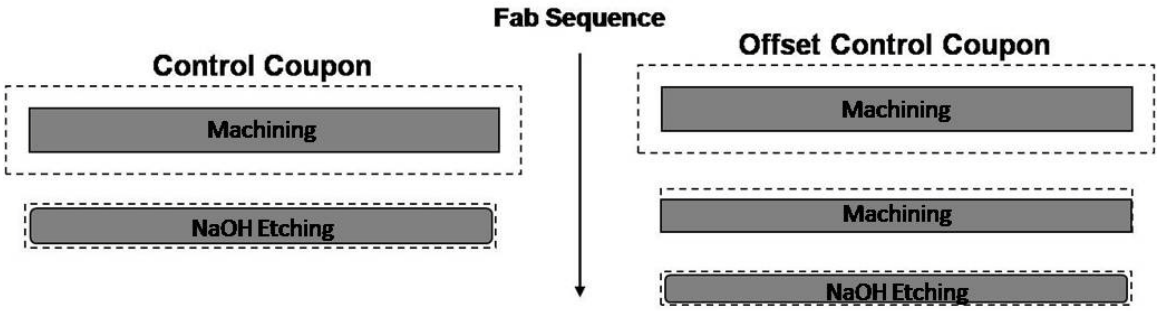

Fig. 4-11 Sequence of material removal for Control and Offset Control Coupons.

4.2 Handling Procedure

4.2.1 Storage

Coupons were stored on edge to prevent the mass of the material causing any stresses that might effectively "flatten" the curvature in storage.

4.3 Heat Treatment

4.3.1 Thermal Chamber Specifications

Coupons were heat treated in Thermotron Thermal Chamber Model RA-42-CHV-30-30. The chamber has very large fans to provide convection heating and heating rates up to 15°C/min to the article being tested. It has a 42 cubic foot chamber and is suitable for the heat treatment of much larger samples than were used in this project. For these reasons, and the very long heat treatment times, any thermal lag of the coupons during heating and cooling can be ignored. The thermal chamber can be seen in **Fig. 4-12**.

Fig. 4-12 The Thermotron thermal chamber used for isothermal heat treating.

4.3.2 Fixturing

In order to prevent the weight of the coupons themselves from creating a bending stress on the coupons during the isothermal heat treatments, a fixture plate was utilized. This plate had a stainless steel series socket head cap screws (SHCS) placed into predrilled holes on the plate. The fasteners were slip fit into the holes and not threaded into place. Once in place, there was about a ¼" gap from the head of one SHCS to the next. Between each set of SHCSs two coupons were placed. The coupons were stood up on the long edge. The coupons were free the move slightly and were in no way clamped by the fasteners. In this manner, the coupons were held in place for the heat treatments, but the curvature was not influenced by their own weight, or by the weight of adjacent coupons. An image of this setup is shown in **Fig. 4-13** below

.

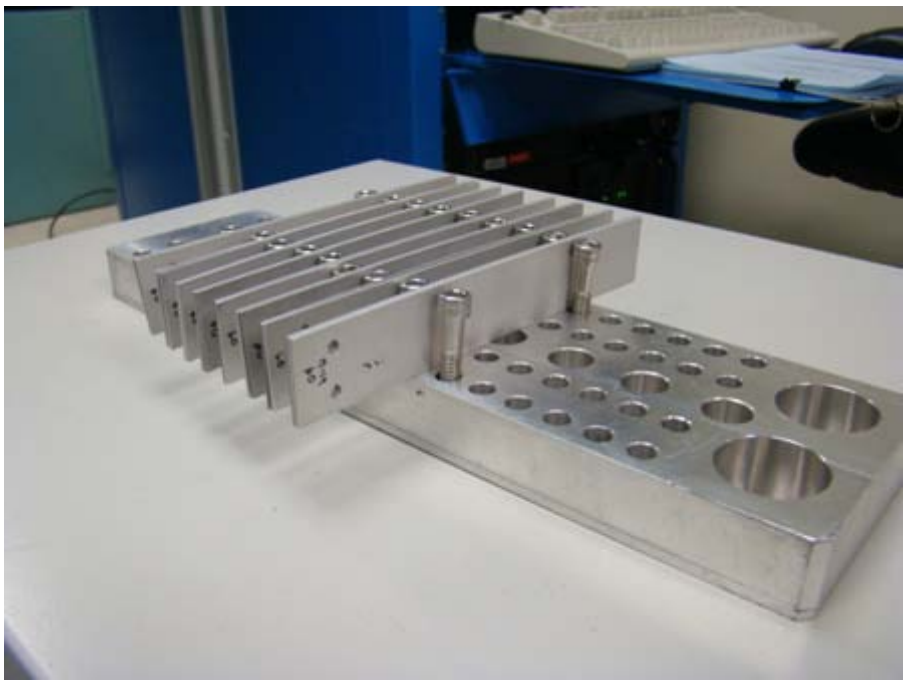

Fig. 4-13 Image of the coupon fixture plate used for the isothermal heat treatments.

Only two coupons were placed in each slot so that each had at least one full surface exposed to the convection of the thermal chamber. The coupons are thin enough, and aluminum conductive enough, and the heat treatments long enough, that any thermal gradients across the coupons thickness would be very brief and can be ignored. The fixture setup can be seen in the thermal chamber in below, see **Fig. 4-14**.

Fig. 4-14 Fixture plate shown in thermal chamber.

4.3.3 Initial Isothermal Exposures

In order to gather curves for time at temperature 6061 samples were exposed to isothermal exposures of 60C, 85C, and 125C. 4032 samples were exposed to isothermal treatments of 40C, 50C, and 60C and 85C. Curvature was monitored periodically.

4.3.4 Use of Control Samples

Control samples were used to evaluate whether there were large internal stresses in the bulk material that might influence curvature. One Control sample and one Offset Control sample per alloy were exposed to isothermal exposures at 85C.

4.4 Microstructure Examinations

Microstructure was characterized by etching samples using Keller's reagent. Samples were etched for approximately 20 seconds at room temperature [32]. Images were taken using a Nikon Eclipse L150 microscope using brightfield lighting. Differential Interference Contrasting (DIC), also known as Nomarski polarized lighting, was also used to examine the structures, but it did not reveal any features not already visible using brightfield only. Baseline microstructure images can be seen in **Fig. 4-15** through **Fig. 4-18**

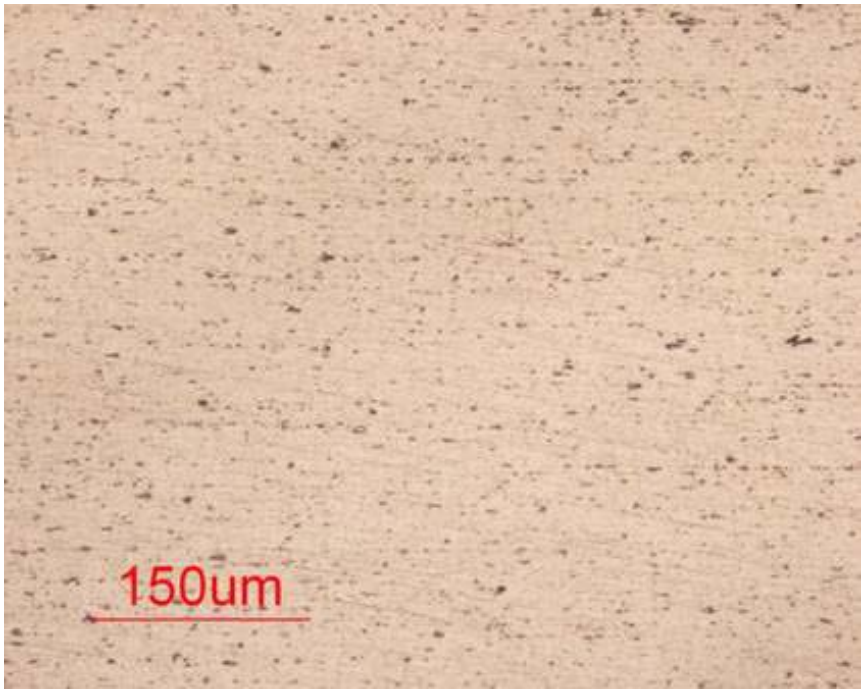

Fig. 4-15 Baseline microstructure of 6061-T6 originally imaged at 200X.

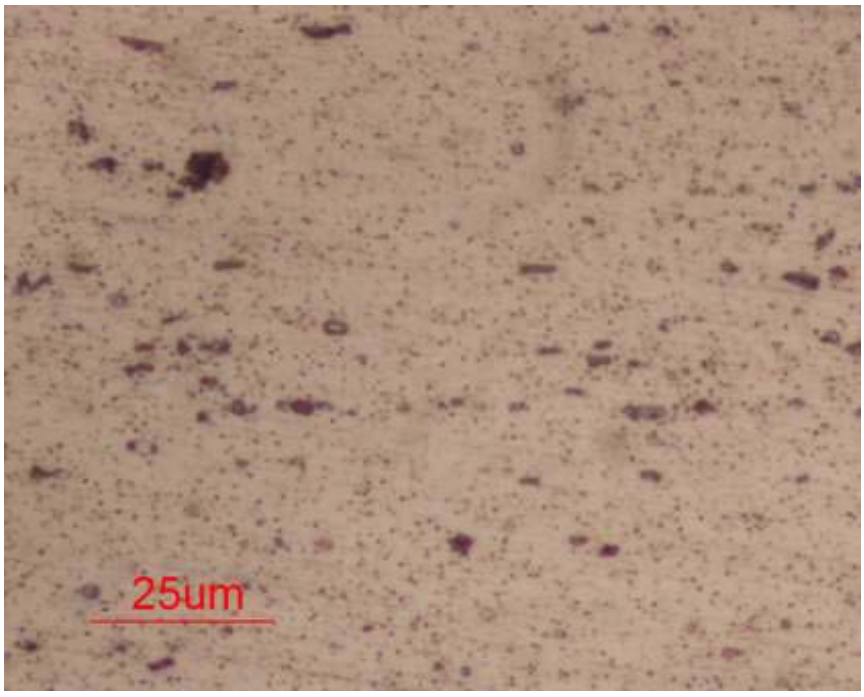

Fig. 4-16 Baseline microstructure of 6061-T6 originally imaged at 1000X.

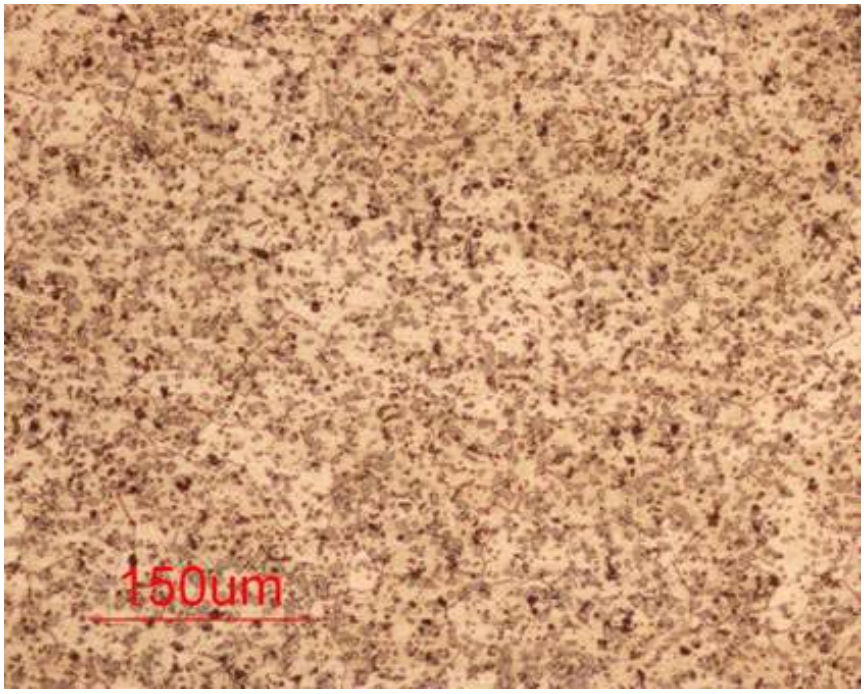

Fig. 4-17 Baseline microstructure of 4032-0 originally imaged at 200X.

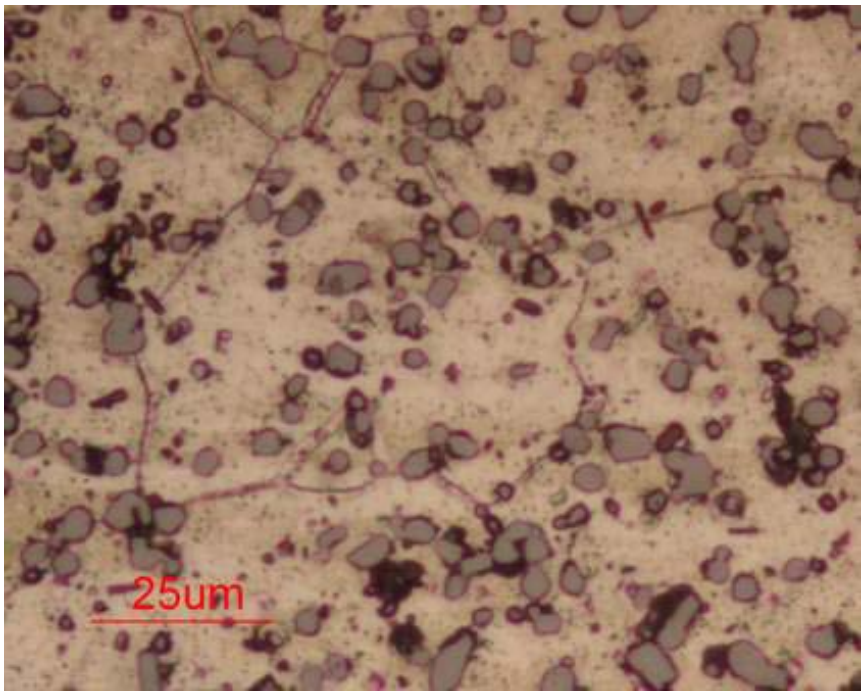

Fig. 4-18 Baseline microstructure of 4032-0 originally imaged at 1000X.

The 6061-T6 microstructure contains a dispersion of Fe_3SiAl_{12} and Mg_2Si particles as expected [33]. The 4032-0 microstructure contained a dispersion of Nickel and Silicon particles [34].

The machined surface was also characterized both before and after the heat treating experiments for any signs of a microstructure change. The pre- and post- heat treating images are presented side by side for comparison. These images can be seen in **Fig. 4-19** through **Fig. 4-34** below.

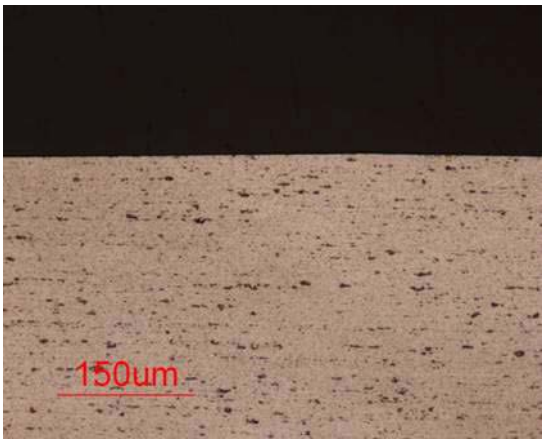

Fig. 4-19 6061-T6 flycut surface prior to heat treatments, originally imaged at 200X.

Fig. 4-20 6061-T6 flycut surface after 1100 hrs at 125C, originally imaged at 200X.

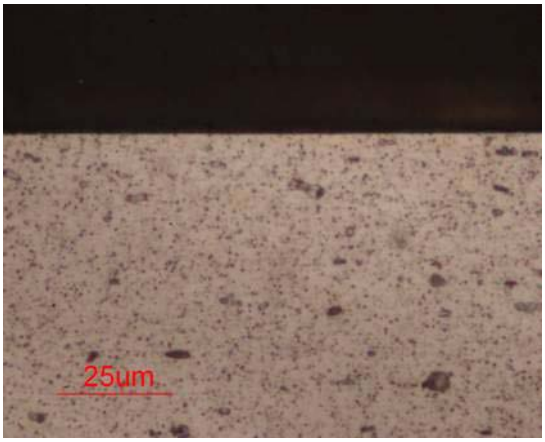

Fig. 4-21 6061-T6 flycut surface prior to heat treatments, originally imaged at 1000X.

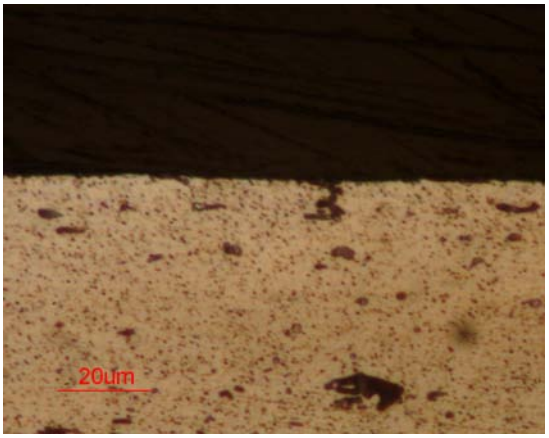

Fig. 4-22 6061-T6 flycut surface after 1100 hours at 125C, originally imaged at 1000X.

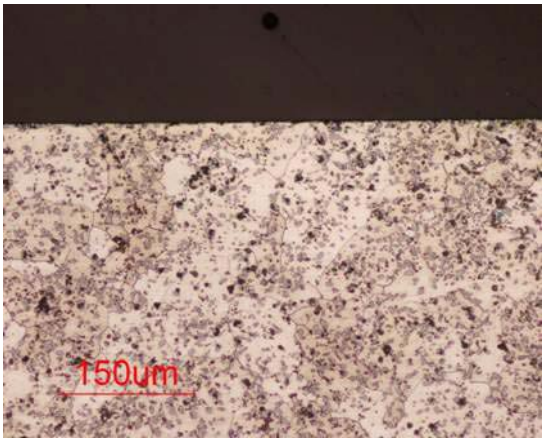

Fig. 4-23 4032-0 flycut surface prior to heat treatments, originally imaged at 200X.

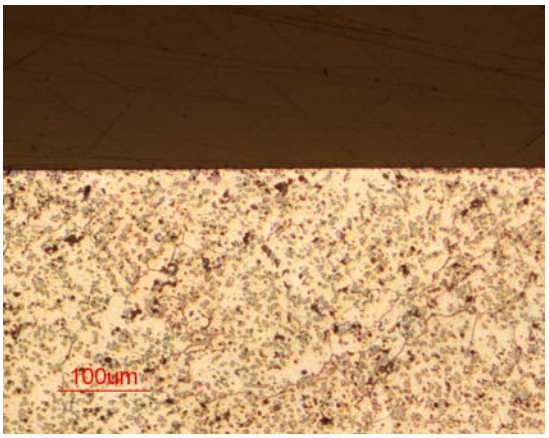

Fig. 4-24 4032-0 flycut surface after 200 hrs at 85C, originally imaged at 200X.

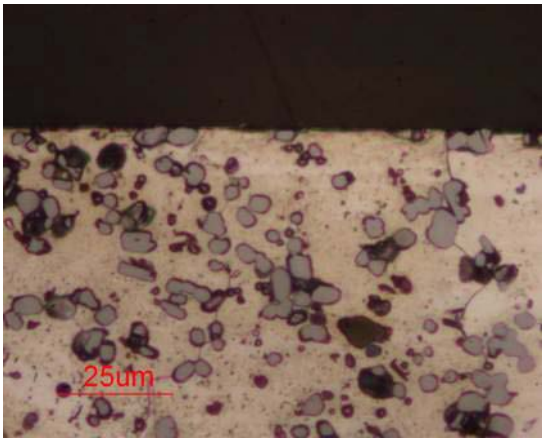

Fig. 4-25 4032-0 flycut surface prior to heat treatments, originally imaged at 1000X.

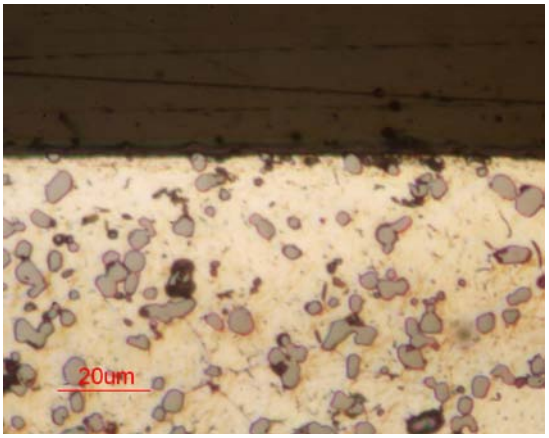

Fig. 4-26 4032-0 flycut surface after 1100 hrs at 85C, originally imaged at 1000X.

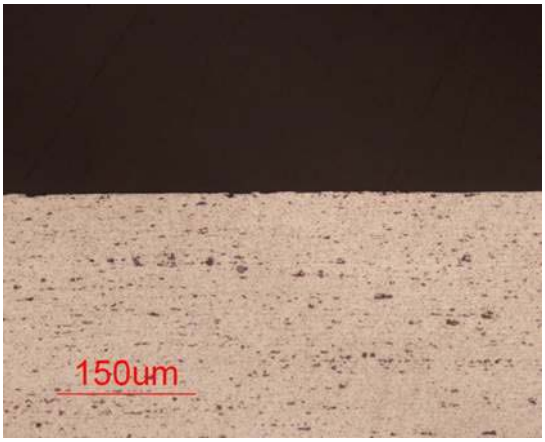

Fig. 4-27 6061-T6 milled surface prior to heat treatments, originally imaged at 200X.

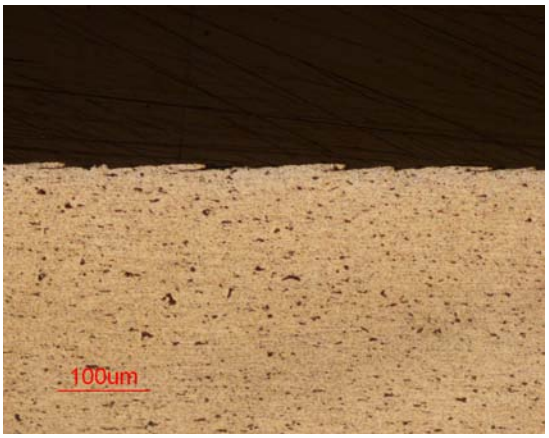

Fig. 4-28 6061-T6 milled surface after 1100 hrs at 125C, originally imaged at 200X.

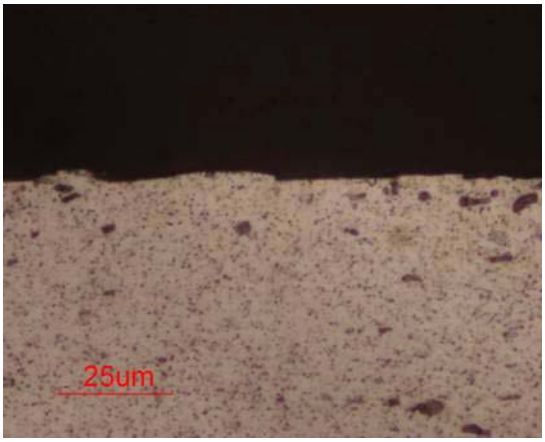

Fig. 4-29 6061-T6 milled surface prior to heat treatments, originally imaged at 1000X.

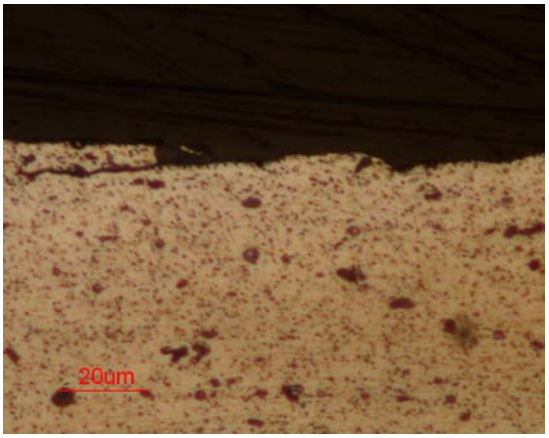

Fig. 4-30 6061-T6 milled surface after 1100 hrs at 125C, originally imaged at 1000X.

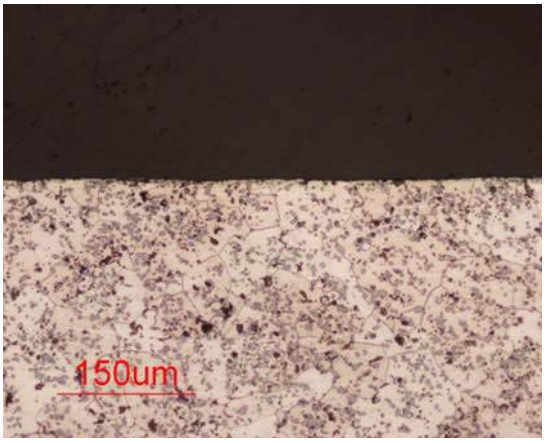

Fig. 4-31 4032-0 milled surface prior to heat treatments, originally imaged at 200X.

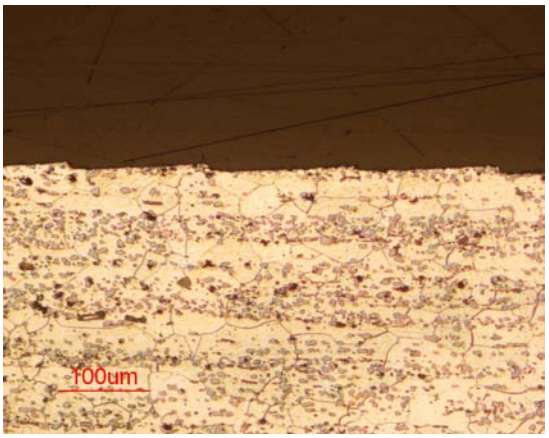

Fig. 4-32 4032-0 milled surface after 1100 hrs at 85C, originally imaged at 200X.

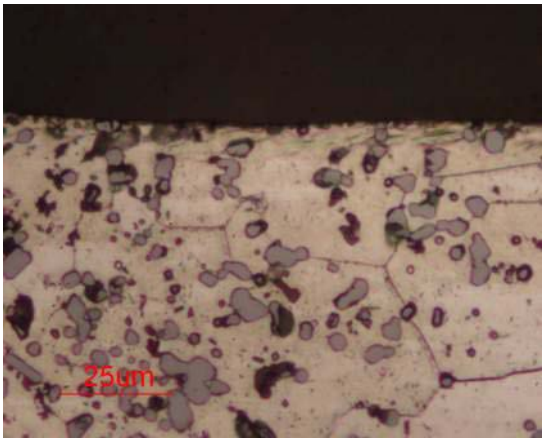

Fig. 4-33 4032-0 milled surface prior to heat treatments, originally imaged at 1000X.

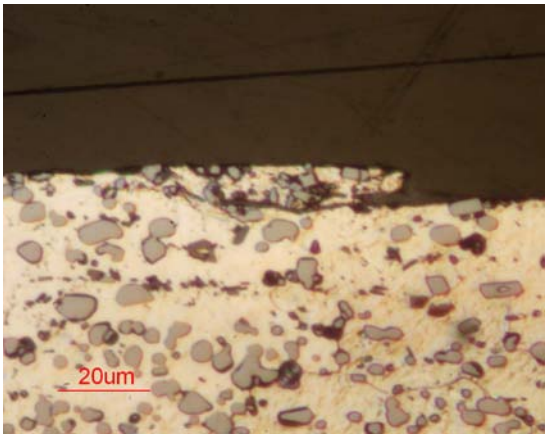

Fig. 4-34 4032-0 milled surface after 1100 hrs at 85C, originally imaged at 1000X.

There were no obvious microstructural changes as a result of the isothermal heat treatments.

4.5 Characterization of Residual Stresses

Residual stress was measured using X-Ray Diffraction. In both the surface only measurements and the depth corrected measurements a previously determined value of the X-Ray Diffraction constant (K_e) was utilized, rather than developing a new value from the samples under study. It is acknowledged that this introduces some error in the

measurement. Ideally a four-point bending fixture would be utilized to produce a known amount of stress onto a sample of the alloy under study. The x-ray constants for a particular peak are determined by measuring the shift of that peak that results from the application of the known applied stress. In the case of the depth corrected stress measurements, which had to be performed at a commercial laboratory, this added significant cost that was considered out of scope of the project.

4.5.1 Surface Only Measurements

Surface only stress measurements were made courtesy of PANalytical in Westborough, MA, using their X'Pert Pro XRD System X'Celerator model. A copper tube was used and the <422> K-α_1 peak was analyzed for all alloys.

An overall scan from ϕ=20-160° was performed in order to verify the location of the <422> aluminum K-α_1 peak. Based on these results, a 2-θ range of 132.6-142.4° was selected in order to capture the <422> peak.

A series of d-spacing measurements were made at Ψ = –58.03, -47.28, -36.86, -25.10, 0, 25.10, 36.86, 47.28, and 58.03°. As step size of 2-θ= 0.1° and sampling time of 2 seconds was used. The peak position was determined by first :

- Correcting for Lorentz polarization
- Correcting for adsorption effect
- Subtracting a linearly sloping background intensity
- Stripping out the K-α_2 peak

Followed by:

- Fitting to an Intermediate Lorentzian peak profile using least squares regression technique. (Some data points did require using other profiles, such as Gaussian, in order to achieve good data alignment).

These values were then used in a psi-squared analysis to determine the magnitude of residual stress on the sample surface.

Two samples of each alloy, and for each machining technique, for a total of 12 samples, were measured on the machined surface for residual stress. The data for each sample has been included in Appendix E. A summary of the results is presented in **Table 4-1** below. Included in the summary is the calculated equivalent thickness associated with the measured surface stress. These calculations were made using the procedure described in 5.1.

The data, in general, revealed much lower than expected stress magnitudes, and therefore thicker than expected equivalent thickness layers when compared to the findings of Frommer and LLoyd.

Table 4-1 Summary of surface residual stress measurements.

Sample	Machining Method	Stress (psi)	Equivalent Layer Thickness (in)
6061-04B	Flycut	-1640 ± 390	0.00775
6061-05B	Milled	-5440 ± 570	0.00275
6061-06B	Flycut	-9530 ± 730	0.00255
6061-07B	Milled	-6060 ± 530	0.00286
4032-04B	Flycut	-7600 ± 1130	0.00426
4032-05B	Milled	-10990 ± 790	0.00201
4032-06B	Flycut	-5930 ± 990	0.00526
4032-07B	Milled	-11250 ± 370	0.00234

1. Negative = Compression
2. Equivalent thickness is from bimetallic strip model

4.5.2 Depth Corrected Measurements

Depth corrected residual stress measurements, or residual stress distributions, were performed in accordance with SAE HS-784. Testing was performed by Lambda Research, Inc, a subsidiary of Lambda Technologies Group. This method uses a series of XRD measurements at increasing depths within the parent material, to characterize the distribution of residual stress as a function of depth. This is required because there is significant relaxation of the material very close to the surface. This effect can be enough to significantly influence the measurements using surface only techniques.

The process is as follows:

A two-angle sine squared psi technique was used.

A chromium K-alpha 1 source was used to analyze the (311) diffraction plane of the FCC structure of the aluminum.

A Pearson VII diffraction peak shape was assumed and used to separate the K-alpha 1 peak from the K alpha doublet.

The peak position was determined by first:

- Correcting for Lorentz polarization
- Correcting for adsorption effect
- Subtracting a linearly sloping background intensity

Followed by:

- Fitting the Pearson VII peak using least squares regression technique.

Samples were rocked around a ±3° around the mean psi angle in order to include additional grains in the measurement, which in effect minimizes the effect of grain size on the measurement.

The diffractometer was fixtured as follows:

- Incident beam divergence was set to 1°
- Detector scintillation was set to accept 90% of the chromium K-alpha energy
- Psi rotation was set to 10.00° and 50.00°
- The irradiated area was .020" by.020"

The X-Ray elastic constant $E/(1+\nu)$ for the (311) plane of 7050-T6 was used for these measurements. This value had been determined empirically using a four point bending fixture to load a7050 specimen to known stress levels, and the resulting change in (311) spacing [35].

The error in measurement was from two sources:

- The random error in determining the diffraction peak positions
- The random error in the determination of the XRD constant $E/(1+\nu)$

A semi-systematic error was also determined by using a powder metal, zero-stress sample monitored in accordance with ASTM E915. This error was determined to be -1.8 ksi.

Two samples of each alloy and each machining technique were submitted for analysis. The stress profiles and the peak width distribution for 6061-T6, and 4032-0 can be seen in **Fig. 4-35** and **Fig. 4-36**, and **Fig. 4-37** and **Fig. 4-38**, respectively.

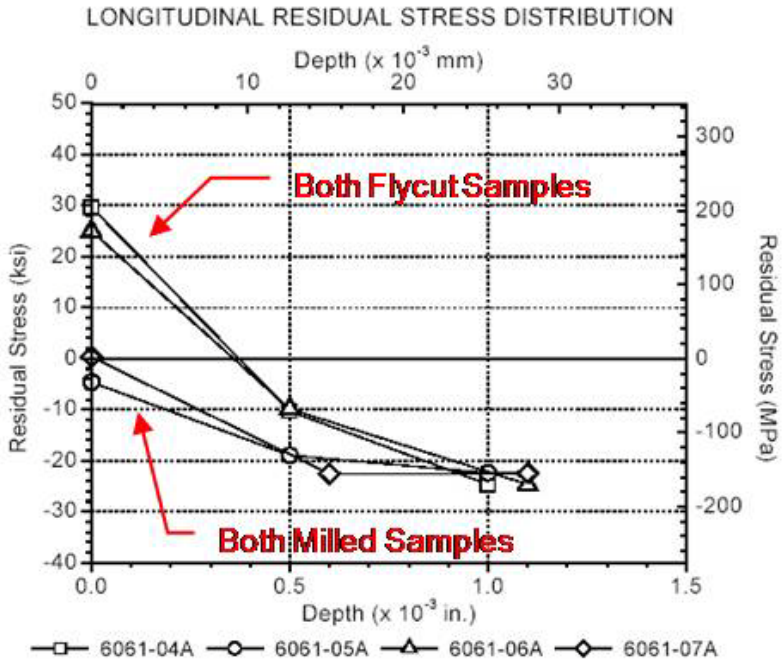

Fig. 4-35 Stress profiles for flycut and milled 6061-T6 samples.

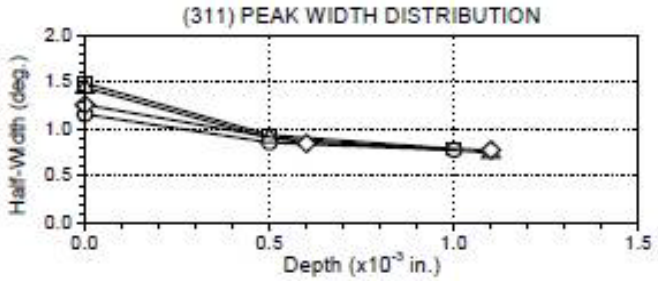

Fig. 4-36 Peak width distribution profile for flycut and milled 6061-T6 samples.

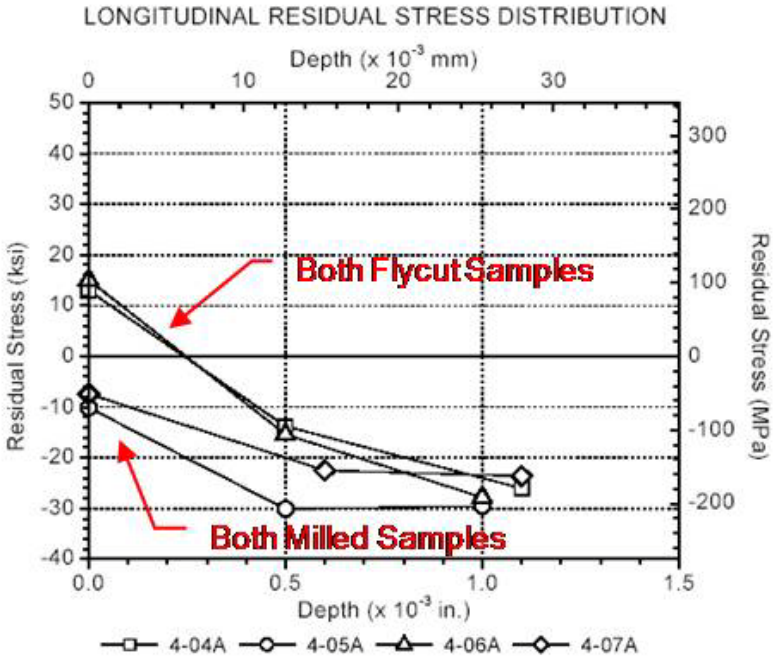

Fig. 4-37 Stress profile for flycut and milled 4032-0 samples.

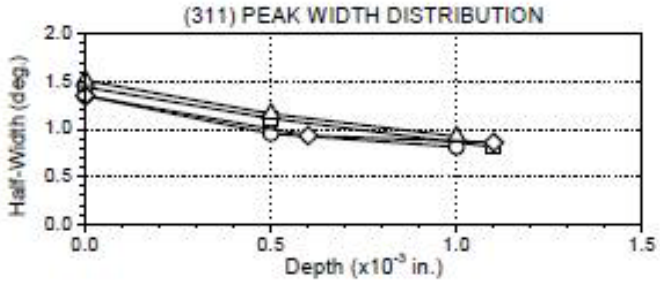

Fig. 4-38 Peak width distribution profiles for flycut and milled 4032-0 samples.

A summary of the can be seen in **Table 4-2** through **Table 4-3** below. The corrected value of stress found just below the material surface is highlighted.

Table 4-2 XRD residual stress distribution data for 6061-T6 samples.

Sample	Depth	Measured (ksi)	Gradient (ksi)	Relaxation (ksi)	B 1/2
6061-04A (Flycut)	0.0000”	3.7 ± 0.4	29.7	29.7	1.49
	0.0005”	-20.3 ± 0.4	-9.9	-10.3	0.94
	0.0010”	-19.8 ± 0.4	-25.3	**-24.7**	0.79
6061-05A (Milled)	0.0000”	-13.8 ± 0.4	-4.6	-4.6	1.16
	0.0005”	-21.8 ± 0.4	-19.7	-19.0	0.86
	0.0010”	-19.0 ± 0.4	-24.2	**-22.4**	0.78
6061-06A (Flycut)	0.0000”	3.0 ± 0.4	25.0	25.0	1.44
	0.0005”	-19.4 ± 0.4	-9.6	-9.9	0.91
	0.0010”	-20.8 ± 0.4	-25.6	**-24.7**	0.75
6061-07A (Milled)	0.0000”	-13.5 ± 0.4	0.3	0.3	1.26
	0.0005”	-20.4 ± 0.4	-23.5	-22.6	0.85
	0.0010”	-7.4 ± 0.3	-24.6	**-22.5**	0.78

It is observed in the XRD stress data that there is a considerable difference in the peak width (B 1/2) term between the flycut and the milled surfaces. Line broadening can be caused by three influences, small crystallite size, non-uniform strain, and stacking faults [36]. Both non-uniform strain and stacking faults are indicators of cold work. Since there should be no difference in the crystallite size of the base allow as a result of a machining operation, it is reasonable to conclude that the peak broadening is due to cold working effects.

Table 4-3 XRD residual stress distribution data for 4032-0 samples.

Sample	Depth	Measured (ksi)	Gradient (ksi)	Relaxation (ksi)	B 1/2
4-04A (Flycut)	0.0000”	-4.2 ± 0.5	13.0	13.0	1.44
	0.0005”	-22.7 ± 0.5	-13.8	-13.8	0.11
	0.0010”	-26.3 ± 0.4	-27.4	**-26.0**	0.81
4-05A (Milled)	0.0000”	-21.7 ± 0.5	-10.1	-10.1	1.35
	0.0005”	-28.5 ± 0.5	-31.2	-30.1	0.95
	0.0010”	-15.2 ± 0.3	-32.2	**-29.5**	0.81
4-06A (Flycut)	0.0000”	-5.0 ± 0.4	15.1	15.1	1.51
	0.0005”	-25.3 ± 0.5	-15.5	-15.4	1.16
	0.0010”	-28.6 ± 0.5	-29.1	**-27.8**	0.92
4-07A (Milled)	0.0000”	-15.5 ± 0.5	-7.4	-7.4	1.35
	0.0005”	-23.6 ± 0.4	-23.5	-22.5	0.93
	0.0010”	-19.3 ± 0.4	-25.9	**-23.6**	0.86

4.5.3 Comparison of Techniques

It is apparent from the XRD stress measurements that the surface only technique was not adequate for capturing the magnitude of the stress created by machining passes. Magnitudes of stress measured using surface only technique were a fraction of those captured using depth corrected measurements. This is unfortunate as it means that destructive methods are required to determine the stress state, and there is not possible to be performed on a part destined for use in service.

4.6 Measurement of Curvature

Curvature has been monitored using a Mitutoyo Quickvision ELF Pro Inspection System. This system utilizes a Z-Axis camera and an X-Y table to perform 3-D inspection on

incoming product. This system is controlled by BAE Systems Calibration program, and is assigned CAL ID ACU01 tracking number for this purpose. Actually calibration procedures are performed by the manufacturer on site at BAE Systems. This system is pictured below in **Fig. 4-39**.

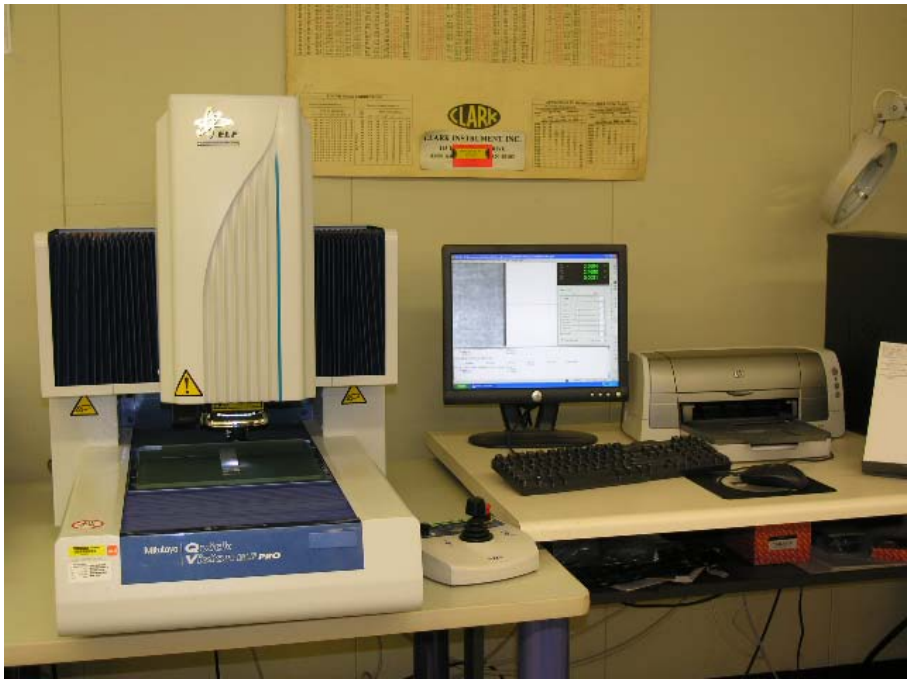

Fig. 4-39 The Mitutoyo Quickvision ELF Pro Inspection System. A coupon can be seen on the X-Y Stage.

A program was written for the inspection of these samples for curvature. This program assessed curvature in the following manner:

1. The part placed on the X-Y table.
2. Aligned was performed within the program by manually picking points at the two corners along the right edge of the coupon (the X-axis).
3. The program then performed a series of 26 height measurements (Z-axis) along each edge of the coupon. These locations were approximate 0.100” in from the edge of the coupon.
4. These points are then used to calculate the radius of a best fit circle using a least sum of squares calculation.
5. The radius of each edge is reported in a printout.
6. These printouts were manually entered in spreadsheets for further calculation and analysis.
7. Approximately 3.5 minutes is required to measure each coupon.

The raw curvature data is provided Appendix G.

4.6.1 Accuracy of Curvature Measurements

Measurement accuracy values are published by Mitutoyo and are functions of the length of the feature being measured. These specifications can be seen below in **Fig. 4-40**

SPECIFICATIONS

Model No. and Type		QVELF202	
		PT machine	PRO machine
Range	X-axis	200mm (8")	
	Y-axis	250mm (10")	
	Z-axis	100mm (4")	
Resolution		0.1µm	
High-sensitivity CCD camera		B&W	
Accuracy* (20°C±0.2°C)	E_{1XY}	(2.0+3L/1000)µm	
	E_{1Z}	(4.0+5L/1000)µm	
Max. drive speed (X/Y/Z-axis)		100mm/s	
Illumination (PRL: Programmable Ring Light)	Surface	Halogen	Halogen
	Contour	Halogen	Halogen
	Ring light	Halogen	LED, White
Magnification change system**		Turret	Turret
Stage glass size		10.59 x 12.24" / 269 x 311mm	
Max workpiece load		10kg / 22 lbs	
Optional accessory		laser auto-focus (factory installed option)	

* The measuring accuracy is defined at the following conditions
Programmable power turret: 1X Objective set: 5X L = Dimension between two arbitrary points (mm)
**Fixed: Optical system with fixed magnification, Turret: Programmable Power Turret

Fig. 4-40 Published measurement accuracy values s for Quickvision ELF Pro System.

The error described by these specifications was used to calculate the error in measuring curvature for two cases; the smallest sample radius of 30 inches, and the largest of 150 inches. The detailed calculations were performed using MathCAD and the complete study can be seen in Appendix H.

Measurement error of Radius due to the machine is:

+/- 0.005" at 150 inch radius

+/- 0.0007" at 30 inch radius

This error is very small compared to the changes in radius that were observed, which was on the order of 0.5 to 10 inches.

4.7 Modulus Determination

Modulus of Elasticity at temperature was determined using an Instron 5500R tensile tester S/N 6089C fitted with a 50,000 lb cell Cat# 2511-307 S/N 072. A 1" MTS extensometer Model # 633.11B-15 S/N 173 was utilized. Testing was performed at room temperature, 60C, 85C and 125C and 175C for 6061 and room temperature, 40C, 60C, and 85C for 4032. The data was fitted with a line to average out test error. A summary of Modulus vs. Temperature with the fitted values is seen in **Table 4-4**. The fitted data is seen in **Fig. 4-41**.

Table 4-4 Summary of Modulus of Elasticity at Temperature.

Temp (C)	**6061-T6**	**4032-0**
	E (kPa)	E (kPa)
25	68815	80447
40	68323	79873
50	67970	79460
60	67597	79024
85	66577	77832
125	64684	75618
175	61865	72323

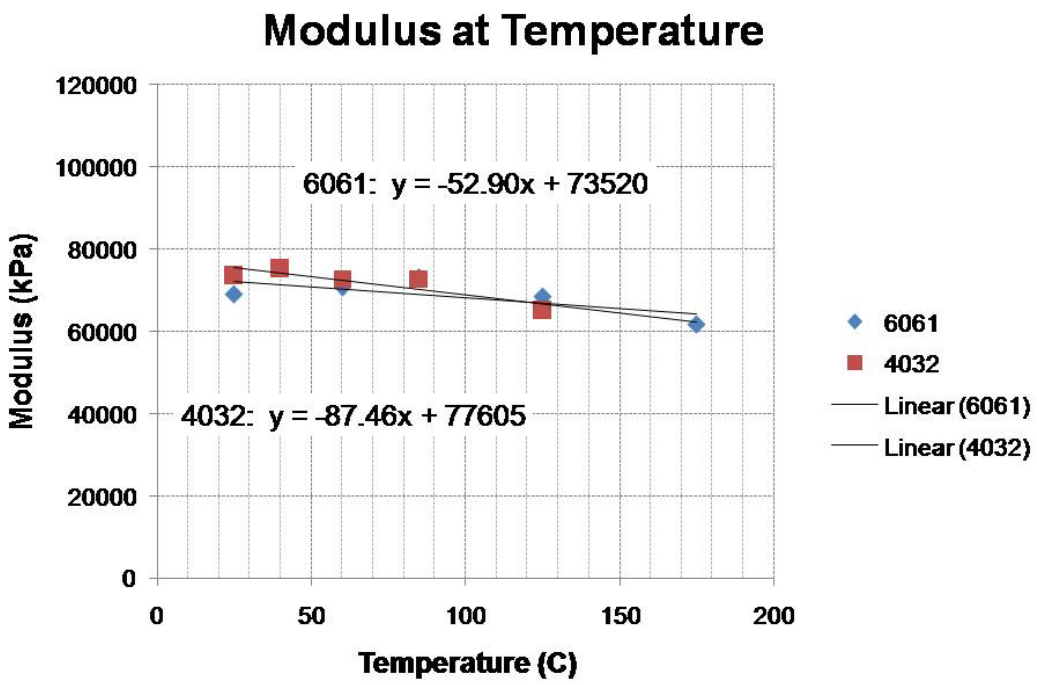

Fig. 4-41 Data fitting of Modulus vs. Temperature testing for each alloy.

4.8 Chemical Composition

Chemical composition of the alloys was verified using a SpectroMax Spectro spark emission spectroscopy system. Software was Spark Analyzer SE 4.00C. A summary of the results is seen in **Table 4-5** below.

Table 4-5 Summary of chemical composition.

wt%	6061-T6	4032-0
Si	0.70	11.16
Mg	0.99	1.28
Cu	0.38	0.83
Mn	0.38	0.013
Ni	0.01	0.72
Fe	0.43	0.232
Zn	0.106	-
Cr	0.198	-
Ti	-	0.04
Al	Re	Re

5 Data Analysis

5.1 Assessing the Depth of the Stressed Layer

Using a bimetallic strip model allows the curvature of a sample to be calculated knowing the thickness and stress state of a surface layer of material along with the thickness of the unstressed layer.

For each alloy and each machining type, two coupons were used to assess the depth and magnitude of the stressed layer. The initial curvature as a result of the controlled machining pass was measured using the procedure described in Paragraph 4.6. The coupons were then sent for depth corrected XRD measurements. Knowing the curvature of the coupon and the magnitude of the stress allowed the depth of the stressed layer to be calculated using **Eq. 3-14**. In the bimetallic strip model, the stress that was measured on the sample surface is referred to as the ***Resultant Stress***. This is the stress after initial curvature has taken place. The stress that is present while the coupon is restrained flat on the machining fixture is a slightly higher magnitude, and is referred to as the ***Pre-Curvature Stress***.

MathCAD was used for the calculations and an example can be seen in Appendix I. A summary of these calculations is seen below in **Table 5-1**.

Table 5-1 Stressed Layer Magnitudes and Equivalent Thicknesses.

Coupon	Machining Method	Thickness (in)	Radius (in)	Resultant Stress (psi)	Equivalent Thickness (in)	Pre-Curvature Stress (psi)
6061-04	Fly-Cut	0.0350	70.838	-24700		
6061-05	Milled	0.0355	107.937	-22400		
6061-06	Fly-Cut	0.0355	67.840	-24700		
6061-07	Milled	0.0355	91.885	-22500		
6061 Avg.	Fly-Cut	0.03525	69.339	-24700	0.001143	-28279
6061 Avg.	Milled	0.0355	99.911	-22450	0.000906	-24947
4-04	Fly-Cut	0.0355	47.543	-26000		
4-05	Milled	0.036	93.799	-29500		
4-06	Fly-Cut	0.0355	42.856	-27800		
4-07	Milled	0.033	64.267	-23600		
4032 Avg.	Fly-Cut	0.0355	45.199	-26900	0.001629	-32696
4032 Avg.	Milled	0.0345	79.033	-26550	0.001029	-29896

5.2 Experimental Error Calculation Due to Stress Uncertainty

The stress values measured using the layer removal method have an associated error that is quantified in accordance with the methodology described in Section 2.4. Using this known uncertainty, the range of stressed layer equivalent thickness can be calculated. Note that the uncertainty is associated with the direct stress measurement, and is proportionally adjusted to apply to the stress measurement that has been corrected for the removed material.

The measurement of the coupon thickness also carried with it a known uncertainty. The Vernier calipers only reported measurements in increments of 0.0005”, so the experimental error associated with thickness is defined as +/- 0.00025”.

For each alloy/machining type, 4 cases were considered for determining the stressed layer equivalent thickness. These were:

1. smallest stress, smallest thickness,
2. smallest stress, largest thickness,
3. largest stress, smallest thickness,
4. largest stress, largest thickness.

The calculation detail for one of the coupons can be seen in Appendix J. The range of possible values of the stressed layer equivalent thickness is summarized in **Table 5-2** below.

Using these calculated ranges for the stressed layer equivalent thickness and the calculated uncertainty in the measurement of radius (see Section 4.6.1), the uncertainty of the strain can be calculated. Because differences in strain are being measured from a single starting point (the initial radius), and therefore measurement errors are not accumulating, the strain observations are extremely accurate. These are summarized below in **Table 5-2**.

Table 5-2 Summary of experimental error in strain measurement.

Coupon	Stress (psi)	Stress Error (psi)	Equivalent Thickness (in)	Equivalent Thickness Error (in)	Total Strain Error (in/in)
6061 Flycut	-24700	+/- 500	.00126	+/- .00007	$6.8 \cdot 10^{-10}$
6061 Milled	-22450	+/- 692	.00087	+/- .000037	$3.5 \cdot 10^{-10}$
4032 Flycut	-26900	+/- 343	.00170	+/- .00004	$1.8 \cdot 10^{-9}$
4032 Milled	-26550	+/- 536	.00109	+/- .00002	$5.4 \cdot 10^{-10}$

The Stress and Stress Error values reported are the averages of two coupons for each alloy/machining combination. For purposes of this summary table, the Stress Error reported is the average of the two uncertainties, not the sum. The values reported in the Equivalent Thickness error column are based on the full range of possible stress values

(e.g. both stress values used in the average are at the minimum, or both are at the maximum).

5.3 Variation in Measurements

The actual variation in measurements was assessed by examining the measured radius of the six control samples. These were periodically measured throughout the isothermal stress relief treatments. The average deviations taken from the 4 data sets is larger than the machine error previously calculated and is therefore taken as the error associated with bulk material movement The resulting strain error is calculated using **Eq. 3-23** and assuming atypical stressed layer thickness of .0015" and a typical overall coupon thickness of .0365". This has been summarized in **Table 5-3**

Table 5-3 Summary of experimental error based on control samples.

		Avg Radius	Average Deviation	Resulting Strain Error
6061-T6	Control	142.9190"	0.0946"	.00000073
	Offset Control	144.3964"	0.1636"	.0000012
4032-0	Control	146.8108"	0.1413"	.0000010
	Offset Control	147.6228"	0.1474"	.0000010

The largest strain error associated with the control samples is $1.2 \cdot 10^{-6}$. The final strains measured in this research ranged from $1.7 \cdot 10^{-5}$ to $2.2 \cdot 10^{-4}$ indicating that the 7% to 0.5%. This level of error is quite acceptable especially when considering that the data is being used to track changes in strain rather than absolute values of strain.

5.4 Determination of Constants

It was hoped that the $\Delta\sigma^{1-m}$ term from **Eq. 3-6** could be assumed to be small and ignored, allowing for the constant Q, k, and m to be solved graphically. Manually curve fitting indicated that the value of k would be extremely small, and therefore $\Delta\sigma^{1-m}$ would be significant. This made solving graphically for the constants not possible.

Constant were found using the least sum of squares method. This was accomplished with the aid of Prism 5 Graphpad software package. This software had the unique capability of being able to share parameters across individual data sets. The feature was required because the m, and Q were unknowns, but needed to be the same value across each data sets.

Finding the constants required the raw radius vs. time data to be converted into strain. The radius data was converted to strain by using the following form of the simplified bimetallic strip model developed in Section 3.2.

$$\varepsilon_{r_1 \to r_2} = \frac{t_B}{6t_A}\left(3t_A + t_B\right)\left(\frac{1}{r_2} - \frac{1}{r_1}\right) \qquad \textbf{Eq. 3-21}$$

Curves were fit holding m and Q constant for both machining operations for each alloy, but k was only held constant within each machining type. This was required to compensate for the observed differential between the flycut final strains and the milled final strains. **Table 5-4** summarizes the results from the curve fitting.

Note that we are considering compressive stresses and compressive creep. These are numerically negative values. Due to the stress exponent in the creep equations, negative stress values are arithmetically inconvenient. For this reason, absolute values of stress and strain are being considered for curve fitting only. To have avoided using absolute values, only the tensile components (having a positive numerical value) of the stress and strain would need to be considered. This would require calculating the tensile component of the out of plane stress and strains (neither of which can be directly determined), determining creep parameters, and converting back to the in-plane components. This would have added no numerical value to the model and would have introduced the errors associated with calculating the out of plane stress component.

Table 5-4 Summary of material parameters determined by curve fitting.

Alloy	Q (kJ/mol)	m	Machining Method	k
6061-T6	28.9	3.583	Flycut	7.994E-22
			Milled	2.717E-21
4032-0	84.38	2.423	Flycut	1.080E-06
			Milled	2.880E-06

Graphs that were used to determine the constants, showing the actual data points vs. the predicted are shown in **Fig. 5-1** through **Fig. 5-4**. Recall that for curve fitting purposes, absolute values of stress and strain are displayed.

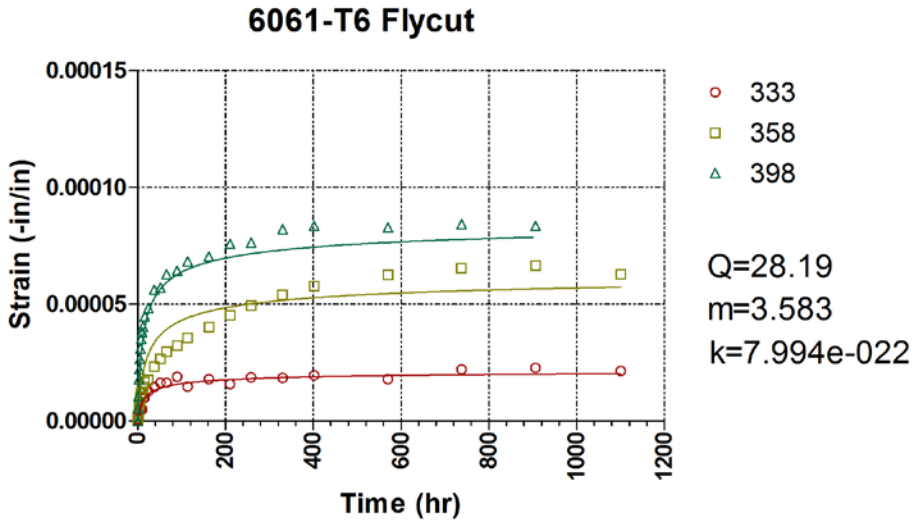

Fig. 5-1 Predicted vs. Actual creep strain for 6061-T6 flycut Coupons.

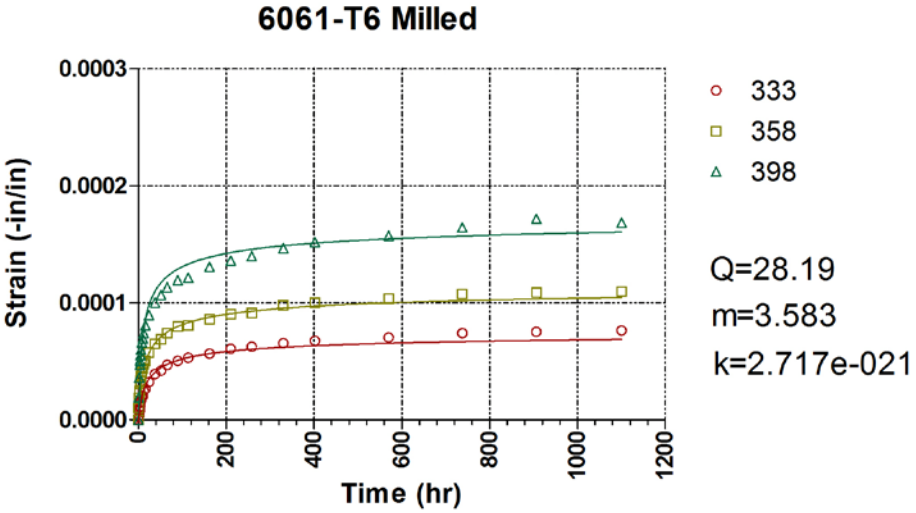

Fig. 5-2 Predicted vs. Actual creep strain for 6061-T6 milled coupons.

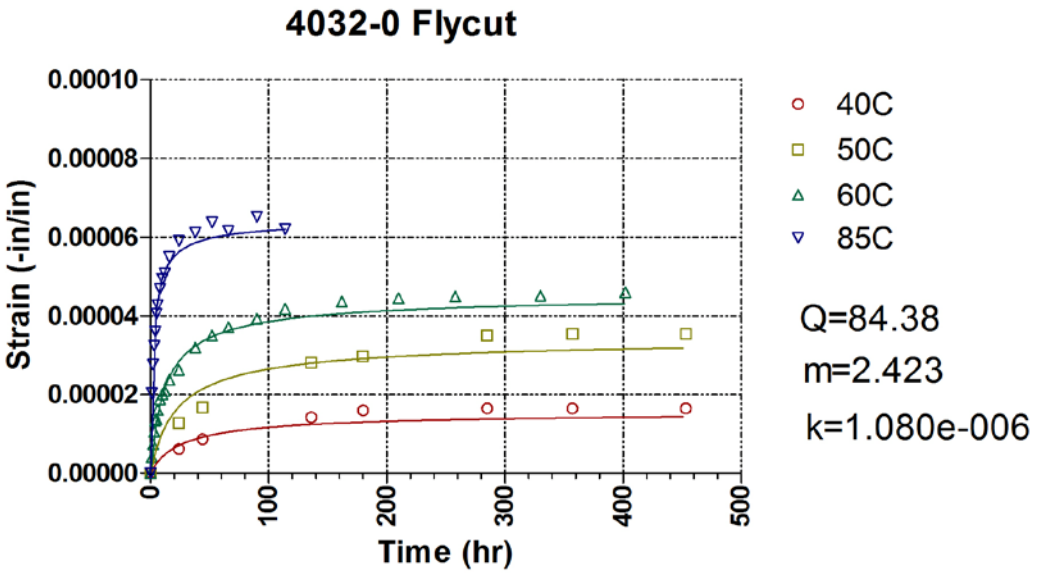

Fig. 5-3 Predicted vs. Actual creep strain for 4032-0 Flycut coupons.

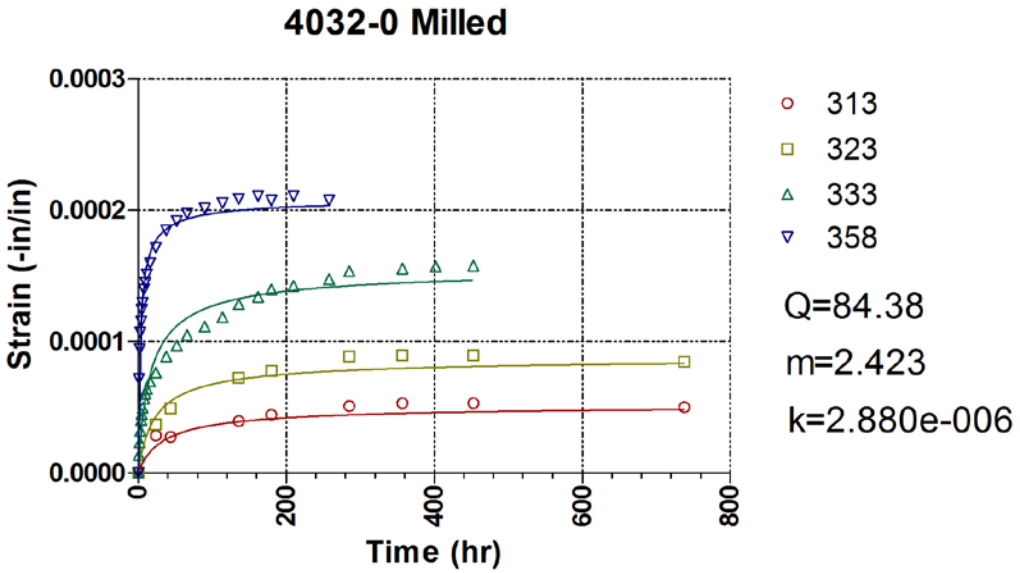

Fig. 5-4 Predicted vs. Actual creep strain of 4032-0 milled coupons.

5.5 Final Strain Temperature Dependence

Final strains were plotted to determine the constants B and n from **Eq. 3-7**. Graphs can be seen in **Fig. 5-5** and **Fig. 5-6** below. Very good linear fits were obtained, particularly when the results were considered in the context of the machining method. The difference in cold working of the flycut samples vs. the milled samples is likely responsible for the difference in the magnitude of the final strains. The results are summarized in **Table 5-5**.

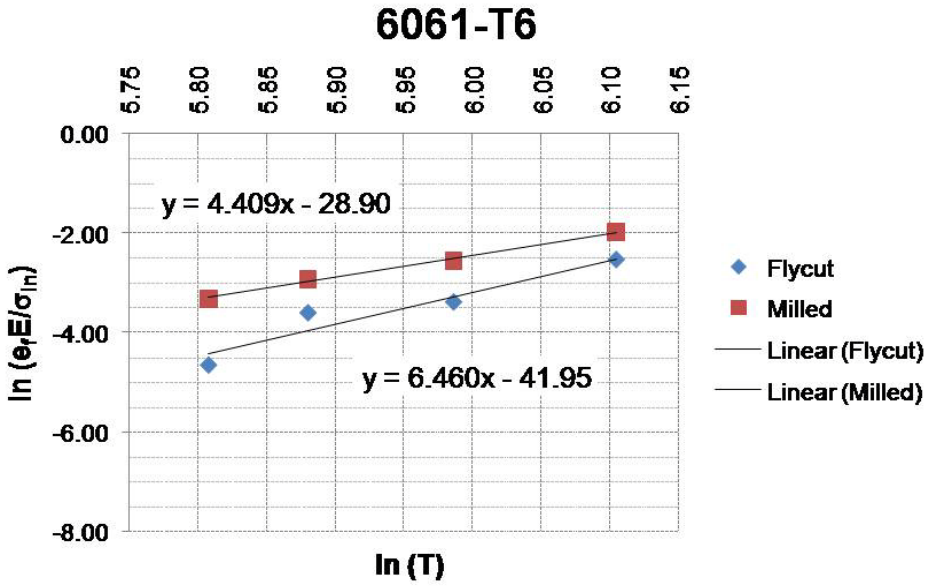

Fig. 5-5 Determination of B and n for 6061-T6.

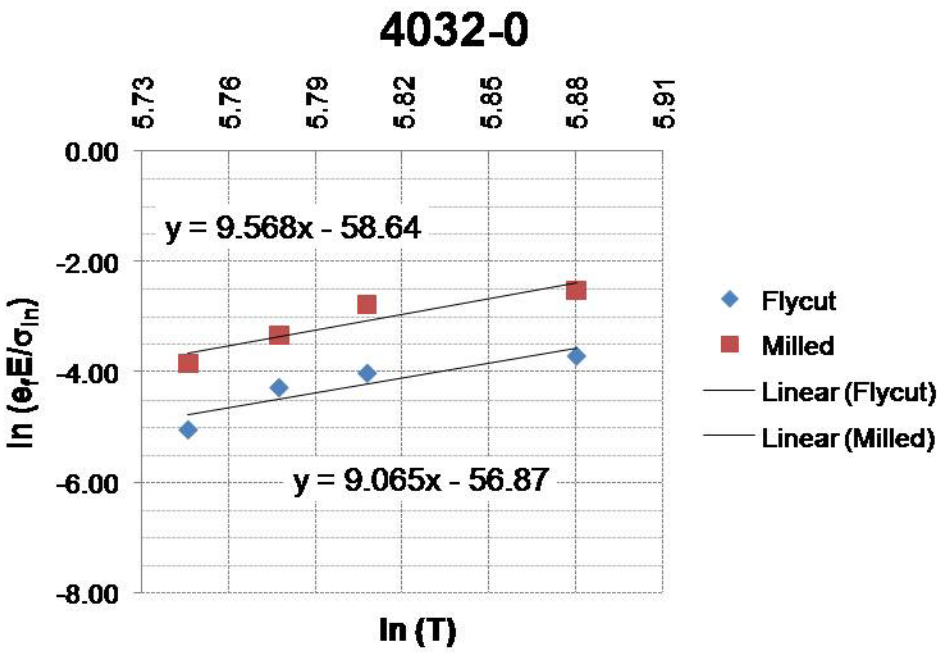

Fig. 5-6 Determination of B and n for 4032-0.

Table 5-5 Summary of B and n values.

	n	ln(B)	B
6061-T6 Flycut	6.460	-41.95	6.044E-19
6061-T6 Milled	4.409	-28.90	2.811E-13
4032-0 Flycut	9.065	-56.87	2.003E-25
4032-0 Milled	9.568	-58.64	3.412E-26

It is noted here that the 6061 plots include a data point collected at 175C. The curvature vs. time data collected on these samples did not fit well into the curve fitting plots, and are therefore not included in the calculation of m, Q and k. The strain rates were too great at the 175C temperature to allow for good fits. This is partly due to the steep nature of the curves (both real and extrapolated) at 175C. The vertical calculation of errors in the least sum of squares results in large errors for curved that are steeper compared to those that are more horizontal.

5.6 Use of Creep Model to Design Stress Relief Schedule

Once the constants have been established, the creep model can be used to develop short term, but higher temperature heat treatment profiles. The stress relief heat treatments would be for the purpose of allowing all surface stresses caused by gross machining passes to creep out under controlled conditions, rather than due to time/temperature exposure in service.

The following procedure can be used for the design of a stress relief heat treatment. First, **Eq. 3-6** is solved for time, t, the result is shown as **Eq. 5-1**. The algebraic details are included in Appendix K.

$$t = \frac{\varepsilon_f T}{(m-1)k\sigma_{in}}\left[\left[\sigma_{in}\left(1-\frac{\varepsilon}{\varepsilon_f}\right)\right]^{1-m} - (\sigma_{in})^{1-m}\right]e^{\frac{Q_c}{RT}} \qquad \textbf{Eq. 5-1}$$

At this point one of two approaches can be used. The first will be to define a fraction of stress that is to be relieved (note that specifying unity as the intended fraction results in an undefined term in the expression). This is specified as $\varepsilon = x\varepsilon_f$, where x=.9 or 90%. **Eq. 5-1** then becomes:

$$t = \frac{\varepsilon_f T}{(m-1)k\sigma_{in}}\left[\left[\sigma_{in}\left(1-\frac{x\varepsilon_f}{\varepsilon_f}\right)\right]^{1-m} - (\sigma_{in})^{1-m}\right]e^{\frac{Q_c}{RT}}$$

or

$$t = \frac{\varepsilon_f T}{(m-1)k\sigma_{in}}\left[[\sigma_{in}(1-x)]^{1-m} - (\sigma_{in})^{1-m}\right]e^{\frac{Q_c}{RT}} \qquad \textbf{Eq. 5-2}$$

Eq. 5-2 can now be used to calculate the time to reach x fraction of ε_f at different temperatures. First substitute **Eq. 3-7** into **Eq. 5-2** which yields:

$$t = \frac{BT^{n+1}}{E(m-1)k}\left[[\sigma_{in}(1-x)]^{1-m} - (\sigma_{in})^{1-m}\right]e^{\frac{Q_c}{RT}}$$

or

$$t = \frac{BT^{n+1}\sigma_{in}^{1-m}}{E(m-1)k}\left[(1-x)^{1-m} - 1\right]e^{\frac{Q_c}{RT}}$$

but since:

$$(1-x)^{1-m} = \frac{1}{(1-x)^{m-1}} >> 1$$

the following simplification is valid:

$$t \cong \frac{BT^{n+1}\sigma_{in}^{1-m}}{E(m-1)k(1-x)^{m-1}}e^{\frac{Q_c}{RT}} \qquad \textbf{Eq. 5-3}$$

It is worth noting at this point that time, t, is a function of both the fraction of stress to be removed, x, and also of final strain, ε_f. Time is far more sensitive to the fraction of stress to be removed due to the exponent m-1 than it is to the value of final strain, which is to the power of unity. This is of practical importance since ε_f is being approximated by **Eq. 3-7**. An example of how this approach to design a stress relief treatment is seen for 4032 Flycut below in **Fig. 5-7**.

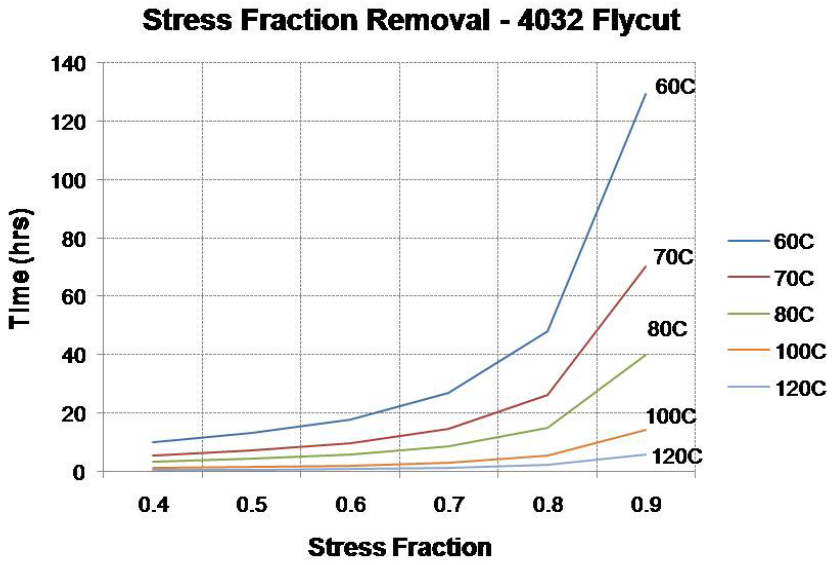

Fig. 5-7 Time required for the removal of a stress fraction from 4032 Flycut samples.

The second approach is to use the service temperature range as a means to specify an appropriate strain to reach during a stress relief treatment. **Eq. 5-1** is again used as the basis for this approach. The ε and ε_f terms are calculated from **Eq. 3-7**, where ε_f is calculated at the stress relief temperature, but ε is the final strain calculated at a lower service temperature,

$$\varepsilon = \varepsilon_{f\,(Service)}$$

$$\varepsilon_f = \varepsilon_{f\,(Stress\ \ relief\ \ temp)}$$

Substituting into **Eq. 5-1**:

$$t = \frac{\varepsilon_{f\,(Stress\ \ relief\ \ temp)} T}{(m-1)k\sigma_{in}} \left[\left[\sigma_{in} \left(1 - \frac{\varepsilon_{f\,(Service)}}{\varepsilon_{f\,(Stress\ \ relief\ \ temp)}} \right) \right]^{1-m} - (\sigma_{in})^{1-m} \right] e^{\frac{Q_c}{RT}}$$

or by substituting **Eq. 3-7** in:

$$t = \frac{BT^{n+1}}{E(m-1)k}\left[\left[\sigma_{in}\left(1-\frac{ET_{Service}^{n}}{E_{service}T^{n}}\right)\right]^{1-m} - (\sigma_{in})^{1-m}\right]e^{\frac{Q_C}{RT}}$$

Eq. 5-4 is established using rationale used in the simplification of **Eq. 5-3**:

$$t = \frac{BT^{n+1}\sigma_{in}^{1-m}}{E(m-1)k}\left[1-\frac{ET_{Service}^{n}}{E_{service}T^{n}}\right]^{1-m} e^{\frac{Q_C}{RT}} \qquad \textbf{Eq. 5-4}$$

Examples of stabilization heat treatment schedules can be seen in **Fig. 5-8**-**Fig. 5-11** below. Values used for determining the stabilizing schedules are seen in **Table 5-6**.

Table 5-6 Summary of values used for determining stabilizing heat treatments.

	6061 Fly	**6061 Mill**	**4032 Fly**	**4032 Mill**	
Q	28.19	28.19	84.38	84.38	kJ/mol
m	3.583	3.583	2.423	2.423	
k	7.99E-22	2.72E-21	2.88E-06	1.08E-06	
R	0.008314	0.008314	0.008314	0.008314	kJ/Mol/k
B	6.04E-19	2.81E-13	2.00E-25	3.41E-26	
n	6.46	4.409	9.065	9.568	
E 25	7.22E+07	7.22E+07	7.41E+07	7.41E+07	kPa
E 40	7.14E+07	7.14E+07	7.41E+07	7.41E+07	kPa
E 45	7.11E+07	7.11E+07	7.37E+07	7.37E+07	kPa
E 50	7.09E+07	7.09E+07	7.32E+07	7.32E+07	kPa
E55	7.06E+07	7.06E+07	7.28E+07	7.28E+07	kPa
E 60	7.03E+07	7.03E+07	7.24E+07	7.24E+07	kPa
E 65	7.01E+07	7.01E+07	7.19E+07	7.19E+07	kPa
E 70	69817000	69817000	71482800	71482800	kPa
E 80	6.93E+07	6.93E+07	7.06E+07	7.06E+07	kPa
E 85	6.90E+07	6.90E+07	7.02E+07	7.02E+07	kPa
E 90	6.88E+07	6.88E+07	6.97E+07	6.97E+07	kPa
E 100	6.82E+07	6.82E+07	6.89E+07	6.89E+07	kPa
E 110	6.77E+07	6.77E+07	6.80E+07	6.80E+07	kPa
E 120	6.72E+07	6.72E+07	6.71E+07	6.71E+07	kPa
E 125	6.69E+07	6.69E+07	6.67E+07	6.67E+07	kPa
E130	6.66E+07	6.66E+07	6.62E+07	6.62E+07	kPa
E140	6.61E+07	6.61E+07	6.54E+07	6.54E+07	kPa
E150	6.56E+07	6.56E+07	6.45E+07	6.45E+07	kPa
σ_{in}	170301	154787	185469	183056	kPa

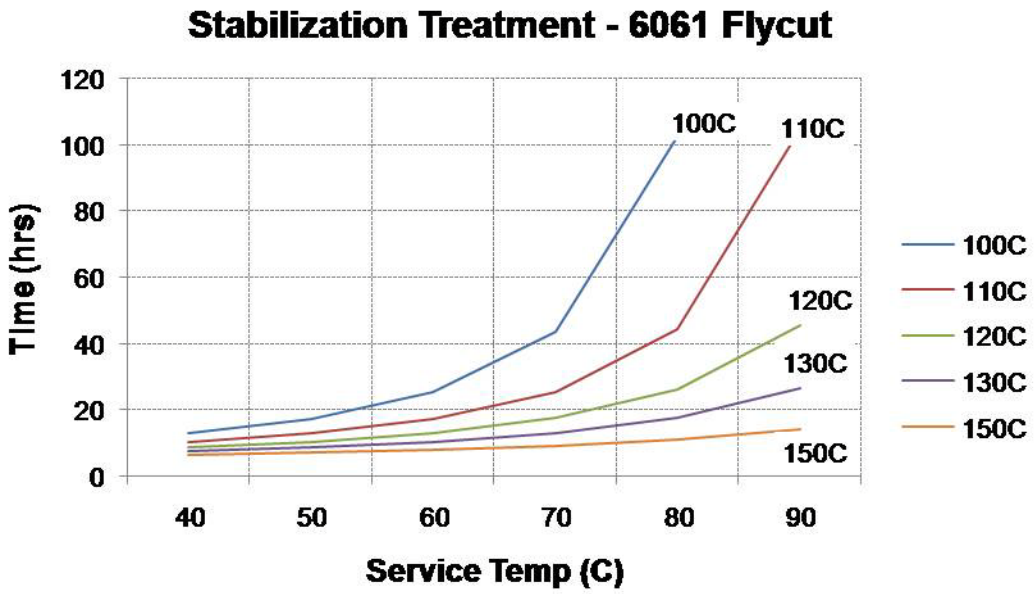

Fig. 5-8 Stabilization treatments for flycut 6061-T6.

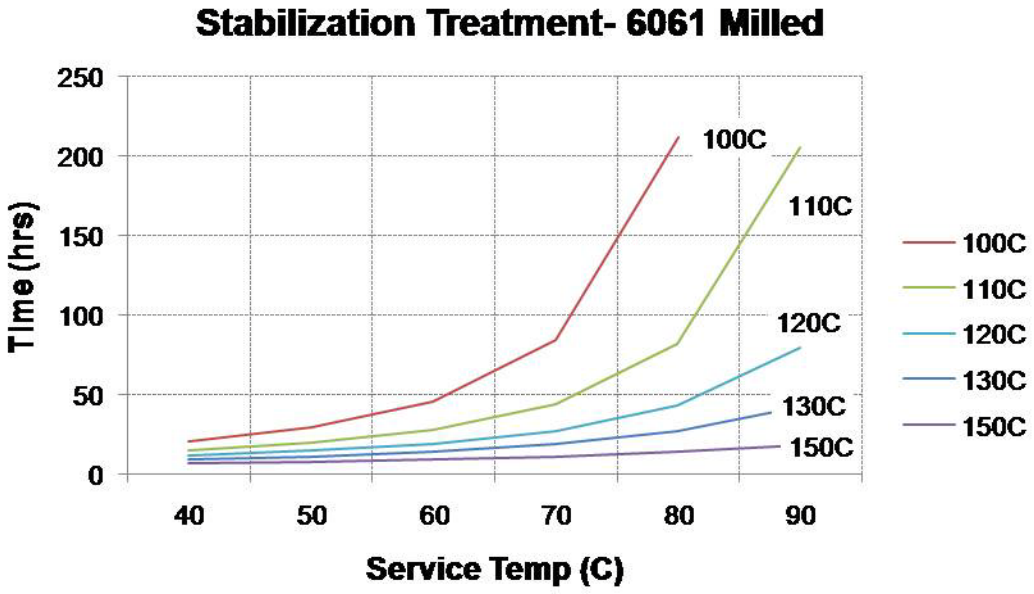

Fig. 5-9 Stabilization treatments for milled 6061-T6.

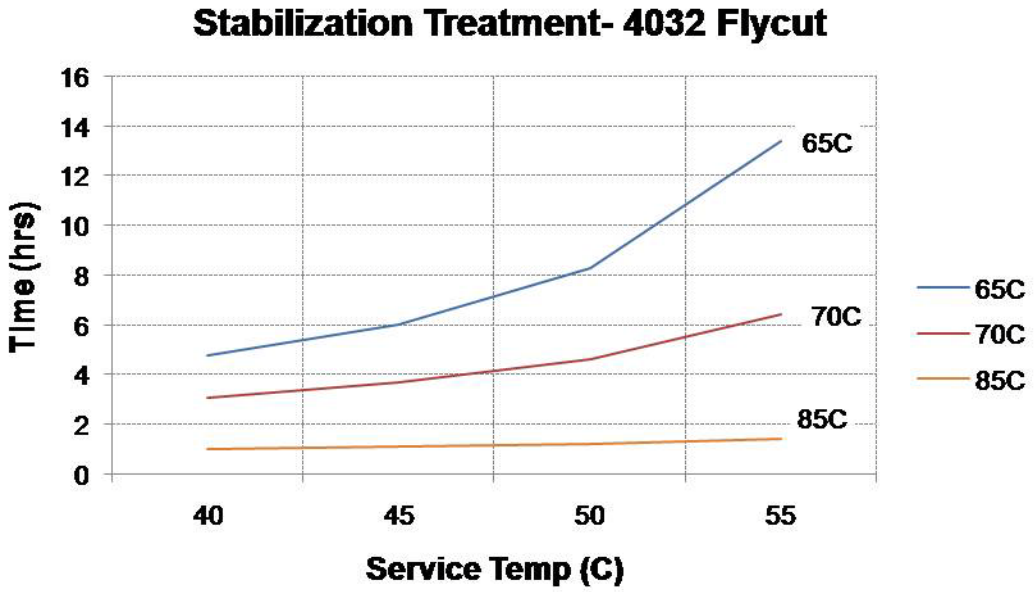

Fig. 5-10 Stabilization treatments for flycut 4032-0.

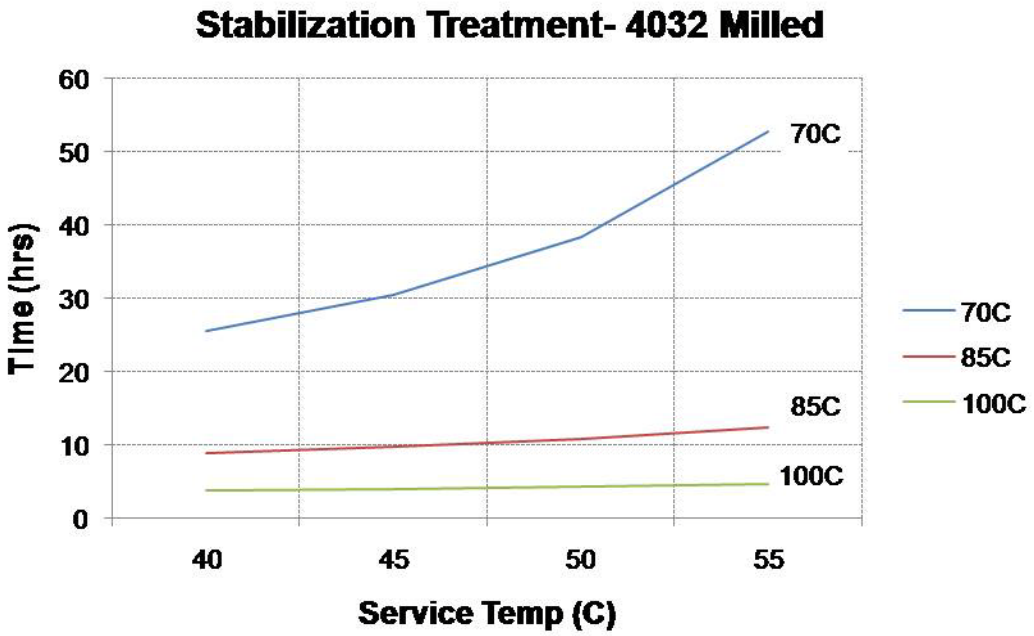

Fig. 5-11 Stabilization treatments for milled 4032-0.

5.7 Isothermal Stress Relief Test

Based on the data collected during the long-term isothermal treatments stress relief treatments can be calculated. The treatments were based on approach achieving stability at a service temperature by exceeding the final strain for the service temperature using a shorter, higher temperature stress relief treatment (the second method described in the previous section).

150C has been slight selected as a stress relief verification temperature based on a slight extension of the range of temperatures investigated to determine the creep model parameters. Because of the shorter times to relieve stress predicted by the model, 85C was retained as a stress relief temp for 4032.

An example treatment for each alloy/machining combination has been identified for testing, see **Table 5-7** below.

Table 5-7 Proposed stress relief treatments for achieving stability at a service temperature.

	Stress Relief Test Temp (C)	**Stress Relief Test Time (hr)**	**Service Temperature**
6061-T6 Flycut	150	12	To achieve stability at 85C service temp
6061-T6 Milled	150	16	
4032-0 Flycut	85	1.5	To achieve stability at 50C service temp
4032-0 Milled	85	11	

Two samples each were stress relived in accordance with the verification temperature schedule. These were then subjected to exposure to the service temperature, and periodic monitoring of curvature.

5.8 Stability Verification

Dimensional stability was verified by exposing the stress relieved samples to a 32 hour exposure at the lower service temperature. The change in curvature resulting from the 32 hour exposure can be compared to the curvature change that was expected with no stabilization treatment performed. The results are summarized in **Table 5-8** below.

Table 5-8 Summary of 32 hour, post stress relief, stability verification test.

	Average Initial Radius (in)	Average Post Exposure Radius (in)	Strain	Expected Strain without Stress Relief	Fraction Creep Strain Removed
6061-T6 Flycut	67.196	67.187	3.6695E-07	-2.497E-05	0.99
6061-T6 Milled	79.116	79.162	-1.7260E-06	-6.08E-05	0.97
4032-0 Flycut	45.408	45.507	-1.0043E-05	-2.17E-05	0.54
4032-0 Milled	58.534	58.459	2.795E-05	-2.98E-05	0.91

It is clear to see from the post exposure data that the stress relief treatment was largely effective in reducing the creep strain associated with residual stresses from machining operations.

The stress relief treatment predicted by the creep model did under-predict the required time for stress relieving the flycut sample of 4032. The time of 1.5 hrs was short due to the low final strain observed in 4032 at the 50C temp. In practice a part would likely have multiple types of machining operations performed on it. The proper stress relief schedule would be associated with the machining operation that required the most time to relieve the stress to an appropriate level.

6 Discussion

6.1 Final Strain Dependence on Temperature

The data presented herein clearly demonstrates that there is a strong temperature dependence on the final strain; increased temperature results in increased distortion. It is likely that this is caused by the distribution of stress within the material. The Timoshenko equations describe this distribution. The 6061 Flycut stress profile is used as an example, see **Fig. 6-1**.

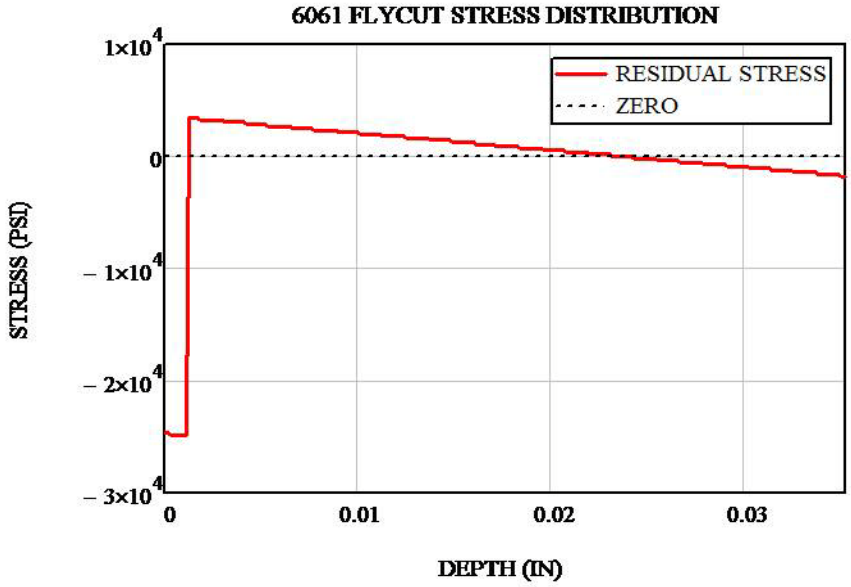

Fig. 6-1 Stress distribution profile of 6061 flycut samples. The machined surface is represented on the left side of the chart as depth 0.

It is clearly seen that just below the compressively stressed machined layer is a portion of material under tensile stress that is elastically balanced with the rest of the stress in the sample. All portions of the sample under stress are subject to some creep over time and temperature. Creeping of the compressed machined layer will results in the following:

- a contraction in-plane
- an expansion out of plane
- a reduction in the level of compressive stress
- a reduction in curvature
- All of these factors work to ***increase*** distortion or final strain, ε_f

The layer below the machined layer is also subject to creep, although its magnitude will be smaller due to a smaller stress magnitude. Since the tensile layer still lies to the same side of the center line as the machined layer, any creeping that occurs in it will results in:

- an expansion in-plane of the machined layer
- a contraction out of plane
- a decrease in the stress level of the machined layer
- an increase in curvature of the surface
- All of these factors work to ***reduce*** distortion or final strain, ε_f

Since the stress magnitude is small, creeping of this layer will have only some influence on the value of final strain. This influence is the greatest at lower temperatures for the following reasons:

- creep rates increase as a function of temperature
- the final strain achieved can be loosely thought of as being proportional to the creep strain achieved by the compressively stressed machined layer, less the creep strain achieved by the tensile sub-layer
- at higher temperatures, both strain rates will be proportionally larger due to the Arrhenius term in the creep model. Proportionally larger strain rates will result in a larger difference in the creep strain achieved by the machined layer vs. the tensile sub-layer

This following argument demonstrates the influence of temperature and stress magnitude on competing strain rates. In order to compare strain rates, the tensile component of each will be considered. The sub-layer is already tensile, so its full magnitude will be used. For illustrative purposes, the compressed layer will be considered in tensile by considering 2/3 the value in accordance with a Poisson Ratio of 1/3. The tensile components then are approximately 15000 psi and 5000 psi for the machined layer and sub-layer respectively (a factor of 3).

Creep strain can be approximated by the power law:

$$\varepsilon = k\sigma^m e^{\frac{-Q}{RT}}\Delta t \qquad \textbf{Eq. 6-1}$$

Now the difference in the amount of strain achieved in a given time at Temperature 1 vs. Temperature 2 will be described. The machined layer will be A, and the tensile sub-layer will be S.

$$\varepsilon_{A,T_1} - \varepsilon_{S,T_1} = ke^{\frac{-Q}{RT_1}} \Delta t\left[(3\sigma)^m - \sigma^m\right] \qquad \textbf{Eq. 6-2}$$

$$\varepsilon_{A,T_1} - \varepsilon_{S,T_1} \propto e^T \qquad \textbf{Eq. 6-3}$$

In short, this means that the larger stress magnitude of the compressed layer is more significant at higher temps, and that higher temps will result in a final strain that more closely approaches the theoretical maximum.

The competing interaction of these two portions of the stress profile are captured by the expression that was used to fit the measured ε_f values, **Eq. 3-7**.

$$\varepsilon_f = B\frac{\sigma_{in}}{E}T^n \qquad \textbf{Eq. 3-7}$$

6.2 Machining of Opposing Faces

The work performed in this project has focused on isolating the stressed layer caused by machining operations, and observing how this layer behaves over time and temperature. In practice there are not real parts manufactured that are completely stressed relieved only to have a single stressed layer imparted on one side.

There are many parts fabricated that would have residual stresses from machining on opposing faces. There are also parts that would have significantly different fabrication n techniques used on opposing surfaces. One example would be a mirror that would have a milled or flycut surface on one side, producing a significant level of residual stress, and the other side would be polished, producing a much less significant layer of residual stress.

A more common situation in the fabrication of real parts is that parallel surfaces are machined using the same process. This will set compressive surface stresses that will artificially stretch the part elastically. As these stressed layers experience creep, which would be in the out-of-plane z-axis, the part will undergo a time-dependant contraction in length. This length contraction will be a function of the total part thickness, and the isothermal exposure temperature. **Eq. 6-4** is used to model the initial elastic response of a part of a certain substrate thickness that has compressively stressed layers on opposing

sides. **Eq. 6-5** describes the potential elastic change as a result of the stressed layers creeping to a final strain. The predicted behavior is seen in **Fig. 6-2** and **Fig. 6-3**.

$$\varepsilon_{in} = \frac{2h_A\sigma_{in}}{h_B E_B} \qquad \textbf{Eq. 6-4}$$

$$\varepsilon = \frac{2h_A(\sigma_{in} - \varepsilon_f E_A)}{h_B E_B} \qquad \textbf{Eq. 6-5}$$

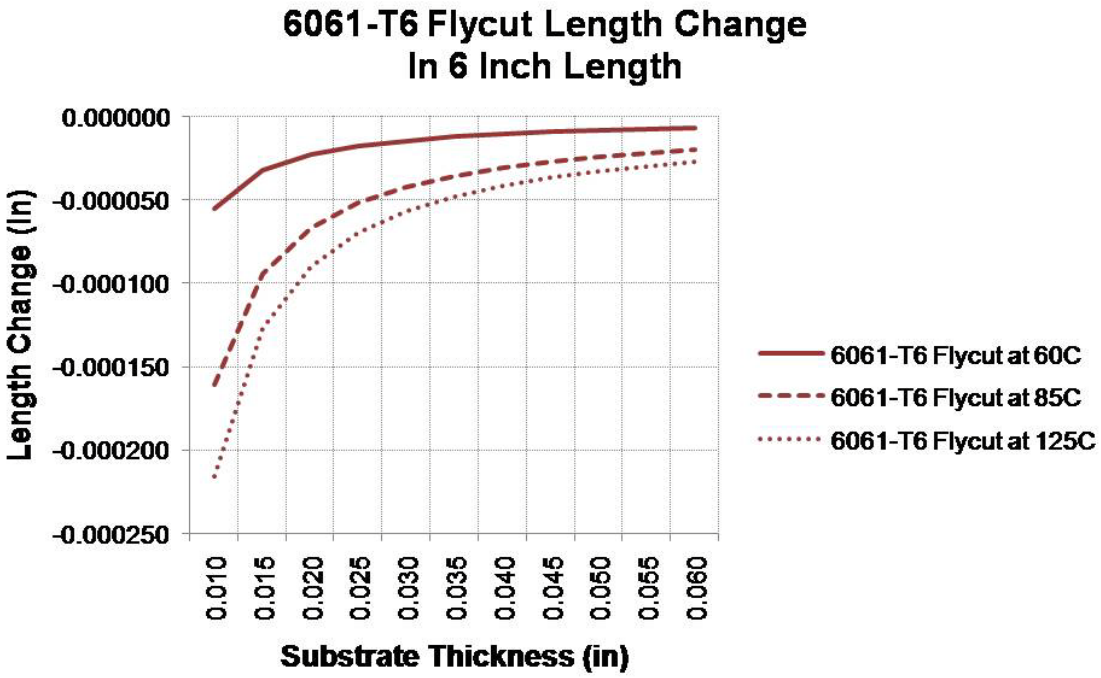

Fig. 6-2 Potential length contraction in Flycut 6061-T6.

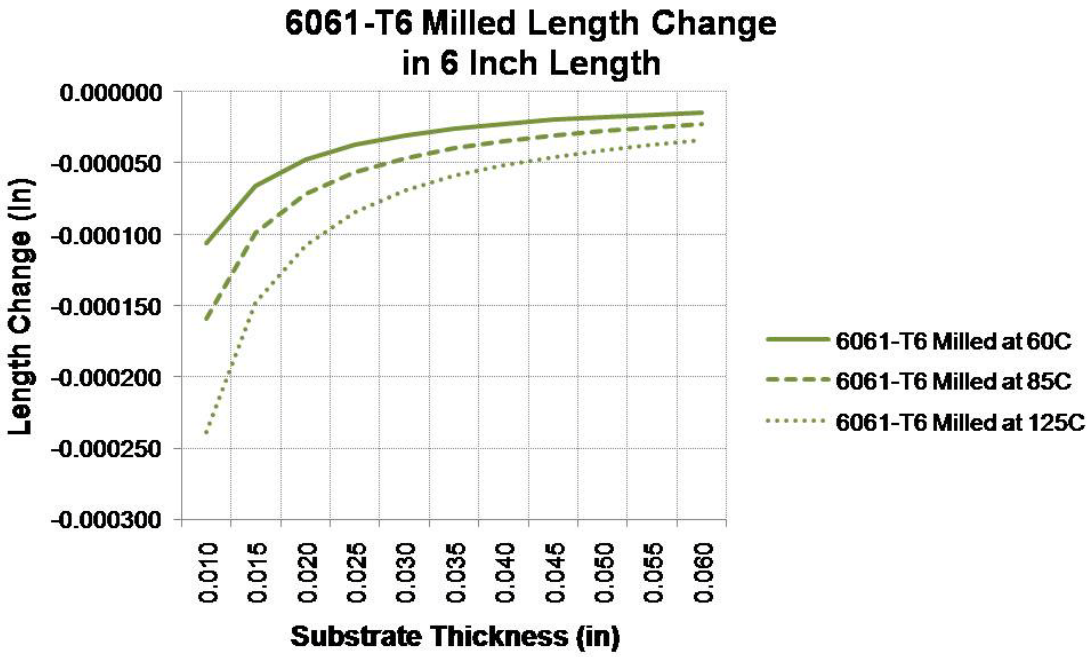

Fig. 6-3 Potential length contraction in milled 6061-T6.

6.3 Use of Creep Model as a Reliability Predictor

Having a method to estimate the final strain of the stressed layer, in addition to knowing the creep model parameters through curve fitting, allows for the use of the model as a tool to predict reliability over long storage times. the following example illustrates the case of a known allowable strain on a part stored at 85C. The allowable design strain will not be reached for nearly 4 years in storage.

$$t = \varepsilon_f \frac{e^{\frac{Q}{RT}}}{(m-1)k\sigma_{in}} \left[\left[\sigma_{in} \left(1 - \frac{\varepsilon}{\varepsilon_f} \right) \right]^{1-m} - \sigma_{in}^{1-m} \right]$$

$$e_f = 1.149 \cdot 10^{-4}$$

$$Q = 28.19 \frac{kJ}{mol}$$

$$k = 2.717 \cdot 10^{-21} \frac{K}{s}$$

$$m = 3.583$$

$$R = .0083144 \frac{KJ}{mol \cdot K}$$

$$allowable\ \ strain\ = .000114$$

$$t = 3.713\, years$$

6.4 Analysis of Complex Parts

Other than in the most simple of cases of the instability real parts, such as the length contraction of a long thin part, it is difficult to see how these findings might be applied to a complex part. An approach to applying the creep model generated in this research to the analysis of complex parts is outlined below.

1. A complex part would be modeled in a solid model program. This is the most common method of part design in industry today.
2. A thin layer is modeled on the surface of the solid part. Existing solid modeling programs have routines built in that perform this task. This layer would reflect the equivalent thickness of the machined layer under study.
3. Using a Finite Element Analysis (FEA) software package, a mesh is applied to both the underlying part and the thin layer.
4. When assigning material properties to the solid part and the thin layer, assign a Coefficient of Thermal Expansion (α) value of zero to the solid part, and a non-zero positive value to the thin layer. Assign a value of 0C to the Temperature of the model.
5. To simulate the initial stress of the machined layer perform a thermal stress simulation at an elevated temperature, T. This will cause the thin layer within the model to expand relative to the base material of the part. This expansion will result in a compressive stress state in the thin layer, and the corresponding elastic response of the solid part. The stress in the thin layer would be the product of the assigned temperature T, the CTE, and the Modulus of the thin layer, so the model temperature would be set per **Eq. 6-6**:

$$T = \frac{\sigma_{in}}{\alpha E} \qquad \textbf{Eq. 6-6}$$

6. To now simulate the effect of the geometry change that would accompany the creeping of the machined layer to its final strain, the Temperature within the FEA model would be reduced so that the product of the temperature reduction and the CTE was equal to the final stain value:

$$\Delta T = \frac{\varepsilon_f}{\alpha} \qquad \textbf{Eq. 6-7}$$

Using this approach, the geometry change due to the stress reduction in the machined layer could be modeled using existing solid modeling and FEA software packages.

6.5 Potential Practical Applications

The original intent of developing this creep model was to predict geometry changes in moderate temperature storage or service conditions, and to be used as a framework to develop short term higher temperature stabilizing stress relief treatments. The potential use of solid model and FEA opens up two additional possibilities:

1. For the designers of precision components, the creep model would help predict when stress relief treatments are required during fabrication. This could be accomplished by comparing the specified drawing tolerances, with the geometry changes calculated using an FEA model.
2. For the fabricators of precision components, the creep model would help predict how much extra material should be left on a part prior to finish machining or lapping/polishing operations. Unexpected creep strain during a stress relief procedure could leave too little material on the part to meet the final required dimensions.

7 Conclusions

The dimensional instability created by machining operations does in general follow the creep model as summarized by the following observations:

- The compressive stresses at the surface do result in an initial curvature away from the compressed (machined) layer.
- The residual compressive stresses remaining on the machined surface do creep and create an increase in radius (a decrease in curvature) over time.
- The creep rate is increased with increasing temperature.
- The amount of total creep strain increases with temperature in a linear fashion.
- The creep rate diminishes with time for any given temperature.

The creep model proposed herein is can be used as a reliability tool to model long term storage.

The creep model proposed herein is can be used as a tool to design high temperature, short term stress relief treatments used for fabricating parts.

The final strain magnitudes found to be between .000023 and .00034 in/in for 6061 and .000016 and .00021 in/in for 4032.

On simple parts such as plates or rods, the length contraction due to creep of surface stresses can be 50-200 micro-inches for substrates in the .040” and smaller size range.

The bimetallic strip model is an effective model for characterizing the curvature created by the residual stresses from machining operations and also for predicting the geometric instability response.

- Higher residual stress magnitudes resulted in greater sample curvature.
- Smaller substrate thicknesses resulted in increased sample curvature.

Performing a non-destructive XRD stress measurement on an external surface of a useable part is not a feasible way to make a prediction of the dimensional stability. Depth profiling and correcting for the removed layers is required to understand the near surface magnitudes of stress.

7.1 Recommendations for Future Work

It is recommended that in any future study of this area, time be spent developing a simple method for fabricating stress free blanks for use as test coupons. The method employed in this study, milling thicker plate stock down to size, and chemically etching the machining stress away prior to performing the final machining pass was tedious. Use of sheet material that is thermally stress relieved only may be feasible

Additional data should be collected at higher temperatures in order to further develop the high temperature stress relief treatment profiles as well as validate the effectiveness of the approach used to design stabilizing heat treatments. Limitations of test articles restricted this portion of the testing.

Appendix A Theoretical Model Derivation

The general equation for Steady State Creep Rate is known as the Mukherjee-Bird-Dorn equation and is as follows (Dowling):

$$\dot{\varepsilon}_{ss} = \frac{d\varepsilon}{dt} = \frac{AGb}{k'T} D \left(\frac{b}{d}\right)^{P} \left(\frac{1}{G}\right)^{m} \sigma^{m} e^{\frac{-Q}{RT}}$$

where:

$\dot{\varepsilon}_{ss}$ = creep strain
t = time
A = material dependant constant
G = Shear Modulus
b = Burger's Vector
k' = Boltzman's Constant
T = temperature
D = Diffusion Constant
σ = stress
d = grain diameter
P = grain size exponent
m = stress exponent
Q = thermal activation energy
R = gas constant

This expression is often represented in the Power Law form as follows:

$$\dot{\varepsilon}_{ss} = \frac{d\varepsilon}{dt} = k\sigma^{m} e^{\frac{-Q}{RT}}$$

$$k = \frac{AGb}{k'T} D_o \left(\frac{b}{d}\right)^{P} \left(\frac{1}{G}\right)^{m}$$

For the case of creep due Dislocation Creep or Glide, the exponent P is zero (Courtney). In the case of crystalline materials, and the temperature dependence of k can be included in the Power Law expression. It is noted that there is an addition, weak temperature dependence of k (Dowling). Due to the relatively small temperature ranges in this research, the value of k is being considered constant. *(Note that in the original source the constant k is assigned A_2.):*

$$\dot{\varepsilon}_{ss} = \frac{d\varepsilon}{dt} = \frac{k}{T}\sigma^m e^{\frac{-Q}{RT}}$$

In the case of the creeping of a thin layer of material on a surface which results in a change of shape of the substrate, the stress will drop as a function of the change on shape. This condition is unlike most creep considerations where the magnitude of stress is constant.

The following expression define stress as a function that decays linearly with increasing strain until it reaches a final strain, which shall be referred to as ε_f:

$$\sigma = \sigma_{in} - \frac{\varepsilon\sigma_{in}}{\varepsilon_f}$$

where:

$$\sigma_{in} = initial \;\; stress$$
$$\varepsilon_f = final \;\; strain$$

substituting this stress expression back into the Power Law Creep expression:

$$\frac{d\varepsilon}{dt} = k\left(\sigma_{in} - \frac{\varepsilon\sigma_{in}}{\varepsilon_f}\right)^m e^{\frac{-Q_c}{RT}}$$

and rearranging the terms to collect strain terms on one side and time on the other side:

$$\frac{d\varepsilon}{\left(\sigma_{in} - \frac{\varepsilon\sigma_{in}}{\varepsilon_f}\right)^m} = ke^{\frac{-Q_c}{RT}}dt$$

The following Chain Rule substitution is made to simplify the integration:

$$u = \sigma_{in} - \frac{\varepsilon \sigma_{in}}{\varepsilon_f}$$

$$du = -\frac{\sigma_{in}}{\varepsilon_f} d\varepsilon$$

$$d\varepsilon = -\frac{\varepsilon_f}{\sigma_{in}} du$$

Substitute u and dε:

$$-\frac{\varepsilon_f}{\sigma_{in}} u^{-m} d\varepsilon = \frac{k}{T} e^{\frac{-Q_c}{RT}} dt$$

$$u^{-m} d\varepsilon = -\frac{\sigma_{in}}{\varepsilon_f} \frac{k}{T} e^{\frac{-Q_c}{RT}} dt$$

Integrating from an initial strain to a subsequent strain and from an initial time to subsequent time:

$$\int u^{-m} du = -\int \frac{\sigma_{in}}{\varepsilon_f} \frac{k}{T} e^{\frac{-Q_c}{RT}} dt$$

$$\left(\frac{1}{1-m} \right) u^{1-m} \Bigg| = -\frac{\sigma_{in}}{\varepsilon_f} \frac{k}{T} e^{\frac{-Q_c}{RT}} t \Bigg|_{t_1}^{t_2}$$

Substituting the stress expression back in:

$$\left(\frac{1}{1-m} \right) \left(\sigma_{in} - \frac{\varepsilon \sigma_{in}}{\varepsilon_f} \right)^{1-m} \Bigg|_{\varepsilon_1}^{\varepsilon_2} = -\frac{\sigma_{in}}{\varepsilon_f} \frac{k}{T} e^{\frac{-Q_c}{RT}} t \Bigg|_{t_1}^{t_2}$$

$$\left(\frac{1}{1-m}\right)\left(\sigma_{in}-\frac{\varepsilon\sigma_{in}}{\varepsilon_f}\right)^{1-m}\Bigg|_{\varepsilon_1}^{\varepsilon_2}=-\frac{\sigma_{in}}{\varepsilon_f}\frac{k}{T}e^{\frac{-Q_c}{RT}}\left(t_2-t_1\right)$$

$$\left(\sigma_{in}-\frac{\varepsilon_2\sigma_{in}}{\varepsilon_f}\right)^{1-m}-\left(\sigma_{in}-\frac{\varepsilon_1\sigma_{in}}{\varepsilon_f}\right)^{1-m}=\frac{(m-1)\sigma_{in}}{\varepsilon_f}\frac{k}{T}e^{\frac{-Q_c}{RT}}\left(t_2-t_1\right)$$

$$\left(\sigma_{in}-\frac{\varepsilon_2\sigma_{in}}{\varepsilon_f}\right)^{1-m}=\frac{(m-1)\sigma_{in}}{\varepsilon_f}\frac{k}{T}e^{\frac{-Q_c}{RT}}\left(t_2-t_1\right)+\left(\sigma_{in}-\frac{\varepsilon_1\sigma_{in}}{\varepsilon_f}\right)^{1-m}$$

$$(1-m)\ln\left(\sigma_{in}-\frac{\varepsilon_2\sigma_{in}}{\varepsilon_f}\right)=\ln\left[\frac{(m-1)\sigma_{in}}{\varepsilon_f}\frac{k}{T}e^{\frac{-Q_c}{RT}}\left(t_2-t_1\right)+\left(\sigma_{in}-\frac{\varepsilon_1\sigma_{in}}{\varepsilon_f}\right)^{1-m}\right]$$

$$\ln\left(\sigma_{in}-\frac{\varepsilon_2\sigma_{in}}{\varepsilon_f}\right)=\frac{1}{1-m}\ln\left[\frac{(m-1)\sigma_{in}}{\varepsilon_f}\frac{k}{T}e^{\frac{-Q_c}{RT}}\left(t_2-t_1\right)+\left(\sigma_{in}-\frac{\varepsilon_1\sigma_{in}}{\varepsilon_f}\right)^{1-m}\right]$$

$$\left(\sigma_{in}-\frac{\varepsilon_2\sigma_{in}}{\varepsilon_f}\right)=\left[\frac{(m-1)\sigma_{in}}{\varepsilon_f}\frac{k}{T}e^{\frac{-Q_c}{RT}}\left(t_2-t_1\right)+\left(\sigma_{in}-\frac{\varepsilon_1\sigma_{in}}{\varepsilon_f}\right)^{1-m}\right]^{\frac{1}{1-m}}$$

$$\frac{\varepsilon_2\sigma_{in}}{\varepsilon_f}=\sigma_{in}-\left[\frac{(m-1)\sigma_{in}}{\varepsilon_f}\frac{k}{T}e^{\frac{-Q_c}{RT}}\left(t_2-t_1\right)+\left(\sigma_{in}-\frac{\varepsilon_1\sigma_{in}}{\varepsilon_f}\right)^{1-m}\right]^{\frac{1}{1-m}}$$

$$\varepsilon_2=\varepsilon_f-\frac{\varepsilon_f}{\sigma_{in}}\left[\frac{(m-1)\sigma_{in}}{\varepsilon_f}\frac{k}{T}e^{\frac{-Q_c}{RT}}\left(t_2-t_1\right)+\left(\sigma_{in}-\frac{\varepsilon_1\sigma_{in}}{\varepsilon_f}\right)^{1-m}\right]^{\frac{1}{1-m}}$$

This is the general expression for strain after a given time with a given initial stress that decays with strain to a final strain value. This will be referred to as the General Creep Model. For the case where initial time is zero seconds, and initial strain is defined as zero, the expression takes the Creep Model takes the following form:

$$\varepsilon=\varepsilon_f-\frac{\varepsilon_f}{\sigma_{in}}\left[\frac{(m-1)\sigma_{in}}{\varepsilon_f}\frac{k}{T}te^{\frac{-Q_c}{RT}}+\left(\sigma_{in}\right)^{1-m}\right]^{\frac{1}{1-m}}$$

The units in this expression are as follows:

$$\varepsilon, \varepsilon_f = \text{unitless}$$
$$\sigma_{in} = \text{kPa}$$
$$m = \text{unitless}$$
$$Q = \frac{\text{kJ}}{\text{mol} \cdot \text{K}}$$
$$k = \text{K}(\text{kPa})^{-m}\,\text{s}^{-1}$$
$$R = .0083144 \frac{\text{kJ}}{\text{mol} \cdot \text{K}}$$
$$T = \text{K}$$

As the data in this project will show, the value of final strain, ε_f, is a function of temperature. Increasing dwell temperature increases the ε_f value. The theoretical maximum creep strain that would be recovered during isothermal temperature exposures would be if the initial stress were completely converted to strain in accordance with Hooke's Law:

$$\varepsilon_{f,\ \text{theoretical maximum}} = \frac{\sigma_{in}}{E}$$

In actuality, the theoretical maximum is not reached, so an expression has been developed to predict ε_f that includes a material constant, B, and Temperature dependence term, T^n:

$$\varepsilon_f = B \frac{\sigma_{in}}{E} T^n$$

The constants B and n can be found graphically using the slope-intercept method by plotting the following:

$$\ln \frac{\varepsilon_f E}{\sigma_{in}} \ \textit{vs.}\ \ln T$$

Using the y=mx+b definition of a line:

$$\text{slope} = m = n$$
$$\text{y intercept} = \exp(b) = B$$

The final strain expression can now be substituted back into the Creep Model:

$$\varepsilon = B\frac{\sigma_{in}}{E}T^{n} - \frac{BT^{n}}{E}\left[\frac{(m-1)E}{B}\frac{k}{T^{n+1}}te^{\frac{-Q_c}{RT}} + (\sigma_{in})^{1-m}\right]^{\frac{1}{1-m}}$$

Appendix B Algebraic Equivalence of Bimetallic Strip Models

From Timoshenko's expression for the curvature of a bimetallic thermometer:

$$\frac{1}{r} = \frac{(\alpha_b - \alpha_a)\Delta T}{\frac{h}{2} + \frac{2(E_a l_a + E_b l_b)}{h}\left(\frac{1}{E_a t_a} + \frac{1}{E_b t_b}\right)}$$

where:

$$h = t_a + t_b$$
$$l_a = \frac{t_a^3}{12}$$
$$l_b = \frac{t_b^3}{12}$$

and the misfit strain term for a CTE differential can be defined as:

$$\Delta\varepsilon = (\alpha_b - \alpha_a)\Delta T$$

substituting these expressions in:

$$\frac{1}{r}=\frac{\Delta\varepsilon}{\frac{t_a+t_b}{2}+\frac{2\left(E_a\frac{t_a^3}{12}+E_b\frac{t_b^3}{12}\right)}{t_a+t_b}\left(\frac{1}{E_at_a}+\frac{1}{E_bt_b}\right)}$$

expanding these terms and multiplying through by $E_aE_b(t_a+t_b)t_at_b$:

$$\frac{1}{r}=\frac{\Delta\varepsilon}{\frac{t_a+t_b}{2}+\frac{2}{t_a+t_b}\left(\frac{t_a^3}{12t_a}+\frac{E_bt_b^3}{12E_at_a}+\frac{E_at_a^3}{12E_bt_b}+\frac{t_b^3}{12t_b}\right)}$$

$$\frac{1}{r}=\frac{6E_aE_b\Delta\varepsilon\left(t_a+t_b\right)t_at_b}{3E_aE_b\left(t_a^2+2t_at_b+t_b^2\right)+E_aE_bt_a^3t_b+E_b^2t_b^4+E_a^2t_a^4+E_aE_bt_at_b^3}$$

Simplifying:

$$\frac{1}{r}=\frac{6E_aE_b\Delta\varepsilon\left(t_a+t_b\right)t_at_b}{E_a^2t_a^4+4E_aE_bt_a^3t_b+6E_aE_bt_a^2t_b^2+4E_aE_bt_at_b^3+E_b^2t_b^4}$$

For our case, the intent is to relate changes in radius, which is easily measured, to changes in stress, which is more difficult to measure. Our samples also have a unique misfit strain based on residual stress rather than a CTE differential, and the Young's modulus' of the two materials are equal. Therefore:

$$\Delta\varepsilon=\frac{\sigma_a}{E_a}$$
$$E_a=E_b=E$$

substituting:

$$\frac{1}{r} = \frac{6E^2 \frac{\sigma_a}{E_a}(t_a + t_b)t_a t_b}{E^2 t_a^4 + 4E^2 t_a^3 t_b + 6E^2 t_a^2 t_b^2 + 4E^2 t_a t_b^3 + E^2 t_b^4}$$

$$\frac{1}{r} = \frac{6\frac{\sigma_a}{E}(t_a + t_b)t_a t_b}{(t_a + t_b)^4}$$

$$\frac{1}{r} = \frac{6\frac{\sigma_a}{E}t_a t_b}{(t_a + t_b)^3}$$

$$r = \frac{t_a^3 + 3t_a^2 t_b + 3t_a t_b^2 + t_b^3}{6\frac{\sigma_a}{E}t_a t_b}$$

In the case of the residual stress left behind by a machining operation, the stressed later, t_a, will be much thinner than the unstressed layer, t_b. Therefore:

$$t_a^3 + 3t_a^2 t_b << 3t_a t_b^2 + t_b^3$$

$$r = \frac{(3t_a + t_b)t_b}{6\frac{\sigma_a}{E}t_a}$$

$$\sigma_a = \frac{Et_b(3t_a + t_b)}{6rt_a}$$

$$\sigma_a = \frac{E}{6}\frac{t_b}{t_a}(3t_a + t_b)\frac{1}{r}$$

and considering the change in stress on the surface as a result of a change in radius:

$$\Delta\sigma_a = \frac{E}{6}\frac{t_b}{t_a}\left(3t_a + t_b\right)\left(\frac{1}{r_2} - \frac{1}{r_1}\right)$$

or considering strain rather than stress:

$$\varepsilon_{r_1 \to r_2} = \frac{t_b}{6t_a}\left(3t_a + t_b\right)\left(\frac{1}{r_2} - \frac{1}{r_1}\right)$$

Appendix C Machined Blank Drawing

	A
P1	.060"
P2	.060"
P3	.060"
P4	.060"

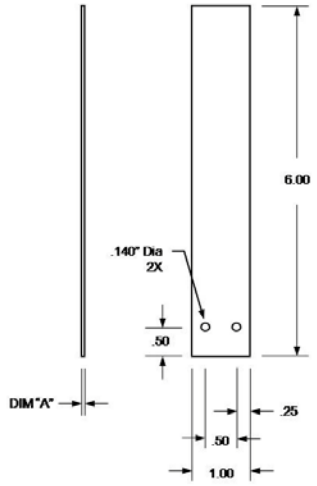

MATERIAL:

P1: ALUMINUM ALLOY 1100-0 IAW ASTM B221

P2: ALUMINUM ALLOY 6061-T6 IAW ASTM B211

P3: ALUMINUM ALLOY 4032-T6 IAW SAE AMS 4319

P4: ALUMINUM ALLOY MIC 6

FINISH:

NONE

ADDITIONAL PROCESSING NOTES:

1. COUPONS TO BE MACHINED FROM 1/8" RAW MATERIAL
2. EQUAL MATERIAL TO BE REMOVED FROM EACH SIDE
3. MACHINING SHALL BE PERFORMED IN THE FOLLOWING SEQUENCE, EDGES, HOLES, FLAT SIDES.
4. OPERATOR SHALL RECORD ENDMILL RPM AND FEED RATE FOR FACE CUTS
5. DEPTH OF FINAL CUT ON FLAT SIDES SHALL BE .020"
6. NO HEAT TRATMENT OR STRAIGHTENING OPERATIONS ARE ALLOWED

STABILITY COUPON 1A

TOL: X.XX +/- .010 X.XXX +/- .002

Appendix D Coupon Drawing

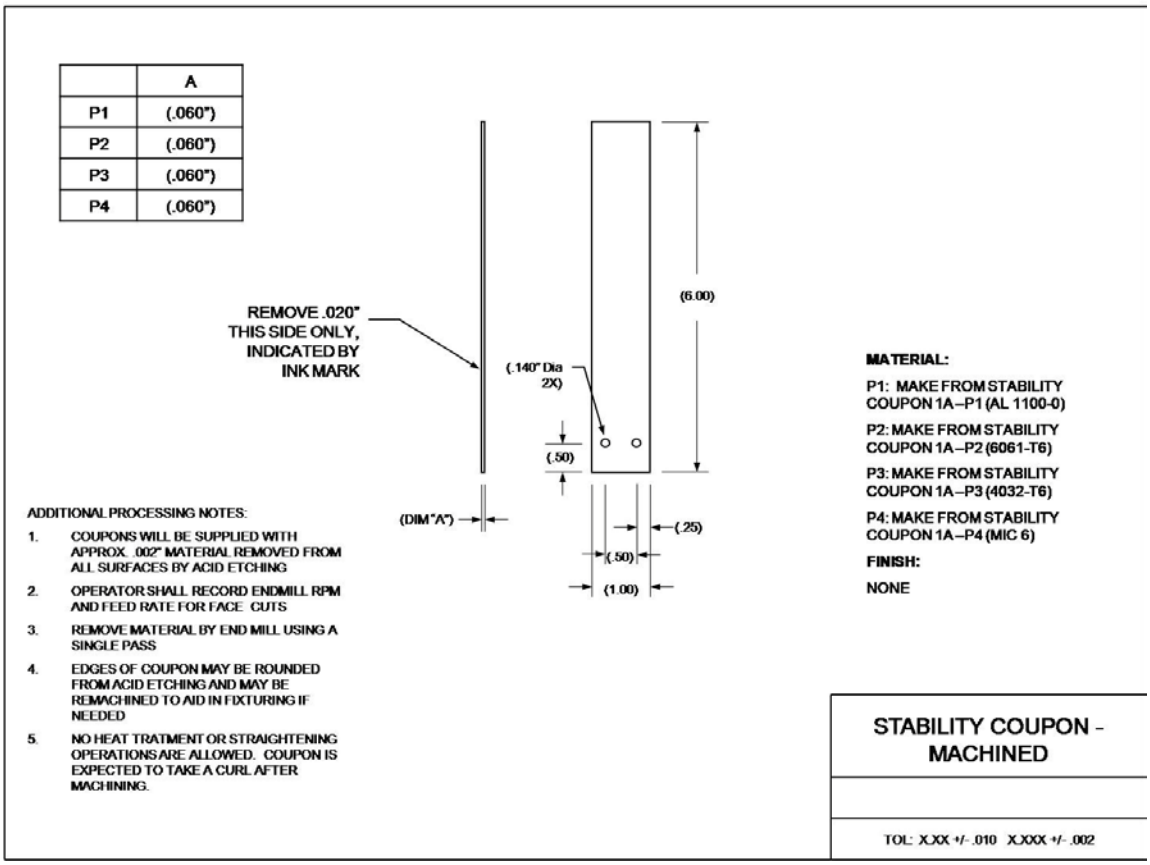

Appendix E Surface Residual Stress Measurements

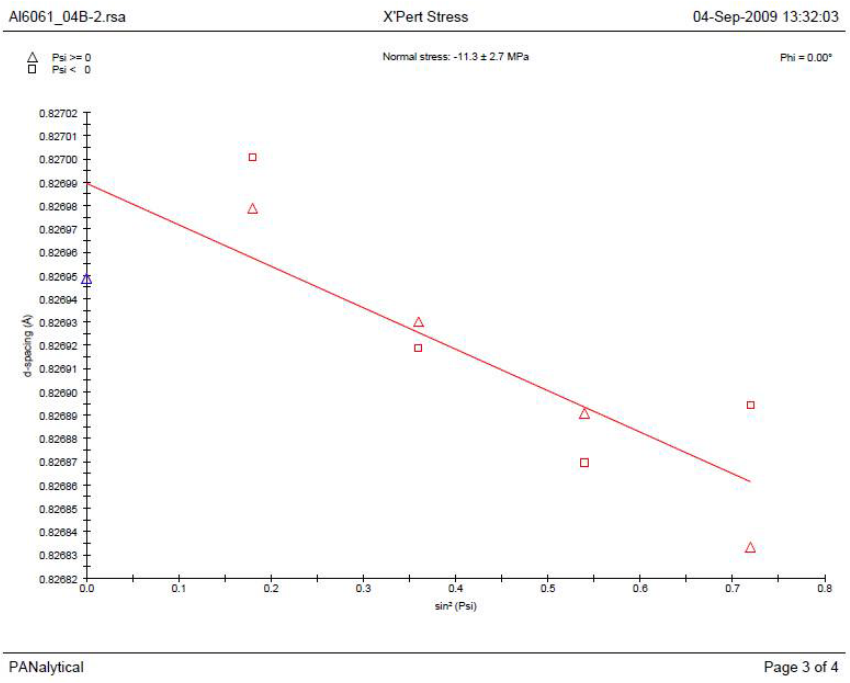

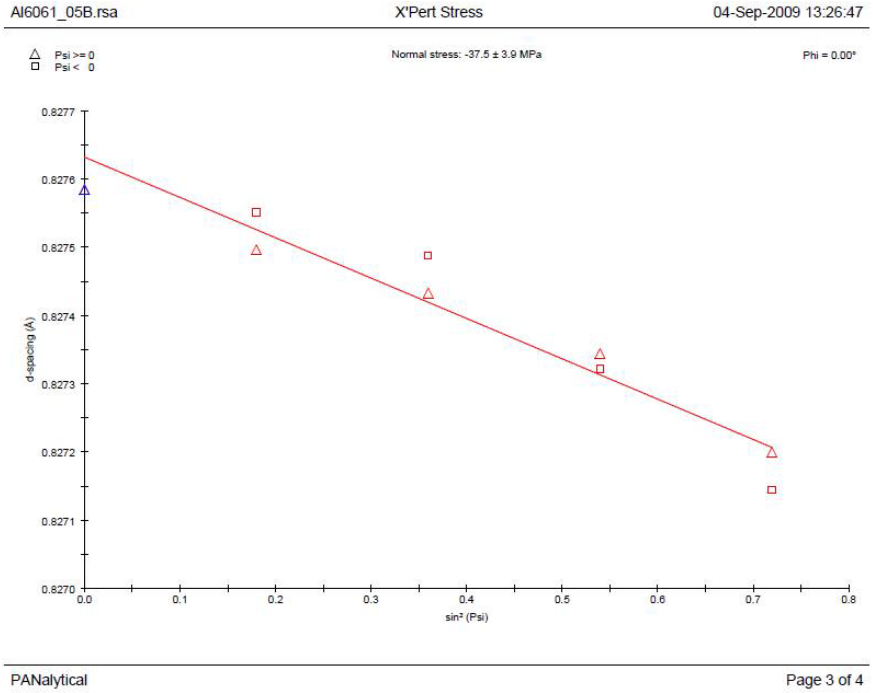

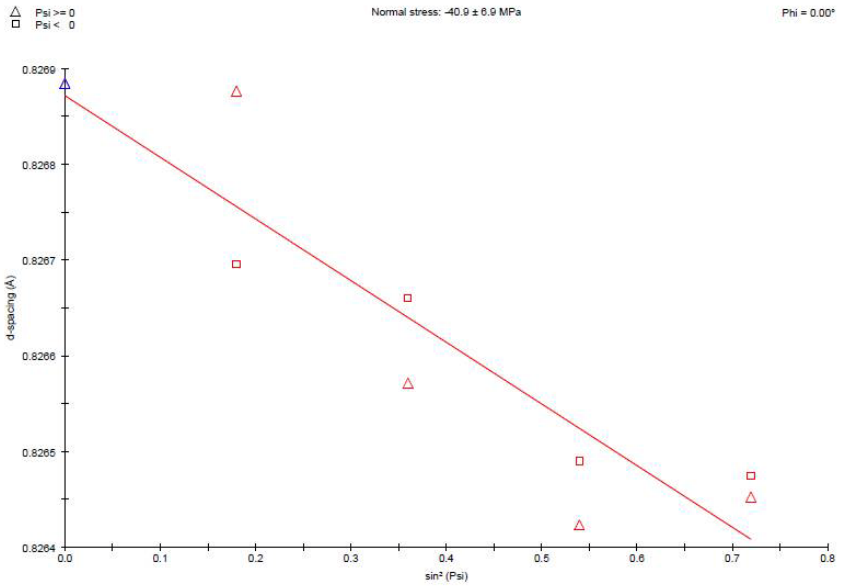
Psi >= 0
Psi < 0
Normal stress: -40.9 ± 6.9 MPa
Phi = 0.00°
d-spacing (Å)
sin² (Psi)

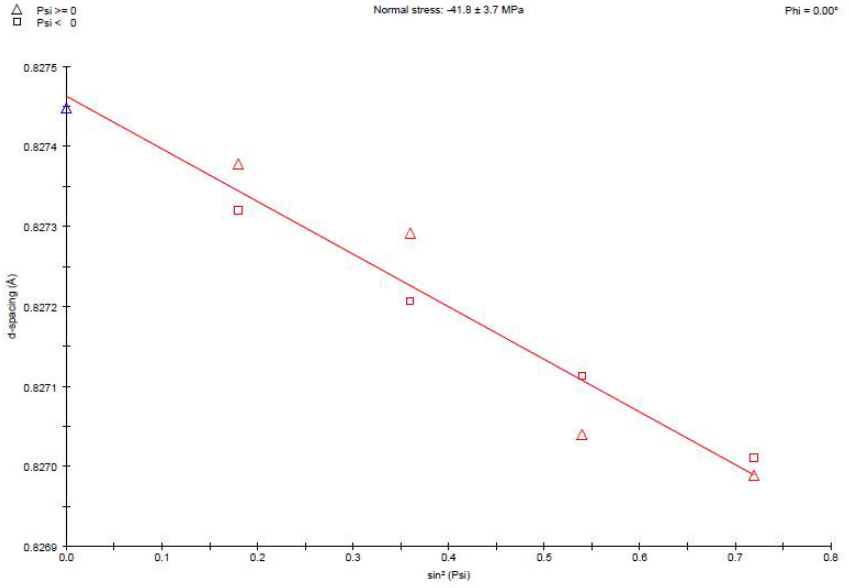
Psi >= 0
Psi < 0
Normal stress: -41.8 ± 3.7 MPa
Phi = 0.00°
d-spacing (Å)
sin² (Psi)

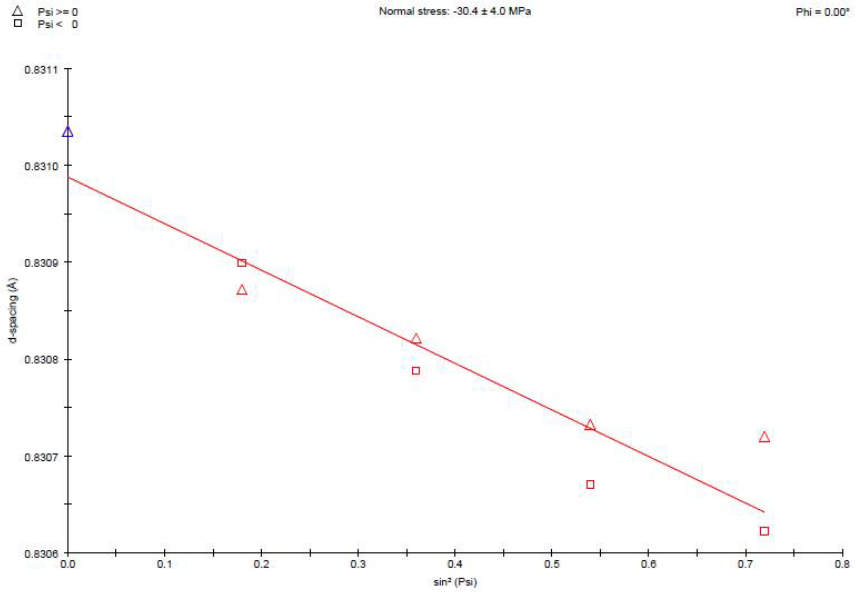
Psi >= 0
Psi < 0
Normal stress: -30.4 ± 4.0 MPa
Phi = 0.00°
d-spacing (Å)
0.8311
0.8310
0.8309
0.8308
0.8307
0.8306
0.0
0.1
0.2
0.3
0.4
0.5
0.6
0.7
0.8
sin² (Psi)

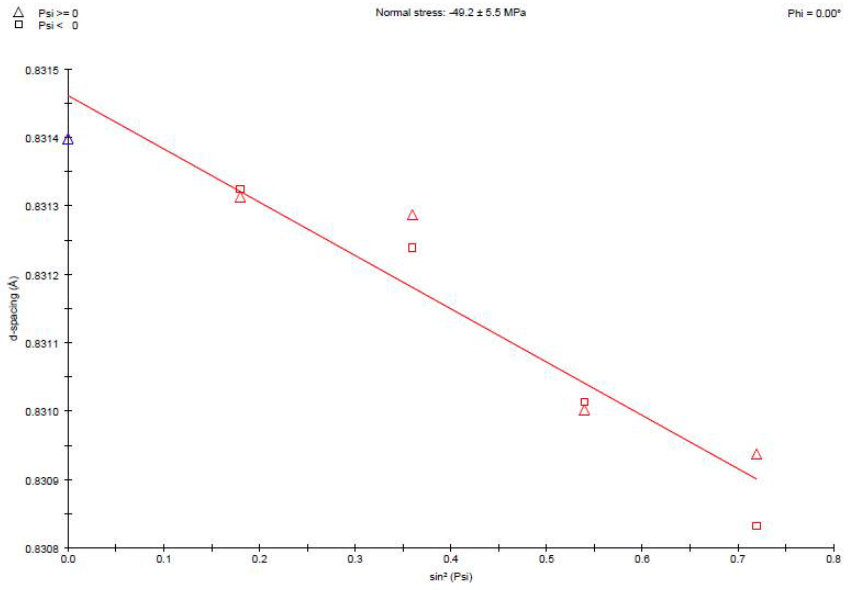
Psi >= 0
Psi < 0
Normal stress: -49.2 ± 5.5 MPa
Phi = 0.00°
d-spacing (Å)
0.8315
0.8314
0.8313
0.8312
0.8311
0.8310
0.8309
0.8308
0.0
0.1
0.2
0.3
0.4
0.5
0.6
0.7
0.8
sin² (Psi)

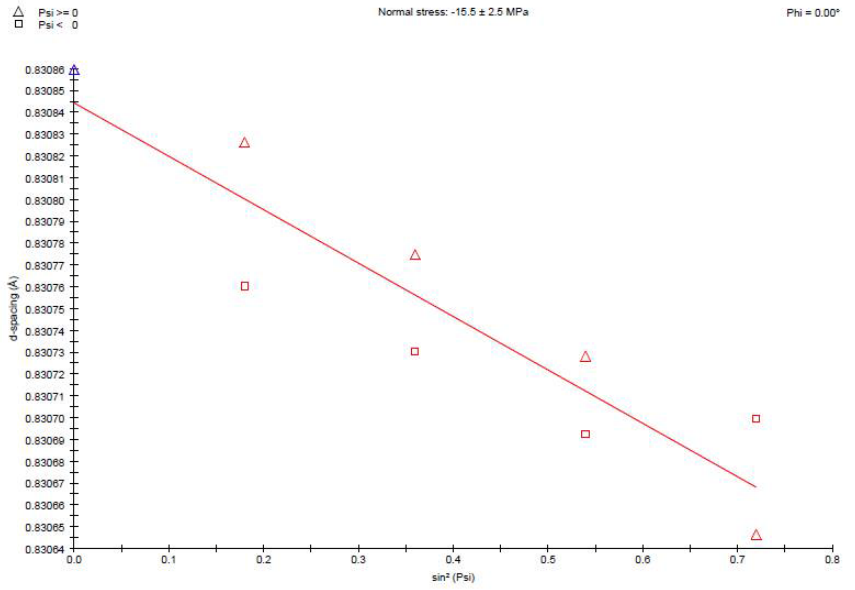
Psi >= 0
Psi < 0
Normal stress: -15.5 ± 2.5 MPa
Phi = 0.00°
d-spacing (Å)
sin² (Psi)

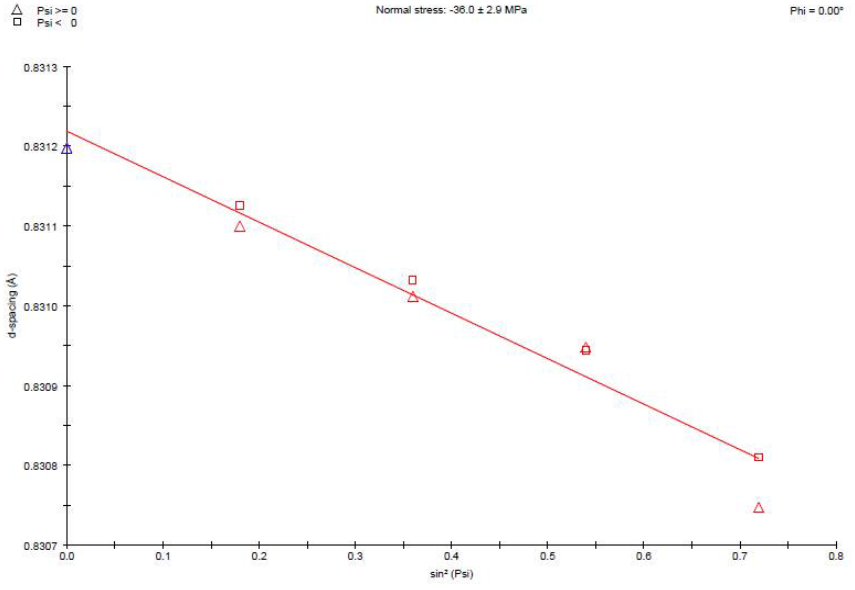
Psi >= 0
Psi < 0
Normal stress: -36.0 ± 2.9 MPa
Phi = 0.00°
d-spacing (Å)
sin² (Psi)

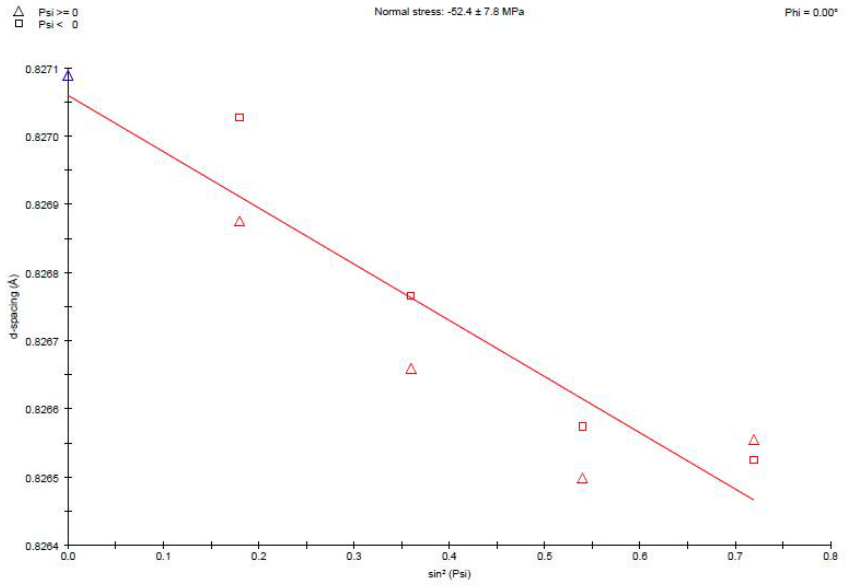
Psi >= 0
Psi < 0
Normal stress: -52.4 ± 7.8 MPa
Phi = 0.00°
d-spacing (Å)
sin² (Psi)
0.8271
0.8270
0.8269
0.8268
0.8267
0.8266
0.8265
0.8264
0.0
0.1
0.2
0.3
0.4
0.5
0.6
0.7
0.8

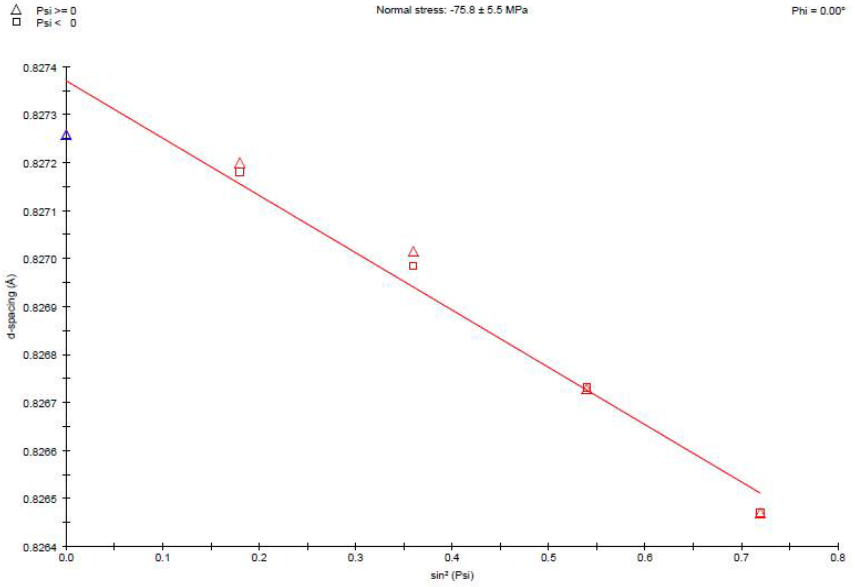
Psi >= 0
Psi < 0
Normal stress: -75.8 ± 5.5 MPa
Phi = 0.00°
d-spacing (Å)
sin² (Psi)
0.8274
0.8273
0.8272
0.8271
0.8270
0.8269
0.8268
0.8267
0.8266
0.8265
0.8264
0.0
0.1
0.2
0.3
0.4
0.5
0.6
0.7
0.8

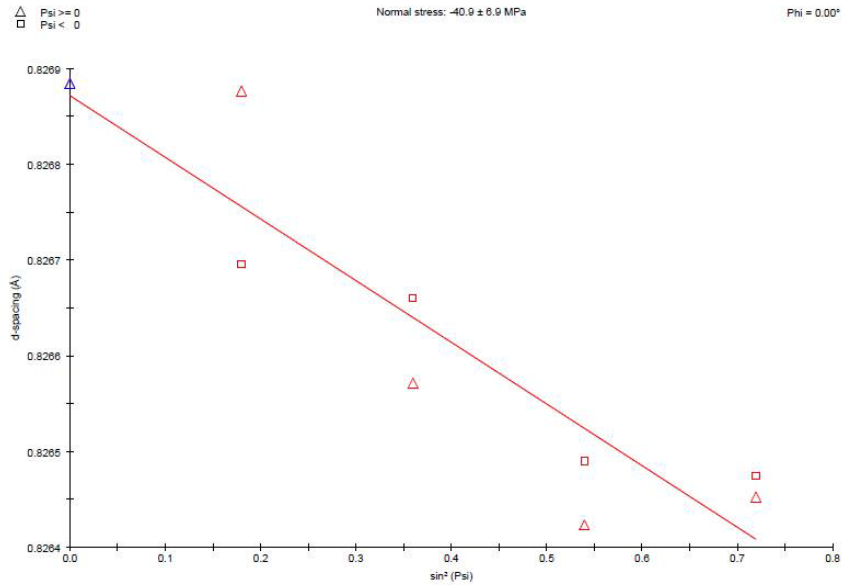
Psi >= 0
Psi < 0
Normal stress: -40.9 ± 6.9 MPa
Phi = 0.00°
d-spacing (Å)
sin² (Psi)

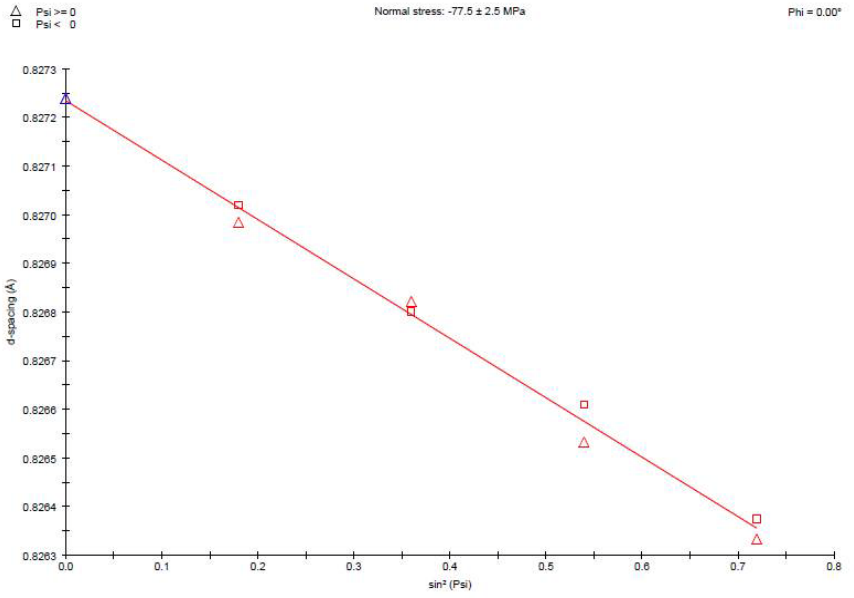
Psi >= 0
Psi < 0
Normal stress: -77.5 ± 2.5 MPa
Phi = 0.00°
d-spacing (Å)
sin² (Psi)

Appendix F Oven Logs

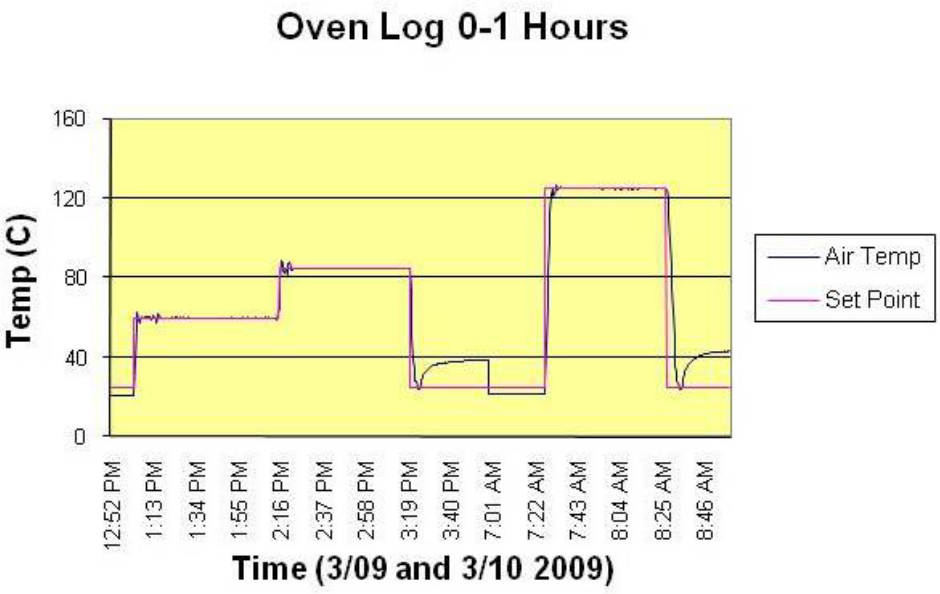

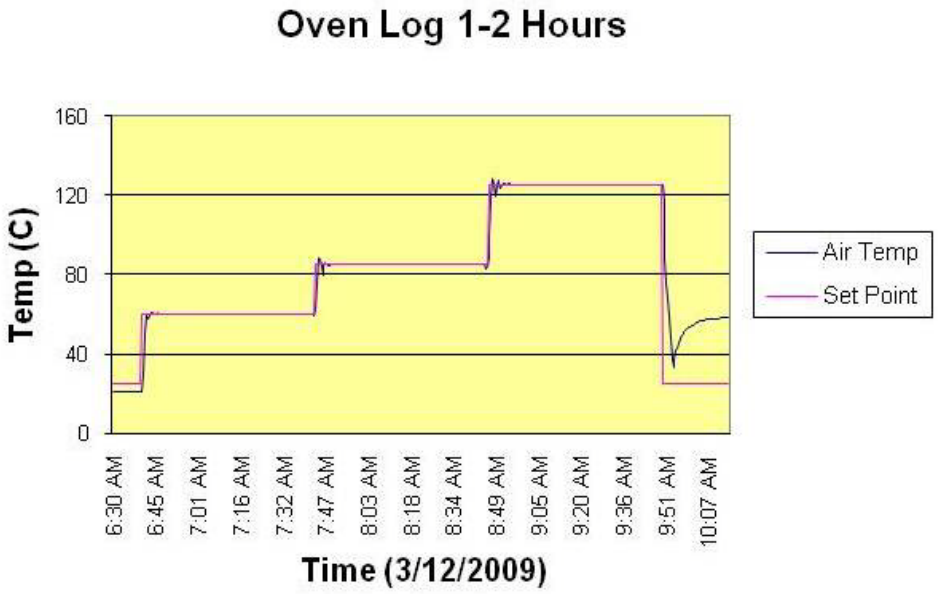

Oven Log 2-3 Hours

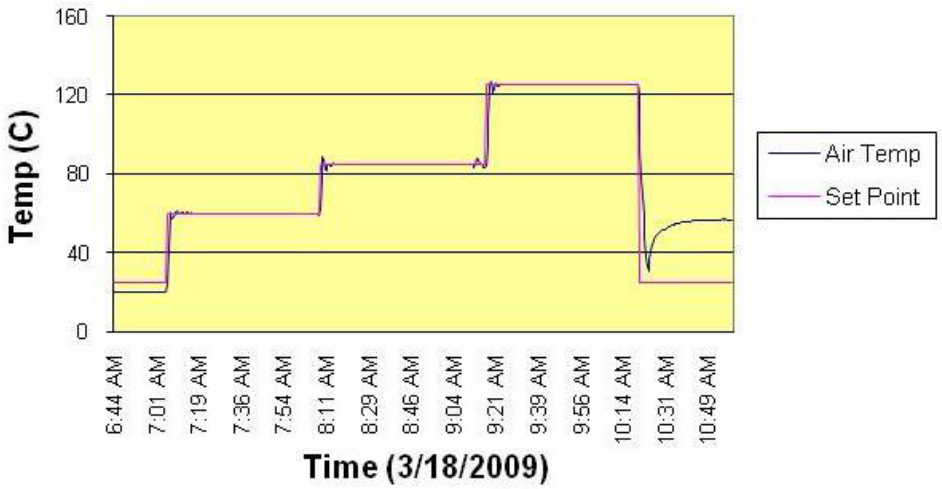

Oven Log 3-4 Hours

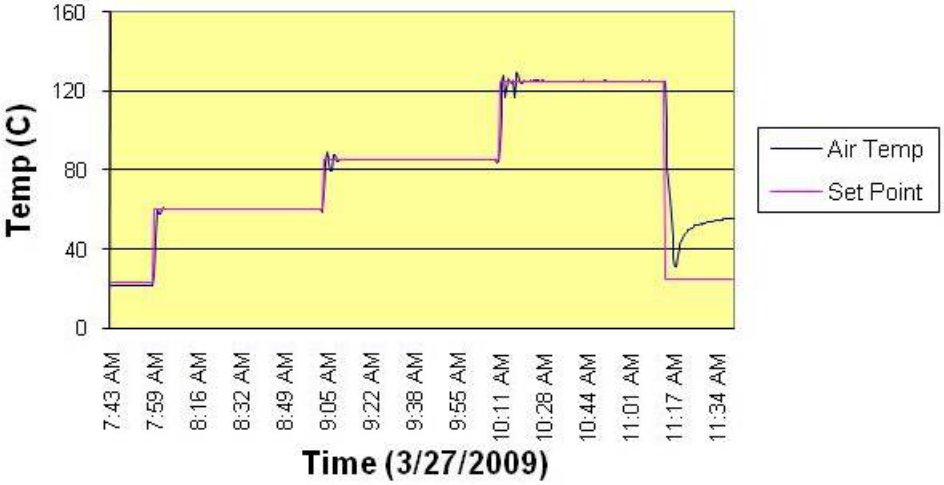

Oven Log 4-5 Hours

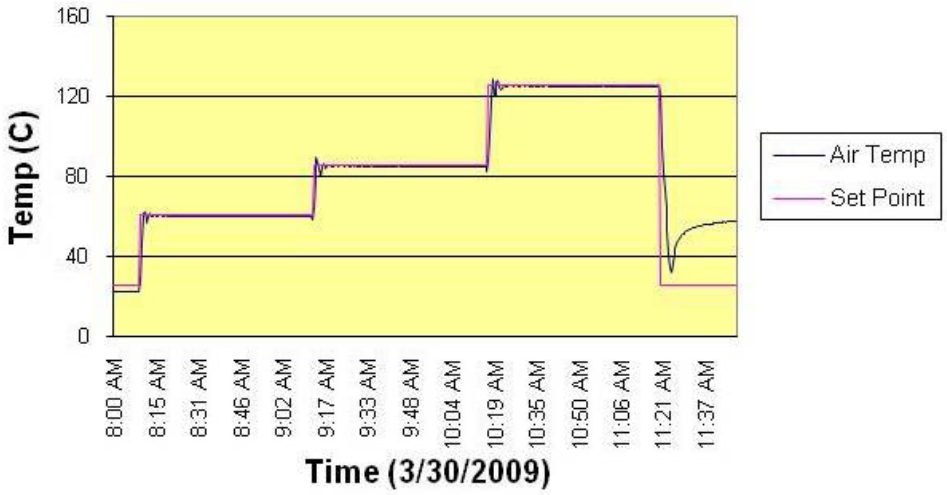

Oven Log 5-6 Hours

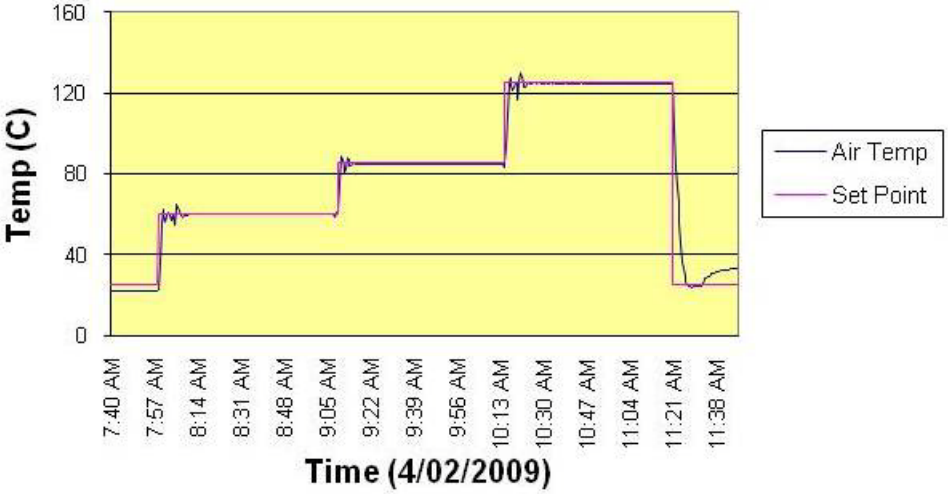

Oven Log 6-8 Hours

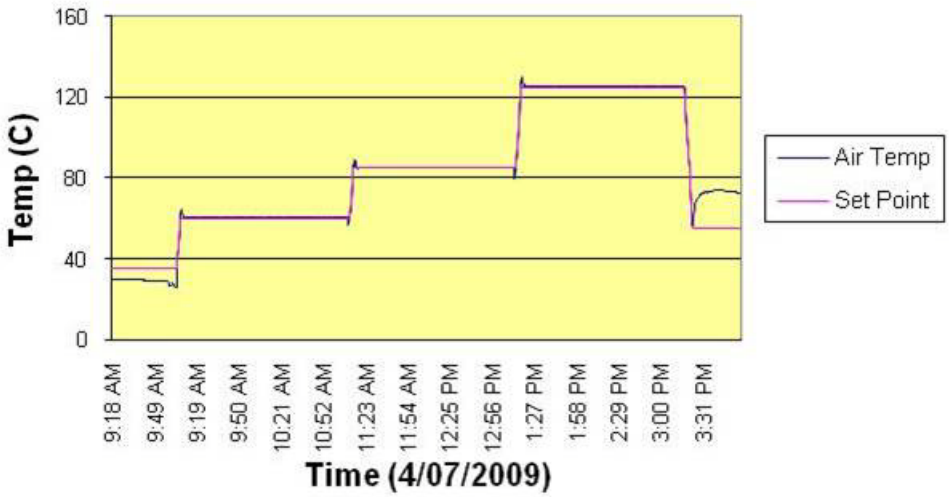

Oven Log 8-10 Hours

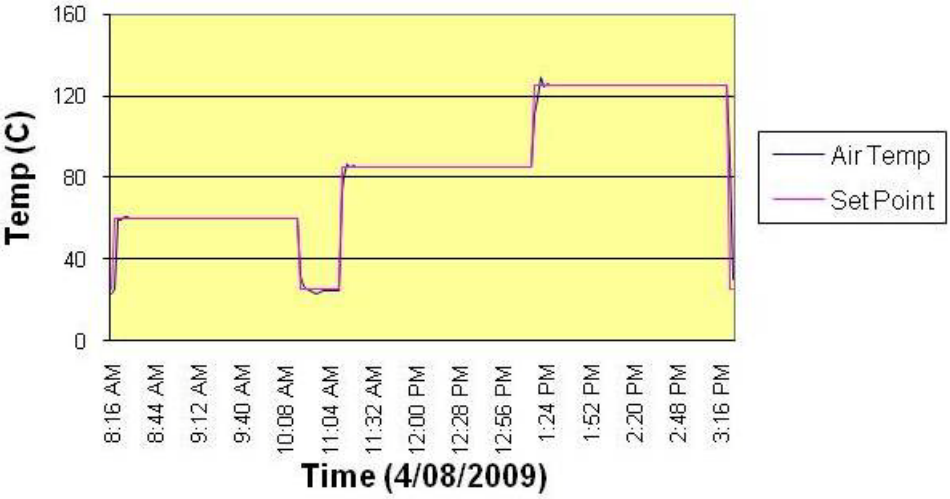

Oven Log 10-12 Hours

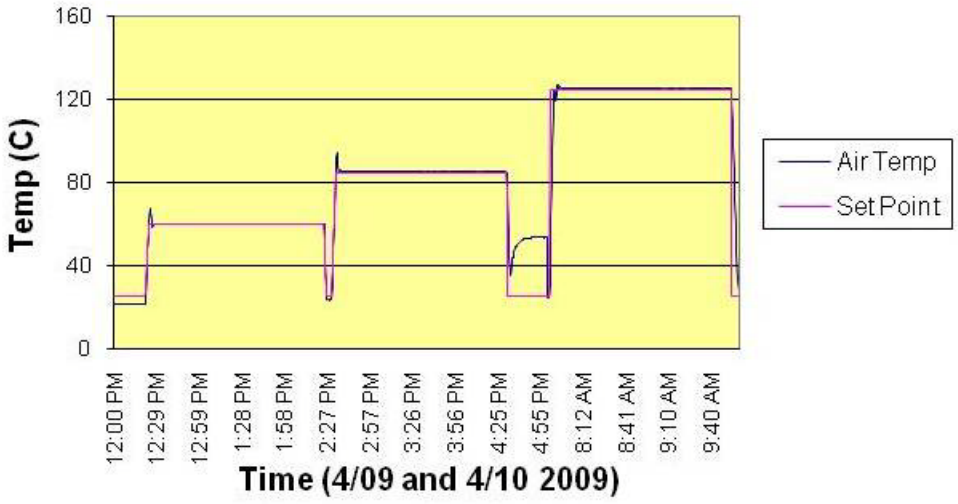

Oven Log 12-16 Hours

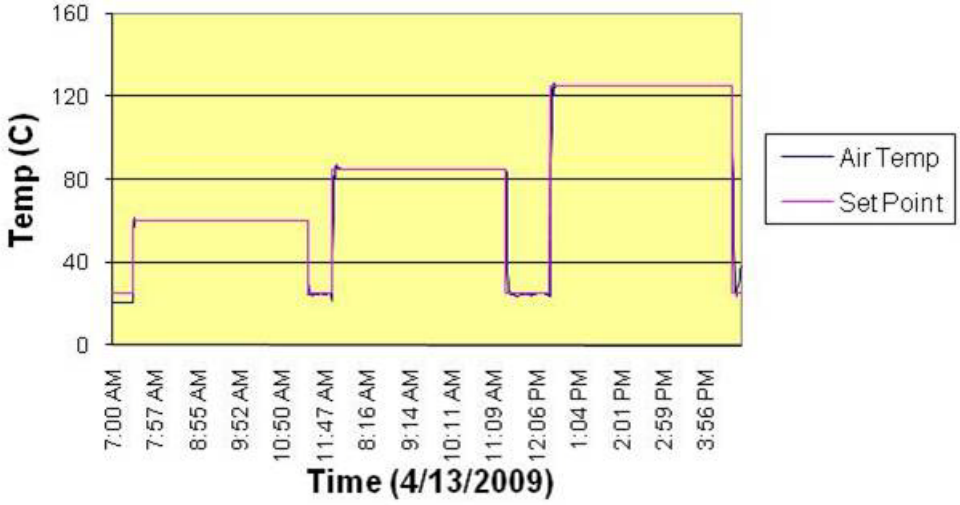

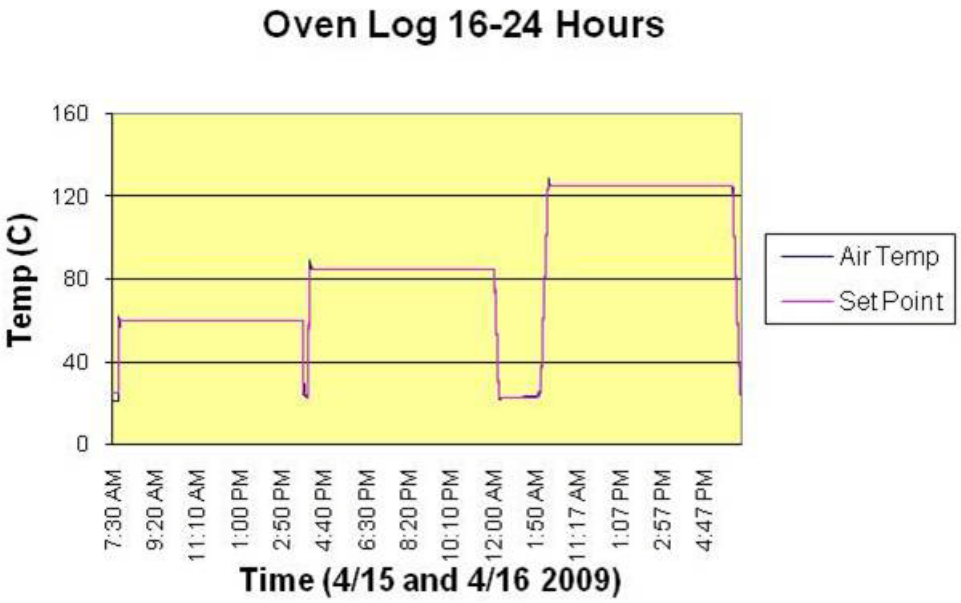
Oven Log 16-24 Hours
160
120
80
40
0
Temp (C)
7:30 AM
9:20 AM
11:10 AM
1:00 PM
2:50 PM
4:40 PM
6:30 PM
8:20 PM
10:10 PM
12:00 AM
1:50 AM
11:17 AM
1:07 PM
2:57 PM
4:47 PM
Time (4/15 and 4/16 2009)
Air Temp
Set Point

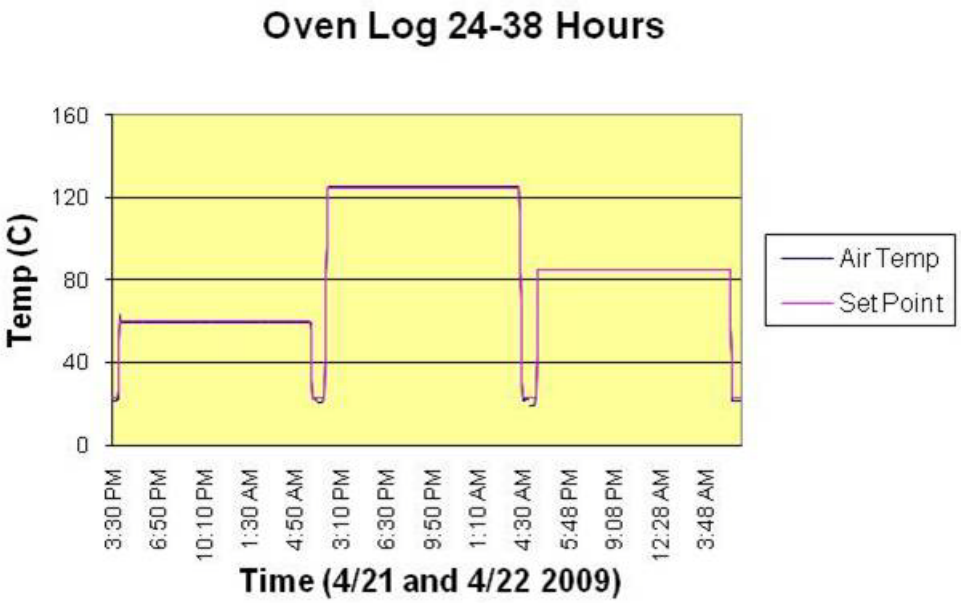
Oven Log 24-38 Hours
160
120
80
40
0
Temp (C)
3:30 PM
6:50 PM
10:10 PM
1:30 AM
4:50 AM
3:10 PM
6:30 PM
9:50 PM
1:10 AM
4:30 AM
5:48 PM
9:08 PM
12:28 AM
3:48 AM
Time (4/21 and 4/22 2009)
Air Temp
Set Point

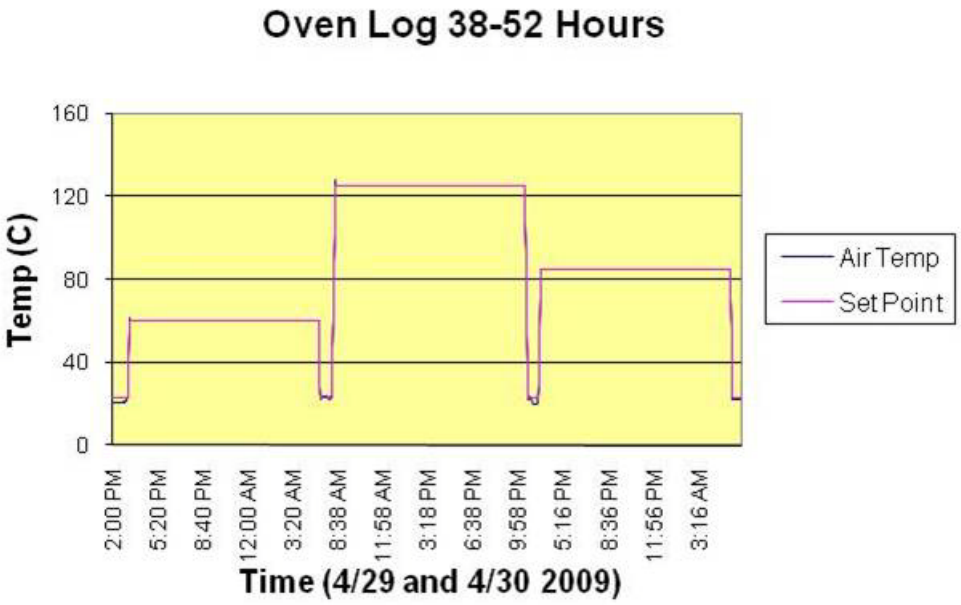
Oven Log 38-52 Hours
160
120
80
40
0
Temp (C)
2:00 PM
5:20 PM
8:40 PM
12:00 AM
3:20 AM
8:38 AM
11:58 AM
3:18 PM
6:38 PM
9:58 PM
5:16 PM
8:36 PM
11:56 PM
3:16 AM
Time (4/29 and 4/30 2009)
Air Temp
Set Point

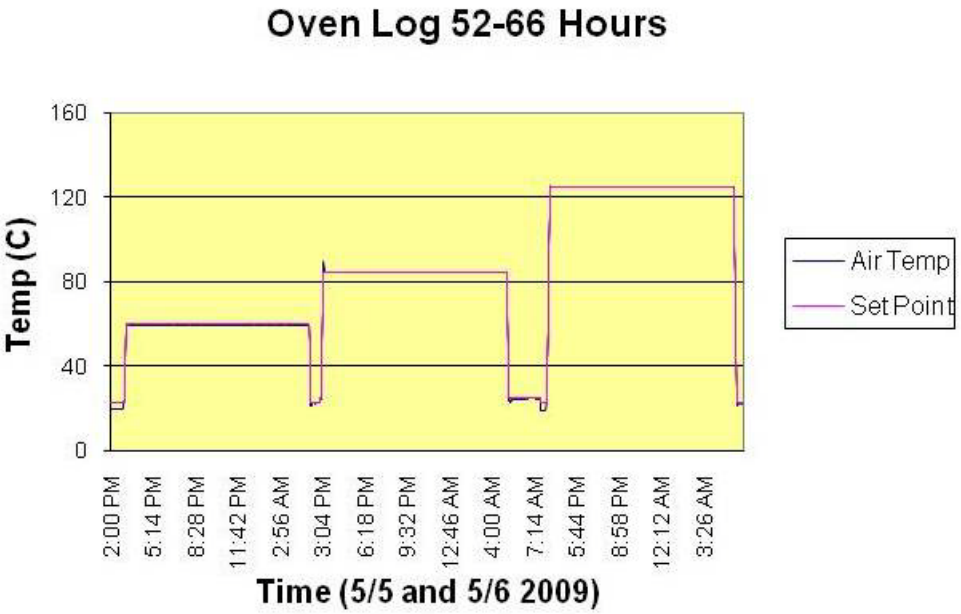
Oven Log 52-66 Hours
160
120
80
40
0
Temp (C)
2:00 PM
5:14 PM
8:28 PM
11:42 PM
2:56 AM
3:04 PM
6:18 PM
9:32 PM
12:46 AM
4:00 AM
7:14 AM
5:44 PM
8:58 PM
12:12 AM
3:26 AM
Time (5/5 and 5/6 2009)
Air Temp
Set Point

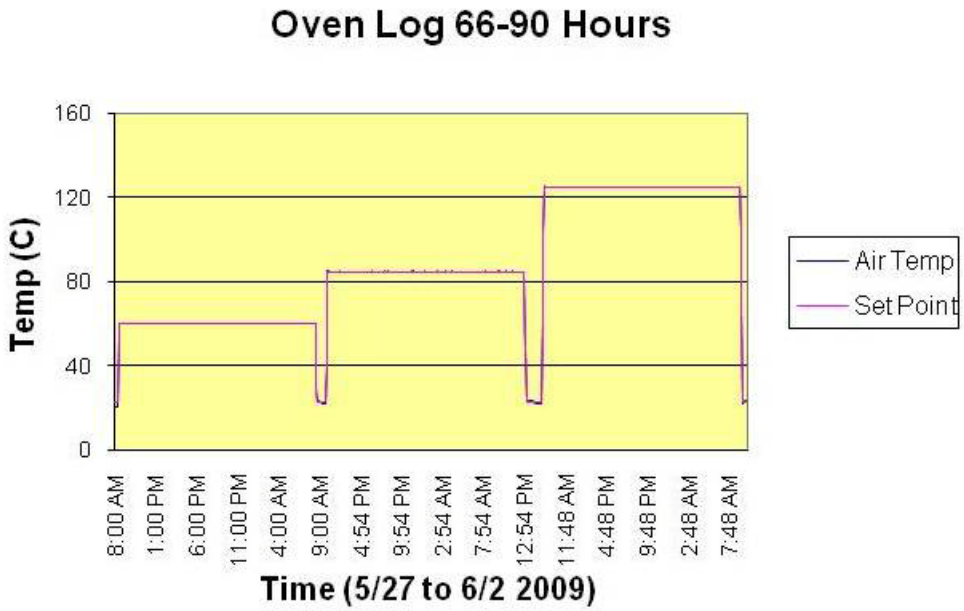
Oven Log 66-90 Hours
160
120
80
40
0
Temp (C)
8:00 AM
1:00 PM
6:00 PM
11:00 PM
4:00 AM
9:00 AM
4:54 PM
9:54 PM
2:54 AM
7:54 AM
12:54 PM
11:48 AM
4:48 PM
9:48 PM
2:48 AM
7:48 AM
Time (5/27 to 6/2 2009)
Air Temp
Set Point

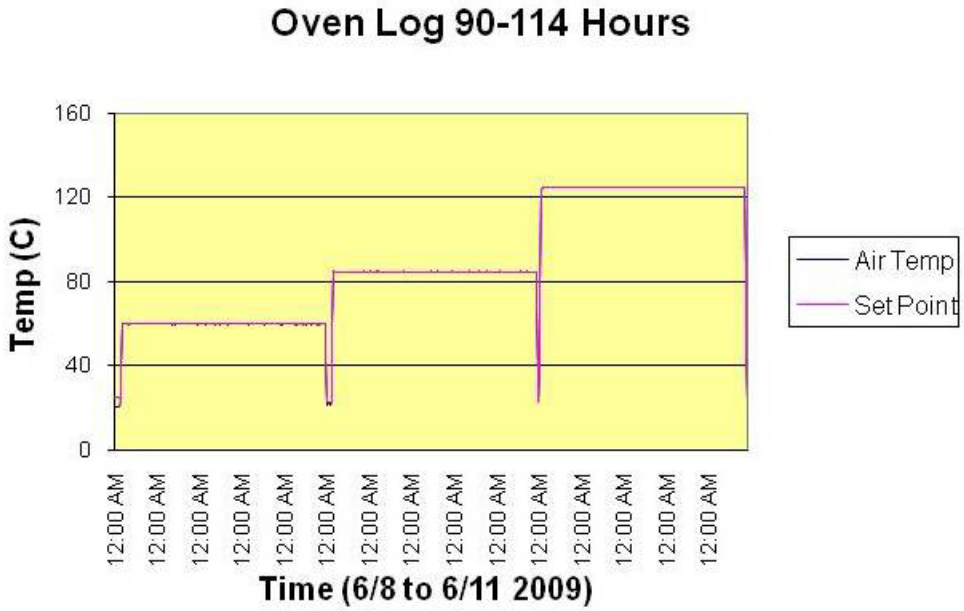
Oven Log 90-114 Hours
160
120
80
40
0
Temp (C)
12:00 AM
12:00 AM
12:00 AM
12:00 AM
12:00 AM
12:00 AM
12:00 AM
12:00 AM
12:00 AM
12:00 AM
12:00 AM
12:00 AM
12:00 AM
12:00 AM
12:00 AM
Time (6/8 to 6/11 2009)
Air Temp
Set Point

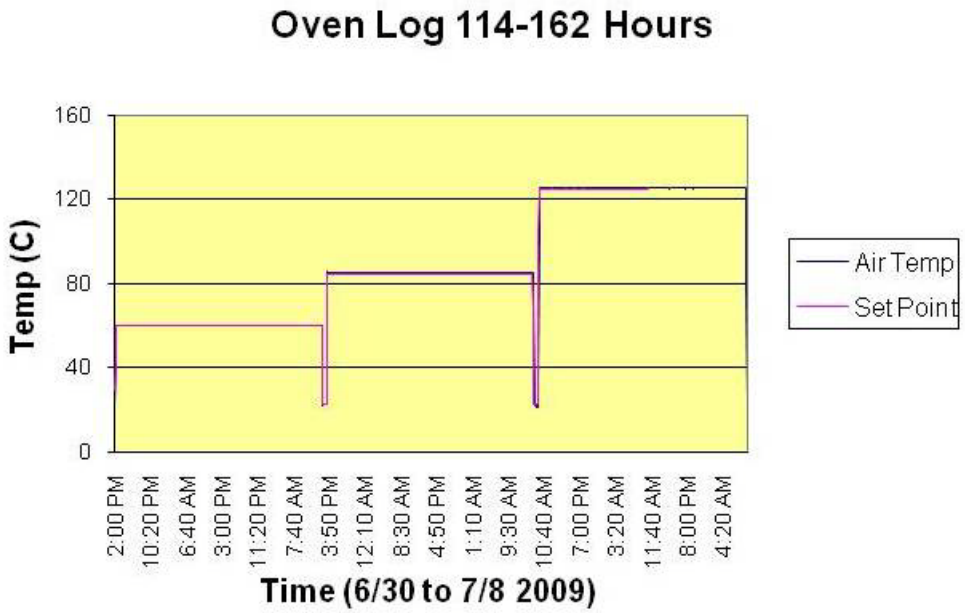
Oven Log 114-162 Hours
160
120
80
40
0
Temp (C)
2:00 PM
10:20 PM
6:40 AM
3:00 PM
11:20 PM
7:40 AM
3:50 PM
12:10 AM
8:30 AM
4:50 PM
1:10 AM
9:30 AM
10:40 AM
7:00 PM
3:20 AM
11:40 AM
8:00 PM
4:20 AM
Time (6/30 to 7/8 2009)
Air Temp
Set Point

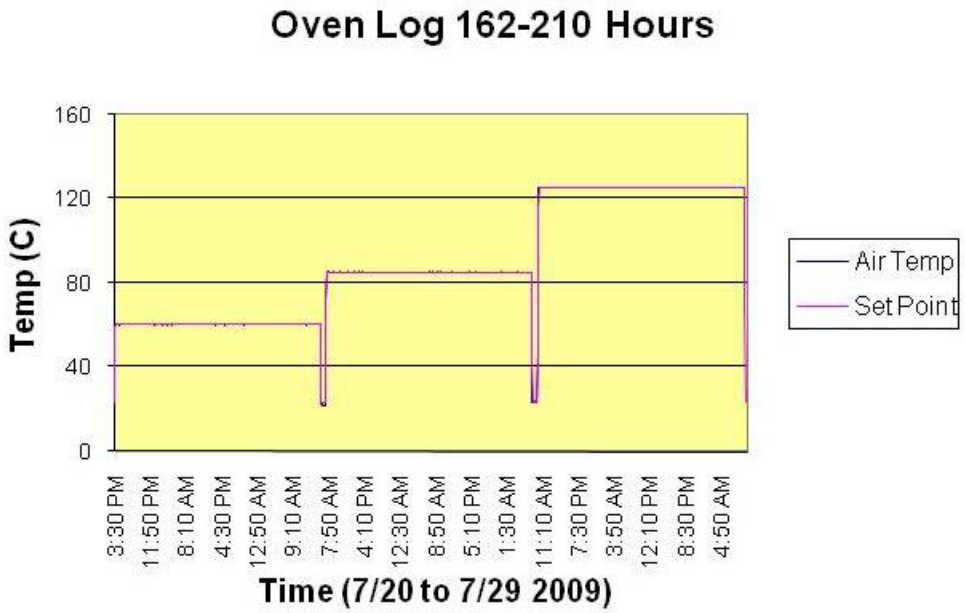
Oven Log 162-210 Hours
160
120
80
40
0
Temp (C)
3:30 PM
11:50 PM
8:10 AM
4:30 PM
12:50 AM
9:10 AM
7:50 AM
4:10 PM
12:30 AM
8:50 AM
5:10 PM
1:30 AM
11:10 AM
7:30 PM
3:50 AM
12:10 PM
8:30 PM
4:50 AM
Time (7/20 to 7/29 2009)
Air Temp
Set Point

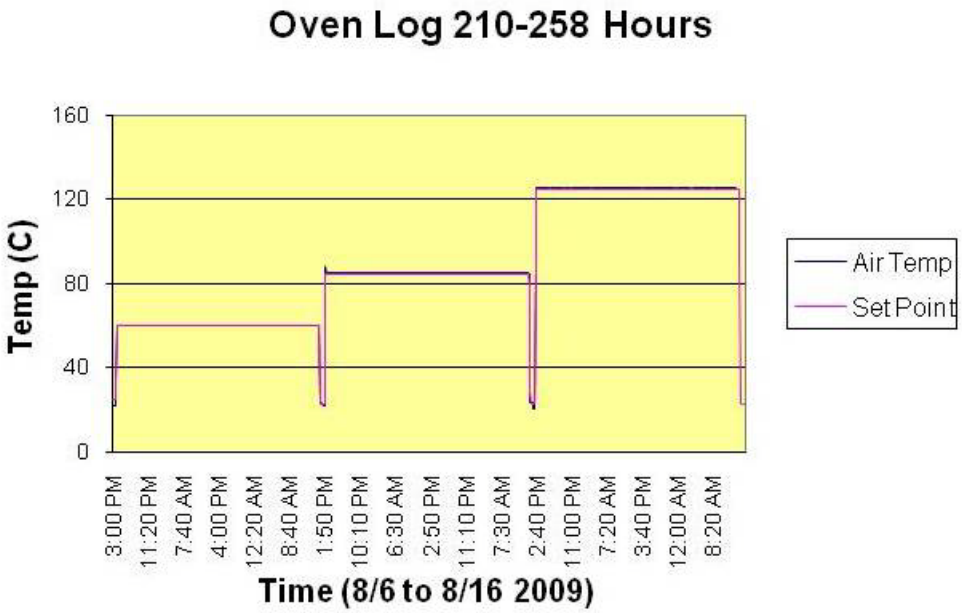
Oven Log 210-258 Hours
160
120
80
40
0
Temp (C)
3:00 PM
11:20 PM
7:40 AM
4:00 PM
12:20 AM
8:40 AM
1:50 PM
10:10 PM
6:30 AM
2:50 PM
11:10 PM
7:30 AM
2:40 PM
11:00 PM
7:20 AM
3:40 PM
12:00 AM
8:20 AM
Time (8/6 to 8/16 2009)
Air Temp
Set Point

Appendix G Curvature Measurements

	6061 Flycut	6061 Flycut	6061 Flycut	6061 Milled	6061 Milled	6061 Milled
Hour	60	85	125	60	85	125
0	68.8069	69.2642	68.8463	90.4225	94.3047	93.9096
1	68.8276	69.3055	68.9828	90.5027	94.6967	94.6968
2	68.8273	69.3345	69.1050	90.5684	95.0455	95.3759
3	68.9190	69.4179	69.2839	90.7329	95.2858	95.8302
4	68.9414	69.4210	69.3859	90.8501	95.5273	95.9813
5	68.9623	69.4667	69.5001	90.9791	95.6297	96.1730
6	68.9553	69.5338	69.6056	91.0260	95.7887	96.3678
8	68.9272	69.5804	69.7093	91.1502	95.9353	96.6438
10	68.9339	69.5923	69.7805	91.1883	96.0580	96.7716
12	69.0524	69.6554	69.8405	91.3503	96.2180	96.9730
16	69.0678	69.7118	69.9553	91.4146	96.3241	97.2505
24	69.1341	69.7387	70.0397	91.6431	96.6121	97.6295
38	69.1794	69.8903	70.2417	91.9014	96.9132	98.0998
44						
52	69.2296	69.9813	70.2619	92.0151	97.0742	98.3891
66	69.2287	70.0664	70.4072	92.1954	97.2970	98.6805
90	69.2964	70.1404	70.4481	92.3368	97.5492	98.9534
114	69.1860	70.2311	70.5503	92.4331	97.5878	99.0378
136						
162	69.2701	70.3594	70.6051	92.5773	97.8069	99.4460
180						
210	69.2140	70.4938	70.7433	92.7331	97.9804	99.6974
258	69.2899	70.6145	70.7558	92.8072	98.0281	99.8667
285						
330	69.2825	70.7397	70.9044	92.9240	98.2995	100.1659
357						
402	69.3125	70.8443	70.9402	93.0002	98.3896	100.4151
453						
570	69.2683	70.9819	70.9236	93.1185	98.5486	100.6608
738	69.3773	71.0621	70.9598	93.2634	98.7202	100.9795
906	69.3949	71.0958	70.9418	93.3038	98.7719	101.3295
1100	69.3603	70.9899		93.3500	98.8221	101.1741

	4032 Flycut	4032 Flycut	4032 Flycut	4032 Flycut	4032 Milled	4032 Milled	4032 Milled	4032 Milled
Hour	40	50	60	85	40	50	60	85
0	150.0833	148.2130	42.1270	37.4241	124.4871	145.7699	70.3455	61.8952
1			42.1796	37.6541			70.6814	63.3105
2			42.2229	37.7369			70.9195	63.7762
3			42.2636	37.7915			71.1373	64.0327
4			42.2998	37.8334			71.3455	64.2061
5			42.3063	37.8852			71.4659	64.3937
6			42.3365	37.9105			71.5806	64.5005
8			42.3723	37.9572			71.7632	64.7192
10			42.3883	37.9873			71.8572	64.8327
12			42.4003	38.0040			71.9447	64.9640
16			42.4363	38.0516			72.0935	65.1429
24	150.8986	150.9722	42.4696	38.0999	126.4108	149.4552	72.2679	65.3988
38			42.5442	38.1248			72.5899	65.6876
44	151.2329	151.7936			126.4070	150.7304		
52			42.5862	38.1544			72.8017	65.8356
66			42.6138	38.1283			73.0073	65.9597
90			42.6423	38.1707			73.1820	66.0473
114			42.6751	38.1347			73.3718	66.1404
136	151.9925	153.8645			127.2951	153.1657		
162			42.7000				73.6442	66.2088
180	152.2313	154.3366			127.6404	153.7795		
210			42.7112				73.7893	66.2560
258			42.7170				73.9414	66.1835
285	152.2992	155.5361			128.1482	154.9020		
330			42.7201				74.0173	
357	152.2968	155.8543			128.3232	154.9955		
402			42.6800				74.1532	
453	152.2945	155.8538			128.3275	154.9961		
570							74.3237	
738								
906								
1100								

Appendix H Sensitivity Analysis

Radii are being measured that are between 30 and 150 inches on samples that are 6 inches long. We will use the published accuracy from Mitutoyo to determine how accurately these radii are being measured. The accuracy of the inspection equpment is provided for X, Y, and Z, only, and is a function of the overall range being measured.

The overall Length will be taken as 5.9 instead of 6 inches for two reasons; (1) the measured X-Y length is slightly less due to the points being slightly inboard of the edges, and (2) due to the curvature of the sample. The range of Z heights being measured is a function of the curvature. The largest and smallest cases of Z range will be examined, correponding to the largest and smallest curvature being measured.

First find the angle over which each case is being measured:

$$5.9\text{in} = 149.860\cdot\text{mm}$$

$$\text{chord} := 149.86\text{mm}$$

$$30\text{in} = 762.000\cdot\text{mm}$$

$$\text{radius}_{\text{small}} := 762.000\text{mm}$$

$$150\text{in} = 3810.000\cdot\text{mm}$$

$$\text{radius}_{\text{large}} := 3810.000\text{mm}$$

Guess Values:

$$\theta_{\text{large}} := .02\text{rad}$$

$$\theta_{\text{small}} := .01\text{rad}$$

Given

$$\sin\left(\theta_{\text{small}}\right) = \frac{0.5\cdot\text{chord}}{\text{radius}_{\text{large}}}$$

$$\sin\left(\theta_{\text{large}}\right) = \frac{0.5\cdot\text{chord}}{\text{radius}_{\text{small}}}$$

$$\text{Find}\left(\theta_{\text{large}}, \theta_{\text{small}}\right) = \begin{pmatrix} 0.0984925 \\ 0.0196679 \end{pmatrix}\cdot\text{rad}$$

Therefore

$$\theta_{large} := .098492rad$$

$$\theta_{small} := .019668rad$$

Now find the delta Z range over these angles:

Guess Value:

$$\Delta z_{small} := 5mm$$

$$\Delta z_{large} := 40mm$$

Given

$$\tan(.019668rad) = \frac{1}{radius_{large} - \Delta z_{small}} \cdot \frac{chord}{2}$$

$$\tan(.098492rad) = \frac{1}{radius_{small} - \Delta z_{large}} \cdot \frac{chord}{2}$$

$$\text{Find}\left(\Delta z_{large}, \Delta z_{small}\right) = \begin{pmatrix} 3.6891457 \\ 0.7495413 \end{pmatrix} \cdot mm$$

Therefore

$$\Delta z_{large.curvature} := 3.6891457mm$$

$$\Delta z_{small.curvature} := 0.7495413mm$$

Now we have the Z range for the largest and smallest curvatures we are measuring. Now determin error associated with each:

Guess Values:

$$Error_{z.large.curvature} := .0001mm$$

$$Error_{z.small.curvature} := .0001mm$$

Given

$$Error_{z.large.curvature} = \left(4mm + 5 \cdot \frac{\Delta z_{large.curvature}}{1000}\right) \cdot 10^{-3}$$

$$Error_{z.small.curvature} = \left(4mm + 5 \cdot \frac{\Delta z_{small.curvature}}{1000}\right) \cdot 10^{-3}$$

$$Find\left(Error_{z.large.curvature}, Error_{z.small.curvature}\right) = \begin{pmatrix} 0.004018 \\ 0.004004 \end{pmatrix} \cdot mm$$

Therefore

$$Error_{z.large.curvature} := .004018mm$$

$$Error_{z.small.curvature} := .004004mm$$

Now find the Error in the XY Measurement. Assume an X-Y range of 5.9 inches for both cases:

$$length := 149.86mm$$

Guess Values:

$$Error_{x.y} := .001mm$$

Given

$$Error_{x.y} \cdot mm = \left(2.2mm + \frac{3 \cdot length}{1000}\right) \cdot 10^{-3} mm$$

$$Find\left(Error_{x.y}\right) = 0.002650 \cdot mm$$

$$Error_{x.y} := .00265mm$$

Now run four cases to determine the error. For each radius extreme (150 and 30 inches), run two cases; one using the maximum length and minimum delta Z, and one using the minimum length and maximum delta Z.

Guess Values

$$r_{max.rad.max.length.min.z} := 3811mm$$

$$r_{max.rad.min.length.max.z} := 3809mm$$

$$r_{min.rad.max.length.min.z} := 763mm$$

$$r_{min.rad.min.length.max.z} := 761mm$$

Given

$$r_{max.rad.max.length.min.z} = \Delta z_{small.curvature} - Error_{z.small.curvature} + \frac{chord + Error_{x.y}}{2\tan(\theta_{small})}$$

$$Find(r_{max.rad.max.length.min.z}) = 3810.0633556 \cdot mm$$

$r_{max.rad.max.length.min.z} := 3810.0633556mm$

Given

$$r_{max.rad.min.length.max.z} = \Delta z_{small.curvature} + Error_{z.small.curvature} + \frac{chord - Error_{x.y}}{2\tan(\theta_{small})}$$

$$Find(r_{max.rad.min.length.max.z}) = 3809.9366444 \cdot mm$$

$r_{max.rad.min.length.max.z} := 3809.9366444mm$

Guess Value

$\Delta r_{max.rad} := .1mm$

Given

$$\Delta r_{max.rad} = r_{max.rad.max.length.min.z} - r_{max.rad.min.length.max.z}$$

$$Find(\Delta r_{max.rad}) = 0.1267112 \cdot mm$$

$0.1267112mm = 0.004989 \cdot in$

Given

$$r_{min.rad.max.length.min.z} = \Delta z_{large.curvature} - Error_{z.large.curvature} + \frac{chord + Error_{x.y}}{2\tan(\theta_{large})}$$

$$Find(r_{min.rad.max.length.min.z}) = 762.0093913 \cdot mm$$

$r_{min.rad.max.length.min.z} := 762.0093913mm$

Given

$$r_{min.rad.min.length.max.z} = \Delta z_{large.curvature} + Error_{z.large.curvature} + \frac{chord - Error_{x.y}}{2\tan(\theta_{large})}$$

$$Find(r_{min.rad.min.length.max.z}) = 761.990609 \cdot mm$$

$$r_{min.rad.min.length.max.z} := 761.9906086mm$$

Guess Values

$$\Delta r_{min.rad} := 0.1mm$$

Given

$$\Delta r_{min.rad} = r_{min.rad.max.length.min.z} - r_{min.rad.min.length.max.z}$$

$$Find(\Delta r_{min.rad}) = 0.018783 \cdot mm$$

$$.018783mm = 0.000739 \cdot in$$

The highest error of the measurement system occurs at the large radii, or the samples with the least curvature. The error in radii measurement is approx 0.13mm or .005 inches. Since the changes in curvature that are seen on machined samples are on the order of 1 inch, it can be concluded that any error contribution from the measuring equipment is negligible.

Appendix I Depth of Stressed Layer Calculation Detail

6061 FLYCUT BIMETALLIC STRIP CALCULATIONS

Assign Known Values. The stress measured directly using XRD is assigned "Resultant Stress" as it was measured after the samples were allowed to elastically curl. "Initial Stress" is the value of the stress in the stressed layer as it was fixtured flat during machining:

$$E_a := 10471297\text{psi}$$

$$E_b := 10471297\text{psi}$$

$$\text{Thickness} := .03525\text{in}$$

$$\sigma_{re} := \frac{-24700 + -24700}{2}\text{psi}$$

$$\kappa := \frac{2}{-70.838\text{in} + -67.840\text{in}}$$

A system of 3 equations and 3 unknowns is used to solve for initial (uncurved) stress, and the two layer thickness. The thin stressed layer is assigned subscript "A":

Guess Values

$$h_a := .004\text{in}$$

$$h_b := .032\text{in}$$

$$\sigma_{initial} := 15000\text{psi}$$

Given

$$\kappa = \frac{6 \cdot E_a \cdot E_b \left(h_a + h_b\right) h_a \cdot h_b \cdot \frac{\sigma_{initial}}{E_a}}{E_a^{\,2} h_a^{\,4} + 4 \cdot E_a E_b \cdot h_a^{\,3} h_b + 6 \cdot E_a E_b \cdot h_a^{\,2} h_b^{\,2} + 4 \cdot E_a E_b \cdot h_a h_b^{\,3} + E_b^{\,2} h_b^{\,4}}$$

$$h_a + h_b = \text{Thickness}$$

$$\sigma_{re} = \frac{-\sigma_{initial} \cdot E_b}{E_a \cdot \left[4 + 6 \cdot \frac{h_a}{h_b} + 4 \cdot \left(\frac{h_a}{h_b}\right)^2 + \frac{E_a}{E_b} \cdot \left(\frac{h_a}{h_b}\right)^3 + \frac{E_b \cdot h_b}{E_a \cdot h_a}\right]} \cdot \left[3 \cdot \frac{h_a}{h_b} + 2 \cdot \left(\frac{h_a}{h_b}\right)^2 - \frac{E_b \cdot h_b}{E_a \cdot h_a}\right]$$

$x := \text{Find}(h_a, h_b, \sigma_{initial})$

$$x \text{ float}, 5 \rightarrow \begin{pmatrix} 0.001143 \cdot in \\ 0.034107 \cdot in \\ -28279.0 \cdot psi \end{pmatrix}$$

These values are now assigned as constant for the remaining stress distribution calcuations:

$$h_A := .001143in$$
$$h_B := .034107in$$
$$\sigma_{in} := -28279psi$$

INTERNAL STRESS CALCULATIONS

The following values of Young's Modulus made by direct measurement at temperature are assigned. Since layer A and B are the same material, the subscript will be dropped from the Modulus term:

$$E_{6061} := 10471297psi$$
$$E_{6061} = 72197051 \cdot kPa$$

The following expressions are used in the bimetallic strip calculations and are taken from Timoshenko (1925). The misfit strain term has been substituted with the misfit strain term that describes the residually stress machining layer:

$$l_A := \frac{h_A^3}{12} \qquad l_B := \frac{h_B^3}{12} \qquad h := h_A + h_B \qquad \Delta\varepsilon := \frac{\sigma_{in}}{E_{6061}}$$

$$\rho := \frac{\frac{h}{2} + 2 \cdot \frac{\left(E_{6061} \cdot l_A + E_{6061} \cdot l_B\right)}{h} \cdot \left(\frac{1}{E_{6061} \cdot h_A} + \frac{1}{E_{6061} \cdot h_B}\right)}{\Delta\varepsilon} \qquad P := 2\frac{\left(E_{6061} \cdot l_A + E_{6061} \cdot l_B\right)}{h \cdot \rho}$$

The stress magnitues are now calculated for each layer at the exterior surface and at the interface:

$$\sigma_{A.surface} := \frac{P}{h_A} - \frac{h_A \cdot E_{6061}}{2 \cdot \rho}$$
$$\sigma_{A.surface} = -24700 \cdot psi$$
$$\sigma_{A.surface} = -170303 \cdot kPa$$

$$\sigma_{A.interface} := \frac{P}{h_A} + \frac{h_A \cdot E_{6061}}{2 \cdot \rho}$$
$$\sigma_{A.interface} = -24873 \cdot psi$$
$$\sigma_{A.interface} = -171493 \cdot kPa$$

$$\sigma_{B.interface} := -\frac{P}{h_B} - \frac{h_B \cdot E_{6061}}{2 \cdot \rho}$$
$$\sigma_{B.interface} = 3406 \cdot psi$$
$$\sigma_{B.interface} = 23484 \cdot kPa$$

$$\sigma_{B.surface} := -\frac{P}{h_B} + \frac{h_B \cdot E_{6061}}{2 \cdot \rho}$$
$$\sigma_{B.surface} = -1745 \cdot psi$$
$$\sigma_{B.surface} = -12029 \cdot kPa$$

The stress magnitues are now plotted as a funcion of depth through the thickness of the coupon:

$$x := 0in, .0001in .. h$$

$$\sigma_{profile}(x) := if\left[x < h_A, \sigma_{A.surface} + \left(\frac{\sigma_{A.interface} - \sigma_{A.surface}}{h_A}\right)\cdot x, \sigma_{B.interface} + \left(\frac{\sigma_{B.surface} - \sigma_{B.interface}}{h_B}\right)\cdot\left(x - h_A\right)\right]$$

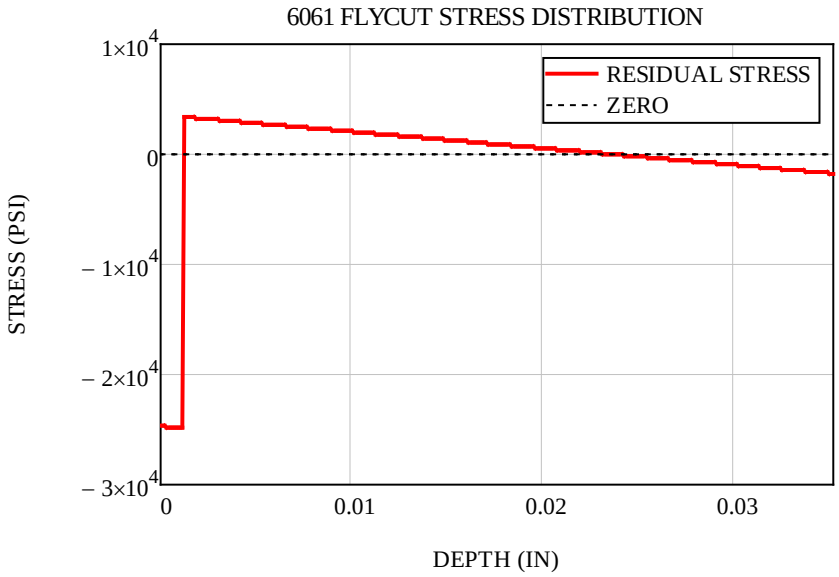

6061 MILLED BIMETALLIC STRIP CALCULATIONS

Assign Known Values. The stress measured directly using XRD is assigned "Resultant Stress" as it was measured after the samples were allowed to elastically curl. "Initial Stress" is the value of the stress in the stressed layer as it was fixtured flat during machining:

$$E_a := 10471297\text{psi}$$

$$E_b := 10471297\text{psi}$$

$$\text{Thickness} := .0355\text{in}$$

$$\sigma_{re} := \frac{-22400 + -22500}{2}\text{psi}$$

$$\kappa := \frac{2}{-107.937\text{in} + -91.885\text{in}}$$

A system of 3 equations and 3 unknowns is used to solve for initial (uncurved) stress, and the two layer thickness. The thin stressed layer is assigned subscript "A":

Guess Values

$$h_a := .004\text{in}$$

$$h_b := .032\text{in}$$

$$\sigma_{initial} := 15000\text{psi}$$

Given

$$\kappa = \frac{6\cdot E_a\cdot E_b\left(h_a + h_b\right)h_a\cdot h_b\cdot\frac{\sigma_{initial}}{E_a}}{E_a{}^2 h_a{}^4 + 4\cdot E_a E_b\cdot h_a{}^3 h_b + 6\cdot E_a E_b\cdot h_a{}^2 h_b{}^2 + 4\cdot E_a E_b\cdot h_a h_b{}^3 + E_b{}^2 h_b{}^4}$$

$$h_a + h_b = \text{Thickness}$$

$$\sigma_{re} = \frac{-\sigma_{initial}\cdot E_b}{E_a\cdot\left[4 + 6\cdot\frac{h_a}{h_b} + 4\cdot\left(\frac{h_a}{h_b}\right)^2 + \frac{E_a}{E_b}\cdot\left(\frac{h_a}{h_b}\right)^3 + \frac{E_b\cdot h_b}{E_a\cdot h_a}\right]}\cdot\left[3\cdot\frac{h_a}{h_b} + 2\cdot\left(\frac{h_a}{h_b}\right)^2 - \frac{E_b\cdot h_b}{E_a\cdot h_a}\right]$$

$x := \text{Find}(h_a, h_b, \sigma_{initial})$

$$x \text{ float}, 5 \rightarrow \begin{pmatrix} 0.00090553 \cdot in \\ 0.034594 \cdot in \\ -24947.0 \cdot psi \end{pmatrix}$$

These values are now assigned as constant for the remaining stress distribution calcuations:

$$h_A := .00090553in$$

$$h_B := .034594in$$

$$\sigma_{in} := -24947psi$$

INTERNAL STRESS CALCULATIONS

The following values of Young's Modulus made by direct measurement at temperature are assigned. Since layer A and B are the same material, the subscript will be dropped from the Modulus term:

$$E_{6061} := 10471297.21psi$$

$$E_{6061} = 72197053 \cdot kPa$$

The following expressions are used in the bimetallic strip calculations and are taken from Timoshenko (1925). The misfit strain term has been substituted with the misfit strain term that describes the residually stress machining layer:

$$I_A := \frac{h_A^3}{12} \qquad I_B := \frac{h_B^3}{12} \qquad h := h_A + h_B \qquad \Delta\varepsilon := \frac{\sigma_{in}}{E_{6061}}$$

$$\rho := \frac{\frac{h}{2} + 2 \cdot \frac{\left(E_{6061} \cdot I_A + E_{6061} \cdot I_B\right)}{h} \cdot \left(\frac{1}{E_{6061} \cdot h_A} + \frac{1}{E_{6061} \cdot h_B}\right)}{\Delta\varepsilon} \qquad P := 2 \frac{\left(E_{6061} \cdot I_A + E_{6061} \cdot I_B\right)}{h \cdot \rho}$$

The stress magnitues are now calculated for each layer at the exterior surface and at the interface:

$$\sigma_{A.surface} := \frac{P}{h_A} - \frac{h_A \cdot E_{6061}}{2 \cdot \rho}$$

$$\sigma_{A.surface} = -22450 \cdot psi$$

$$\sigma_{A.surface} = -154789 \cdot kPa$$

$$\sigma_{A.interface} := \frac{P}{h_A} + \frac{h_A \cdot E_{6061}}{2 \cdot \rho}$$

$$\sigma_{A.interface} = -22545 \cdot psi$$

$$\sigma_{A.interface} = -155444 \cdot kPa$$

$$\sigma_{B.interface} := -\frac{P}{h_B} - \frac{h_B \cdot E_{6061}}{2 \cdot \rho}$$

$$\sigma_{B.interface} = 2402 \cdot psi$$

$$\sigma_{B.interface} = 16560 \cdot kPa$$

$$\sigma_{B.surface} := -\frac{P}{h_B} + \frac{h_B \cdot E_{6061}}{2 \cdot \rho}$$

$$\sigma_{B.surface} = -1224 \cdot psi$$

$$\sigma_{B.surface} = -8439 \cdot kPa$$

The stress magnitues are now plotted as a funcion of depth through the thickness of the coupon:

$$x := 0in, .0001in .. h$$

$$\sigma_{profile}(x) := if\left[x < h_A, \sigma_{A.surface} + \left(\frac{\sigma_{A.interface} - \sigma_{A.surface}}{h_A}\right)\cdot x, \sigma_{B.interface} + \left(\frac{\sigma_{B.surface} - \sigma_{B.interface}}{h_B}\right)\cdot\left(x - h_A\right)\right]$$

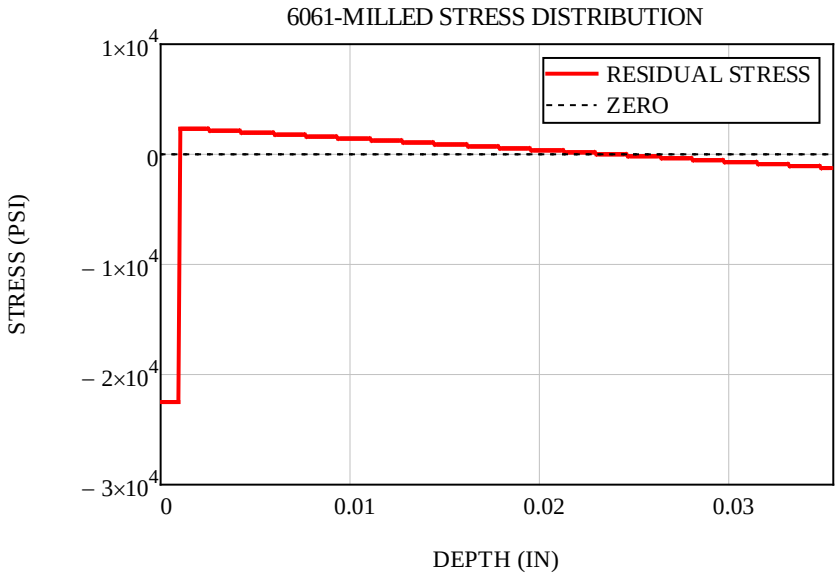

4032 FLYCUT BIMETALLIC STRIP CALCULATIONS

Assign Known Values. The stress measured directly using XRD is assigned "Resultant Stress" as it was measured after the samples were allowed to elastically curl. "Initial Stress" is the value of the stress in the stressed layer as it was fixtured flat during machining:

$$E_a := 10938460\text{psi}$$

$$E_b := 10938460\text{psi}$$

$$\text{Thickness} := .0355\text{in}$$

$$\sigma_{re} := \frac{-26000 + -27800}{2}\text{psi}$$

$$\kappa := \frac{2}{-47.543\text{in} + -42.856\text{in}}$$

A system of 3 equations and 3 unknowns is used to solve for initial (uncurved) stress, and the two layer thickness. The thin stressed layer is assigned subscript "A":

Guess Values

$$h_a := .004\text{in}$$

$$h_b := .032\text{in}$$

$$\sigma_{initial} := 15000\text{psi}$$

Given

$$\kappa = \frac{6\cdot E_a\cdot E_b\left(h_a + h_b\right)h_a\cdot h_b\cdot\frac{\sigma_{initial}}{E_a}}{E_a{}^2 h_a{}^4 + 4\cdot E_a E_b\cdot h_a{}^3 h_b + 6\cdot E_a E_b\cdot h_a{}^2 h_b{}^2 + 4\cdot E_a E_b\cdot h_a h_b{}^3 + E_b{}^2 h_b{}^4}$$

$$h_a + h_b = \text{Thickness}$$

$$\sigma_{re} = \frac{-\sigma_{initial}\cdot E_b}{E_a\cdot\left[4 + 6\cdot\frac{h_a}{h_b} + 4\cdot\left(\frac{h_a}{h_b}\right)^2 + \frac{E_a}{E_b}\cdot\left(\frac{h_a}{h_b}\right)^3 + \frac{E_b\cdot h_b}{E_a\cdot h_a}\right]}\cdot\left[3\cdot\frac{h_a}{h_b} + 2\cdot\left(\frac{h_a}{h_b}\right)^2 - \frac{E_b\cdot h_b}{E_a\cdot h_a}\right]$$

$x := \text{Find}(h_a, h_b, \sigma_{initial})$

$$x \text{ float}, 5 \rightarrow \begin{pmatrix} 0.0016294 \cdot in \\ 0.033871 \cdot in \\ -32696.0 \cdot psi \end{pmatrix}$$

These values are now assigned as constant for the remaining stress distribution calcuations:

$$h_A := .0016294in$$
$$h_B := .033871in$$
$$\sigma_{in} := -32696.0psi$$

INTERNAL STRESS CALCULATIONS

The following values of Young's Modulus made by direct measurement at temperature are assigned. Since layer A and B are the same material, the subscript will be dropped from the Modulus term:

$$E_{4032} := 10938460psi$$
$$E_{4032} = 75418027 \cdot kPa$$

The following expressions are used in the bimetallic strip calculations and are taken fromTimoshenko (1925). The misfit strain term has been substituted with the misfit strain term that describes the residually stressmachining layer:

$$l_A := \frac{h_A^3}{12} \qquad l_B := \frac{h_B^3}{12} \qquad h := h_A + h_B \qquad \Delta\varepsilon := \frac{\sigma_{in}}{E_{4032}}$$

$$\rho := \frac{\frac{h}{2} + 2 \cdot \frac{\left(E_{4032} \cdot l_A + E_{4032} \cdot l_B\right)}{h} \cdot \left(\frac{1}{E_{4032} \cdot h_A} + \frac{1}{E_{4032} \cdot h_B}\right)}{\Delta\varepsilon} \qquad P := 2\frac{\left(E_{4032} \cdot l_A + E_{4032} \cdot l_B\right)}{h \cdot \rho}$$

The stress magnitues are now calculated for each layer at the exterior surface and at the interface:

$$\sigma_{A.surface} := \frac{P}{h_A} - \frac{h_A \cdot E_{4032}}{2 \cdot \rho}$$
$$\sigma_{A.surface} = -26900 \cdot psi$$
$$\sigma_{A.surface} = -185468 \cdot kPa$$

$$\sigma_{A.interface} := \frac{P}{h_A} + \frac{h_A \cdot E_{4032}}{2 \cdot \rho}$$
$$\sigma_{A.interface} = -27294 \cdot psi$$
$$\sigma_{A.interface} = -188187 \cdot kPa$$

$$\sigma_{B.interface} := -\frac{P}{h_B} - \frac{h_B \cdot E_{4032}}{2 \cdot \rho}$$
$$\sigma_{B.interface} = 5402 \cdot psi$$
$$\sigma_{B.interface} = 37244 \cdot kPa$$

$$\sigma_{B.surface} := -\frac{P}{h_B} + \frac{h_B \cdot E_{4032}}{2 \cdot \rho}$$
$$\sigma_{B.surface} = -2795 \cdot psi$$
$$\sigma_{B.surface} = -19269 \cdot kPa$$

The stress magnitues are now plotted as a funcion of depth through the thickness of the coupon:

$$x := 0in, .0001in .. h$$

$$\sigma_{profile}(x) := if\left[x < h_A, \sigma_{A.surface} + \left(\frac{\sigma_{A.interface} - \sigma_{A.surface}}{h_A}\right)\cdot x, \sigma_{B.interface} + \left(\frac{\sigma_{B.surface} - \sigma_{B.interface}}{h_B}\right)\cdot\left(x - h_A\right)\right]$$

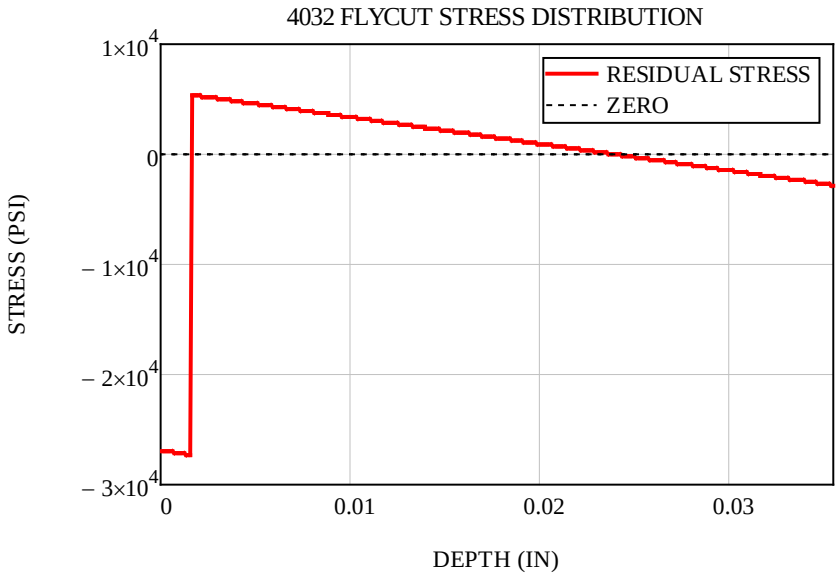

4032 MILLED BIMETALLIC STRIP CALCULATIONS

Assign Known Values. The stress measured directly using XRD is assigned "Resultant Stress" as it was measured after the samples were allowed to elastically curl. "Initial Stress" is the value of the stress in the stressed layer as it was fixtured flat during machining:

$$E_a := 10938460\text{psi}$$

$$E_b := 10938460\text{psi}$$

$$\text{Thickness} := .036\text{in}$$

$$\sigma_{re} := \frac{-29500 + -23600}{2}\text{psi}$$

$$\kappa := \frac{2}{-93.799\text{in} + -64.267\text{in}}$$

A system of 3 equations and 3 unknowns is used to solve for initial (uncurved) stress, and the two layer thickness. The thin stressed layer is assigned subscript "A":

Guess Values

$$h_a := .004\text{in}$$

$$h_b := .032\text{in}$$

$$\sigma_{initial} := 15000\text{psi}$$

Given

$$\kappa = \frac{6\cdot E_a\cdot E_b\left(h_a + h_b\right)h_a\cdot h_b\cdot\frac{\sigma_{initial}}{E_a}}{E_a^{\,2}h_a^{\,4} + 4\cdot E_a E_b\cdot h_a^{\,3}h_b + 6\cdot E_a E_b\cdot h_a^{\,2}h_b^{\,2} + 4\cdot E_a E_b\cdot h_a h_b^{\,3} + E_b^{\,2}h_b^{\,4}}$$

$$h_a + h_b = \text{Thickness}$$

$$\sigma_{re} = \frac{-\sigma_{initial}\cdot E_b}{E_a\cdot\left[4 + 6\cdot\frac{h_a}{h_b} + 4\cdot\left(\frac{h_a}{h_b}\right)^2 + \frac{E_a}{E_b}\cdot\left(\frac{h_a}{h_b}\right)^3 + \frac{E_b\cdot h_b}{E_a\cdot h_a}\right]}\cdot\left[3\cdot\frac{h_a}{h_b} + 2\cdot\left(\frac{h_a}{h_b}\right)^2 - \frac{E_b\cdot h_b}{E_a\cdot h_a}\right]$$

$$x := \text{Find}(h_a, h_b, \sigma_{initial})$$

$$x \text{ float}, 5 \rightarrow \begin{pmatrix} 0.0010294 \cdot in \\ 0.034971 \cdot in \\ -29896.0 \cdot psi \end{pmatrix}$$

These values are now assigned as constant for the remaining stress distribution calcuations:

$$h_A := .0010294in$$

$$h_B := .034971in$$

$$\sigma_{in} := -29896.0psi$$

INTERNAL STRESS CALCULATIONS

The following values of Young's Modulus made by direct measurement at temperature are assigned. Since layer A and B are the same material, the subscript will be dropped from the Modulus term:

$$E_{4032} := 10938460.87psi$$

$$E_{4032} = 75418033 \cdot kPa$$

The following expressions are used in the bimetallic strip calculations and are taken fromTimoshenko (1925). The misfit strain term has been substituted with the misfit strain term that describes the residually stressmachining layer:

$$l_A := \frac{h_A^3}{12} \qquad l_B := \frac{h_B^3}{12} \qquad h := h_A + h_B \qquad \Delta\varepsilon := \frac{\sigma_{in}}{E_{4032}}$$

$$\rho := \frac{\frac{h}{2} + 2 \cdot \frac{\left(E_{4032} \cdot l_A + E_{4032} \cdot l_B\right)}{h} \cdot \left(\frac{1}{E_{4032} \cdot h_A} + \frac{1}{E_{4032} \cdot h_B}\right)}{\Delta\varepsilon} \qquad P := 2\frac{\left(E_{4032} \cdot l_A + E_{4032} \cdot l_B\right)}{h \cdot \rho}$$

The stress magnitues are now calculated for each layer at the exterior surface and at the interface:

$$\sigma_{A.surface} := \frac{P}{h_A} - \frac{h_A \cdot E_{4032}}{2 \cdot \rho}$$

$$\sigma_{A.surface} = -26550 \cdot psi$$

$$\sigma_{A.surface} = -183055 \cdot kPa$$

$$\sigma_{A.interface} := \frac{P}{h_A} + \frac{h_A \cdot E_{4032}}{2 \cdot \rho}$$

$$\sigma_{A.interface} = -26692 \cdot psi$$

$$\sigma_{A.interface} = -184038 \cdot kPa$$

$$\sigma_{B.interface} := -\frac{P}{h_B} - \frac{h_B \cdot E_{4032}}{2 \cdot \rho}$$

$$\sigma_{B.interface} = 3204 \cdot psi$$

$$\sigma_{B.interface} = 22088 \cdot kPa$$

$$\sigma_{B.surface} := -\frac{P}{h_B} + \frac{h_B \cdot E_{4032}}{2 \cdot \rho}$$

$$\sigma_{B.surface} = -1636 \cdot psi$$

$$\sigma_{B.surface} = -11282 \cdot kPa$$

The stress magnitues are now plotted as a funcion of depth through the thickness of the coupon:

$$x := 0in, .0001in .. h$$

$$\sigma_{profile}(x) := if\left[x < h_A, \sigma_{A.surface} + \left(\frac{\sigma_{A.interface} - \sigma_{A.surface}}{h_A}\right)\cdot x, \sigma_{B.interface} + \left(\frac{\sigma_{B.surface} - \sigma_{B.interface}}{h_B}\right)\cdot\left(x - h_A\right)\right]$$

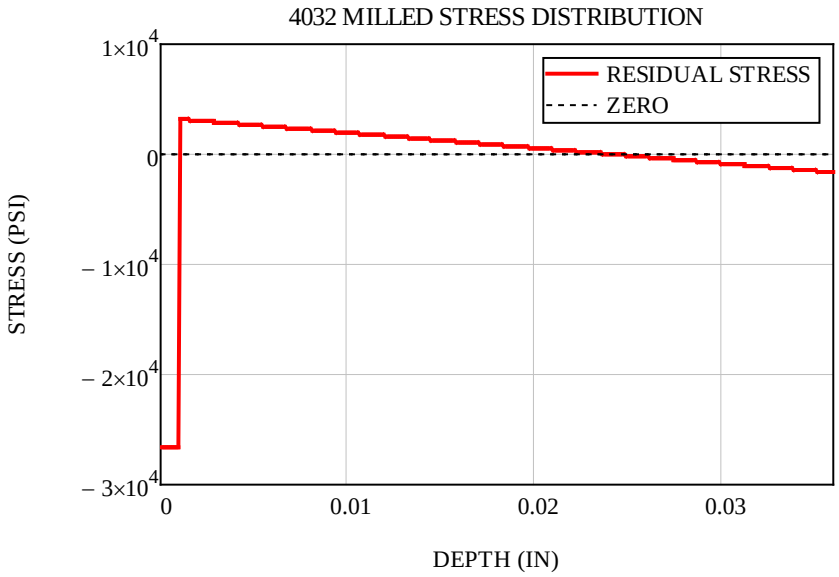

Appendix J Stress and Strain Uncertainty Analysis

6061 FLYCUT STRAIN ERROR

Elastic Modulus is defined:

$$68.9 \cdot 10^{9}\,\text{Pa} = 9.993 \times 10^{6} \cdot \text{psi}$$

$$E_a := 9993000\,\text{psi}$$

$$E_b := 9993000\,\text{psi}$$

Sample thickness is defined by including the thickness measurement uncertainty:

$$\text{Thickness\_low} := \frac{(.035\text{in} - .00025 \cdot \text{in} + .0355 \cdot \text{in} - .00025\text{in})}{2}$$

$$\text{Thickness\_high} := \frac{(.035\text{in} + .00025 \cdot \text{in} + .0355 \cdot \text{in} + .0025\text{in})}{2}$$

Surface stress is defined and includes the reported uncertainty of the measurement. The uncertainty has been scaled to reflect the depth corrected stress measurement, not the raw measurement:

$$\sigma_{re\_low} := \frac{24700 - \frac{24700 \cdot 400}{19800} + 24700 - \frac{24700 \cdot 400}{19800}}{2}\,\text{psi}$$

$$\sigma_{re\_high} := \frac{24700 + \frac{24700 \cdot 400}{19800} + 24700 + \frac{24700 \cdot 400}{19800}}{2}\,\text{psi}$$

Sample curvature is defined as the average of the two radii measurements:

$$\kappa := \frac{2}{70.838\text{in} + 67.840\text{in}}$$

Four cases are considered using the high and low value of both the stress and the sample thickness. A system of 3 equations and 3 unknowns (the general bimetallic curvature equation, the sum of the layer thicknesses, and the equation describing the surface stress on the curved sample) is used to solve for the 3 unknowns (layer A thickness, layer B thickness, and the initial stress in the machined layer of the flat sample prior to springing to its intial curvature):

CASE 1: SMALLEST STRESS, SMALLEST THICKNESS

Guess Values

$$h_a := .004in$$

$$h_b := .032in$$

$$\sigma_{initial} := 17000psi$$

Given

$$\kappa = \frac{6 \cdot E_a \cdot E_b \left(h_a + h_b\right) h_a \cdot h_b \cdot \frac{\sigma_{initial}}{E_a}}{E_a^{\,2} h_a^{\,4} + 4 \cdot E_a E_b \cdot h_a^{\,3} h_b + 6 \cdot E_a E_b \cdot h_a^{\,2} h_b^{\,2} + 4 \cdot E_a E_b \cdot h_a h_b^{\,3} + E_b^{\,2} h_b^{\,4}}$$

$$h_a + h_b = Thickness\_low$$

$$\sigma_{re\_low} = \frac{-\sigma_{initial} \cdot E_b}{E_a \cdot \left[4 + 6 \cdot \frac{h_a}{h_b} + 4 \cdot \left(\frac{h_a}{h_b}\right)^2 + \frac{E_a}{E_b} \cdot \left(\frac{h_a}{h_b}\right)^3 + \frac{E_b \cdot h_b}{E_a \cdot h_a}\right]} \cdot \left[3 \cdot \frac{h_a}{h_b} + 2 \cdot \left(\frac{h_a}{h_b}\right)^2 - \frac{E_b \cdot h_b}{E_a \cdot h_a}\right]$$

$$x := Find\left(h_a, h_b, \sigma_{initial}\right)$$

$$x\,float, 3 \rightarrow \begin{pmatrix} 0.0011 \cdot in \\ 0.0339 \cdot in \\ 27591.0 \cdot psi \end{pmatrix}$$

CASE 2: SMALLEST STRESS, LARGEST THICKNESS

Guess Values

$h_a := .004in$

$h_b := .032in$

$\sigma_{initial} := 15000psi$

Given

$$\kappa = \frac{6 \cdot E_a \cdot E_b \left(h_a + h_b\right) h_a \cdot h_b \cdot \frac{\sigma_{initial}}{E_a}}{E_a^{\,2} h_a^{\,4} + 4 \cdot E_a E_b \cdot h_a^{\,3} h_b + 6 \cdot E_a E_b \cdot h_a^{\,2} h_b^{\,2} + 4 \cdot E_a E_b \cdot h_a h_b^{\,3} + E_b^{\,2} h_b^{\,4}}$$

$$h_a + h_b = Thickness\_high$$

$$\sigma_{re\_low} = \frac{-\sigma_{initial} \cdot E_b}{E_a \cdot \left[4 + 6 \cdot \frac{h_a}{h_b} + 4 \cdot \left(\frac{h_a}{h_b}\right)^2 + \frac{E_a}{E_b} \cdot \left(\frac{h_a}{h_b}\right)^3 + \frac{E_b \cdot h_b}{E_a \cdot h_a}\right]} \cdot \left[3 \cdot \frac{h_a}{h_b} + 2 \cdot \left(\frac{h_a}{h_b}\right)^2 - \frac{E_b \cdot h_b}{E_a \cdot h_a}\right]$$

$x := Find\left(h_a, h_b, \sigma_{initial}\right)$

$$x\ float, 3 \rightarrow \begin{pmatrix} 0.0012 \cdot in \\ 0.0354 \cdot in \\ 27749.0 \cdot psi \end{pmatrix}$$

CASE 3: LARGEST STRESS, SMALLEST THICKNESS

Guess Values

$h_a := .004in$

$h_b := .032in$

$\sigma_{initial} := 15000psi$

Given

$$\kappa = \frac{6 \cdot E_a \cdot E_b \left(h_a + h_b\right) h_a \cdot h_b \cdot \frac{\sigma_{initial}}{E_a}}{E_a^{\,2} h_a^{\,4} + 4 \cdot E_a E_b \cdot h_a^{\,3} h_b + 6 \cdot E_a E_b \cdot h_a^{\,2} h_b^{\,2} + 4 \cdot E_a E_b \cdot h_a h_b^{\,3} + E_b^{\,2} h_b^{\,4}}$$

$$h_a + h_b = Thickness\_low$$

$$\sigma_{re\_high} = \frac{-\sigma_{initial} \cdot E_b}{E_a \cdot \left[4 + 6 \cdot \frac{h_a}{h_b} + 4 \cdot \left(\frac{h_a}{h_b}\right)^2 + \frac{E_a}{E_b} \cdot \left(\frac{h_a}{h_b}\right)^3 + \frac{E_b \cdot h_b}{E_a \cdot h_a}\right]} \cdot \left[3 \cdot \frac{h_a}{h_b} + 2 \cdot \left(\frac{h_a}{h_b}\right)^2 - \frac{E_b \cdot h_b}{E_a \cdot h_a}\right]$$

$x := Find\left(h_a, h_b, \sigma_{initial}\right)$

$$x \text{ float}, 3 \rightarrow \begin{pmatrix} 0.00106 \cdot in \\ 0.0339 \cdot in \\ 28588.0 \cdot psi \end{pmatrix}$$

CASE 4: LARGEST STRESS, LARGEST THICKNESS

Guess Values

$h_a := .004in$

$h_b := .032in$

$\sigma_{initial} := 15000psi$

Given

$$\kappa = \frac{6 \cdot E_a \cdot E_b \left(h_a + h_b\right) h_a \cdot h_b \cdot \frac{\sigma_{initial}}{E_a}}{E_a^{\,2} h_a^{\,4} + 4 \cdot E_a E_b \cdot h_a^{\,3} h_b + 6 \cdot E_a E_b \cdot h_a^{\,2} h_b^{\,2} + 4 \cdot E_a E_b \cdot h_a h_b^{\,3} + E_b^{\,2} h_b^{\,4}}$$

$$h_a + h_b = Thickness\_high$$

$$\sigma_{re\_high} = \frac{-\sigma_{initial} \cdot E_b}{E_a \cdot \left[4 + 6 \cdot \frac{h_a}{h_b} + 4 \cdot \left(\frac{h_a}{h_b}\right)^2 + \frac{E_a}{E_b} \cdot \left(\frac{h_a}{h_b}\right)^3 + \frac{E_b \cdot h_b}{E_a \cdot h_a}\right]} \cdot \left[3 \cdot \frac{h_a}{h_b} + 2 \cdot \left(\frac{h_a}{h_b}\right)^2 - \frac{E_b \cdot h_b}{E_a \cdot h_a}\right]$$

$x := Find\left(h_a, h_b, \sigma_{initial}\right)$

$$x \text{ float}, 3 \rightarrow \begin{pmatrix} 0.00116 \cdot in \\ 0.0355 \cdot in \\ 28746.0 \cdot psi \end{pmatrix}$$

RANGE OF VALUES IS .00106 - .0012" OR +/- .00007

Now use this range of values for the stressed layer thickness, the measured curvature, and the calculated error of curvature measurement (due to the inspection equipment) to determine the strain uncertainty. Using the simplified bimetallic strip model, is is obvious by inspection that the largest strain error will be at the largest possible value of the substrate layer h_B.

It was previously shown that the machine error ranges from +/- .0007" at a 30" radius to +/- .005" at a 150" radius. A linear relationship will be assumed for simplicity. The radius error for this radius is calculated below:

$$\text{radius}_{error} := \frac{1}{\kappa} \cdot \frac{.005\text{in} - .0007\text{in}}{150\text{in} - 30\text{in}}$$

$$\text{radius}_{error} = 0.00248 \cdot \text{in}$$

$$r_{low} := \frac{1}{\kappa} - \text{radius}_{error}$$

$$r_{high} := \frac{1}{\kappa} + \text{radius}_{error}$$

The strain error is now calulated:

$$h_B := .0012\text{in}$$

$$\varepsilon_{error} := \frac{h_B}{6h_a} \cdot \left(3h_a + h_B\right)\left(\frac{1}{r_{low}} - \frac{1}{r_{high}}\right)$$

$$\varepsilon_{error} = 6.822 \times 10^{-10}$$

Appendix K Curve Fitting Software Code

6061 Data

<A>stress_in=170300

<B>stress_in=170300

<C>stress_in=170300

<D>stress_in=154787

<E>stress_in=154787

<F>stress_in=154787

R=.00831447

<A>ef=0.000023

<B>ef=0.000067

<C>ef=0.00009

<D>ef=0.00008

<E>ef=0.00012

<F>ef=0.00018

<A>k=k1

<B>k=k1

<C>k=k1

<D>k=k2

<E>k=k2

<F>k=k2

Y=ef-(ef/stress_in)*[{(m-1)*(stress_in/ef)*(k/T)*X*3600*
(exp[-Q/(R*T)])+[(stress_in)^(1-m)]}^[1/(1-m)]]

Time (hrs)	6061 Flycut 60C	6061 Flycut 85C	6061 Flycut 125C	6061 Milled 60C	6061 Milled 85C	6061 Milled 125C
0.0001	0	0	0	0	0	0
1	8.0459E-07	0.00000154	5.593E-06	2.1572E-06	9.95E-06	1.95E-05
2	7.9423E-07	2.6186E-06	1.058E-05	3.9226E-06	1.87E-05	3.61E-05
3	4.3521E-06	5.7184E-06	1.785E-05	8.3325E-06	2.47E-05	4.7E-05
4	5.2212E-06	5.8328E-06	2.1979E-05	1.1464E-05	3.08E-05	5.06E-05
5	6.031E-06	7.5297E-06	2.659E-05	1.4902E-05	3.33E-05	5.52E-05
6	5.7568E-06	1.0015E-05	3.0832E-05	1.6148E-05	3.72E-05	5.98E-05
8	4.6705E-06	1.174E-05	3.4992E-05	1.9445E-05	4.09E-05	6.64E-05
10	4.9287E-06	1.2179E-05	3.7841E-05	2.0455E-05	4.39E-05	6.94E-05
12	9.5132E-06	1.4509E-05	4.0236E-05	2.4739E-05	4.78E-05	7.41E-05
16	1.0108E-05	1.6585E-05	4.4809E-05	2.6433E-05	5.04E-05	8.06E-05
24	1.2661E-05	1.7576E-05	4.8162E-05	3.2442E-05	5.74E-05	8.94E-05
38	1.4406E-05	2.3141E-05	5.6152E-05	3.9196E-05	6.47E-05	0.0001
52	1.6337E-05	2.647E-05	5.6946E-05	4.2157E-05	6.86E-05	0.000107
66	1.6301E-05	2.9574E-05	6.2663E-05	4.6838E-05	7.39E-05	0.000113
90	1.89E-05	3.2269E-05	6.4267E-05	5.0498E-05	7.99E-05	0.00012
114	1.4658E-05	3.5563E-05	6.8268E-05	5.2981E-05	8.09E-05	0.000121
162	1.7892E-05	0.00004021	7.0408E-05	5.6694E-05	8.61E-05	0.000131
210	1.5737E-05	4.5059E-05	7.5792E-05	6.069E-05	9.02E-05	0.000136
258	1.865E-05	4.9398E-05	7.6278E-05	6.2587E-05	9.13E-05	0.00014
330	1.8364E-05	5.388E-05	8.2044E-05	6.557E-05	9.77E-05	0.000146
402	1.9515E-05	5.7615E-05	8.3427E-05	6.7511E-05	9.98E-05	0.000152
570	1.7819E-05	6.2511E-05	8.2786E-05	7.0521E-05	0.000104	0.000157
738	2.1995E-05	6.5357E-05	8.4186E-05	7.4196E-05	0.000108	0.000164
906	2.2669E-05	6.6552E-05	8.3492E-05	7.5218E-05	0.000109	0.000172
1100	2.1347E-05	6.2795E-05		7.6386E-05	0.00011	0.000168

Parameter	Rules For initial Values		Default Constraints
	Initial Value	Rule	
k1	1.00E-15	Initial value, to be fit	Shared value for all data sets
k2	1.00E-15	Initial value, to be fit	Shared value for all data sets
Q	2.8	Initial value, to be fit	Shared value for all data sets
T	325	Initial value, to be fit	Data set constant (=column title)
k	50	Initial value, to be fit	Shared value for all data sets

4032 Data

<A>stress_in=185469

<B>stress_in=185469

<C>stress_in=185469

<D>stress_in=185469

<E>stress_in=183056

<F>stress_in=183056

<G>stress_in=183056

<H>stress_in=183056

<A>k=k1

<B>k=k1

<C>k=k1

<D>k=k1

<E>k=k2

<F>k=k2

<G>k=k2

<H>k=k2

R=.00831447

<A>ef=.000016

<B>ef=.000035

<C>ef=0.000046

<D>ef=0.000065

<E>ef=0.000053

<F>ef=.000089

<G>ef=.000158

<H>ef=0.00021

Y=ef-(ef/stress_in)*[{(m-1)*(stress_in/ef)*(k/T)*X*3600*

(exp[-Q/(R*T)])+[(stress_in)^(1-m)]}^[1/(1-m)]]

Time (hrs)	4032 Flycut 40C	4032 Flycut 50C	4032 Flycut 60C	4032 Flycut 85C	4032 Milled 40C	4032 Milled 50C	4032 Milled 60C	4032 Milled 85C
0.0001	0	0	0	0	0	0	0	0
1			4.05E-06	2.03E-05			1.36E-05	7.16E-05
2			7.38E-06	2.76E-05			2.32E-05	9.44E-05
3			1.05E-05	3.24E-05			3.19E-05	0.000107
4			1.33E-05	3.6E-05			4.02E-05	0.000115
5			1.38E-05	4.05E-05			4.5E-05	0.000124
6			1.61E-05	4.27E-05			4.95E-05	0.000129
8			1.88E-05	4.67E-05			5.67E-05	0.00014
10			2E-05	4.93E-05			6.04E-05	0.000145
12			2.09E-05	5.08E-05			6.38E-05	0.000151
16			2.37E-05	5.49E-05			6.96E-05	0.00016
24	6.11E-06	1.27E-05	2.62E-05	5.9E-05	2.85E-05	3.7E-05	7.64E-05	0.000171
38			3.18E-05	6.12E-05			8.87E-05	0.000185
44	8.6E-06	1.67E-05			2.73E-05	4.92E-05		
52			3.5E-05	6.37E-05			9.68E-05	0.000192
66			3.71E-05	6.15E-05			0.000105	0.000197
90			3.92E-05	6.51E-05			0.000111	0.000201
114			4.17E-05	6.2E-05			0.000118	0.000205
136	1.42E-05	2.8E-05			3.95E-05	7.22E-05	0.000129	0.000209
162			4.36E-05				0.000134	0.000211
180	1.6E-05	2.97E-05			4.42E-05	7.77E-05	0.00014	0.000207
210			4.44E-05				0.000142	0.000211
258			4.48E-05				0.000147	0.000207
285	1.65E-05	3.5E-05			5.1E-05	8.84E-05	0.000154	
330			4.51E-05					
357	1.64E-05	3.54E-05			5.3E-05	8.94E-05	0.000155	

Parameter	Rules for Initial Values		Default Constraint
	Initial Value	Rule	
k1	1.00E-11	Initial value, to be fit	Shared value for all data sets
k2	1.00E-11	Initial value, to be fit	Shared value for all data sets
Q	2.5	Initial value, to be fit	Shared value for all data sets
T	325	Initial value, to be fit	Data set constant (=column title)

Appendix L Derivation of Time Expression

Beginning with the expression previously derived for creep strain over time, an expression for time (t) can be attained:

$$\varepsilon = \varepsilon_f - \frac{\varepsilon_f}{\sigma_{in}}\left[\frac{(m-1)\sigma_{in}}{\varepsilon_f}\frac{k}{T}te^{\frac{-Q_c}{RT}} + (\Delta\sigma)^{1-m}\right]^{\frac{1}{1-m}}$$

Rearrange terms in the following manner:

$$\frac{\sigma_{in}}{\varepsilon_f}(\varepsilon_f - \varepsilon) = \left[\frac{(m-1)\sigma_{in}}{\varepsilon_f}\frac{k}{T}te^{\frac{-Q_c}{RT}} + (\sigma_{in})^{1-m}\right]^{\frac{1}{1-m}}$$

$$(1-m)\ln\left[\frac{\sigma_{in}}{\varepsilon_f}(\varepsilon_f - \varepsilon)\right] = \ln\left[\frac{(m-1)\sigma_{in}}{\varepsilon_f}\frac{k}{T}te^{\frac{-Q_c}{RT}} + (\sigma_{in})^{1-m}\right]$$

$$\left[\frac{\sigma_{in}}{\varepsilon_f}(\varepsilon_f - \varepsilon)\right]^{1-m} = \frac{(m-1)\sigma_{in}}{\varepsilon_f}\frac{k}{T}te^{\frac{-Q_c}{RT}} + (\sigma_{in})^{1-m}$$

and solving for time (t):

$$\frac{(m-1)\sigma_{in}}{\varepsilon_f}\frac{k}{T}te^{\frac{-Q_c}{RT}} = \left[\frac{\sigma_{in}}{\varepsilon_f}\left(\varepsilon_f - \varepsilon\right)\right]^{1-m} - \left(\sigma_{in}\right)^{1-m}$$

$$t = \frac{\varepsilon_f T}{(m-1)k\sigma_{in}}\left[\left[\sigma_{in}\left(1-\frac{\varepsilon}{\varepsilon_f}\right)\right]^{1-m} - \left(\sigma_{in}\right)^{1-m}\right]e^{\frac{Q_c}{RT}}$$

This expression can now be used to calculate the time required to *approach* the final strain condition at different temperatures. The following prevents a direct calculation of time for the final strain condition:

when

$\varepsilon = \varepsilon_f$

$\sigma_{in}\left(1-\frac{\varepsilon}{\varepsilon_f}\right) = 0$

and

$0^{1-m} = undefined$

Appendix M References

1 Marschall, Charles W. and Maringer, Robert E., Dimensional Instability: An Introduction; Battelle Columbus Laboratories, pp 139-212, Pergamon Press, New York, NY (1967).

2 Paquin, Roger, “Dimensional Stability: An Overview”, Hughes Danbury Optical Systems, *Proceedings of SPIE - The International Society for Optical Engineering*, Volume 1335, pp 2-19 (1990).

3 Paquin, Roger, “Dimensional Stability: An Overview”, Hughes Danbury Optical Systems, *Proceedings of SPIE - The International Society for Optical Engineering*, Volume 1335, pp 2-19 (1990).

4 Lindig, O. and Pannhorst, W., "Thermal Expansion and Length Stability of Zerodur in Dependence on Temperature and Time". *Applied Optics (0003-6935)*, 24 (20), p. 3330 (1985).

5 Emerson, W.B., “Secular Length Changes of Gage Blocks During 25 Years, Metrology of Gage Blocks”, *US National Bureau of Standards*, Circular 581, p 71 (1957).

6 Finnie I., and Heller, W.R., Creep of Engineering Materials, McGraw-Hill, Chapter 3, New York, (1959).

7 Brunet, S. et al., “Influence of Residual Stresses Induced by Milling on Fatigue Life of Aluminum Workpieces” *Residual Stresses III*, pp 1344-49, ICRS (1991).

8 Field, M, "Surface integrity in machining and grinding". *American Society of Tool and Manufacturing Engineers -- Creative Manufacturing Seminars, Technical Papers, 2*, p. 21 (1968).

9 Marschall, Charles W. and Maringer, Robert E., Dimensional Instability: An Introduction; Battelle Columbus Laboratories, p. 156, Pergamon Press, New York, NY (1967)..

10 Brunet, S. et al., “Influence of Residual Stresses Induced by Milling on Fatigue Life of Aluminum Workpieces” *Residual Stresses III*, pp 1344-49, ICRS (1991).

11 Imgram, A. G., Hoskins, M. E., Sovik, J. H., Maringer, R.E., and Holden, F. C., Study of Microplastic Properties and Dimensional Stability of Materials, Technical Report AFML-TR-67-232, Part II, Battelle Memorial Institute, Aug. p. 24 (1968).

12 Treuting, R. G., Jynch, J. J., Wishart, H. B., and Richards D. G., Residual Stress Measurements, American Society for Metals, Cleveland, OH, 1952, p 161 (1952).

13 Frommer, L. and Lloyd, E.H., "The Measurement of Residual Stresses in Metals by the X-Ray back Reflection Method, With Special Reference to Industrial Components in Aluminum Alloys, *Journal of the Institute of Metals*, Vol. 70, p. 122 (1944).

14 Lester, H.H., Aborn, R.H., "The Behavior Under Stress of the Iron Crystals in steel", *Army Ordnance*, vol. 6, 33, pp 200-207 (1925).

15 Cullity, B. D. and Stock, S. R., Elements of X-Ray Diffraction, 3rd Edition, pp 440-442, Prentice Hall, Upper Saddle River, NJ (2001).

16 Moore, M.G and Evans, W.P. "Mathematical Correction for Removed Layers in X-Ray Diffraction Residual Stress Analysis", *Transactions of the Society of Automotive Engineers*, Volume 66, pp. 340-345 (1958).

17 Evans, W. P., Residual Stress Measurement by X-Ray Diffraction, SAE HS784, pp 76-79, Society of Automotive Engineering, Warrendale, PA, (2003).

18 Kang, Z. Q., Li, J. B., and Wang, Z. G., "Stress Correction for Material Removal in X-Ray Stress Determination", *Journal of Evaluation and Testing*, Vol., 22, No. 3, pp 217-222 (May 1994).

19 England, Roger, Measurement of Residual Stresses in Diesel Components Using X-Ray, Synchrotron, and Neutron Diffraction, University of Cincinnati, Materials Science Dept., Master of Science Thesis, (2000).

20 ASTM International, ASTM B209 Standard Specification for Aluminum and Aluminum-Alloy Sheet and Plate, ASTM International, West Conshohocken, PA (2007).

21 Alcoa Corporation, "Global Cold Finished Products Guide: Deltalloy® 4032",http://www.alcoa.com/gcfp/catalog/pdf/alcoa_deltalloy_4032.pdf, (Accessed October2007).

22 Courtney, T. Mechanical Behavior of Materials, pp 268-309, Dept. of Materials Science, University of Virginia, McGraw-Hill Publishing Company, New York, (1990).

23 Callister, W., Materials Science and Engineering: An Introduction, 3rd Edition, p. 221, John Wiley & Sons, New York, New York, (1993).

24 Callister, W., Materials Science and Engineering: An Introduction, 3rd Edition, p. 219, John Wiley & Sons, New York, New York, (1993).

25 Mukherjee, A.K. "Experimental Correlations For High-Temperature Creep", *ASM (American Society for Metals) Transactions*, 62 (1), p. 155, (1969).

26 Dowling, Norman E., Mechanical Behavior of Materials, 2nd Edition, p. 718 Prentice Hall Publishing Company, Upper Saddle River, NJ, (1998).

27 Ahmadieh, A., and Mukherjee, A. K., "Stress-Temperature-Time Correlations for High Temperature Creep Curves", Materials Science and Engineering, Vol. 21, pp 115-124, (1975).

28 Timoshenko, S., "Analysis of Bi-Metal Thermostats", *Optical Society of America – Journal*, Vol. 11, n 3, pp 233-255 (1925).

29 Rourke, R. J., and Young, W. C., Formulas for Stress and Strain, Fifth Edition, pp 112-115, McGraw Hill Book Company, New York, New York (1975).

30 Frommer, L., and Lloyd, E. H., "The Measurements of Residual Stresses in Metals by the X-Ray Back Reflection Method, With Special Reference to Industrial Components in Aluminum Alloys," *Journal: Institute of Metals*, Vol. 70, pp 118-122, (1944).

31 Vossen, J. and Kern, W., Thin Film Measurement, pp 220-221, Academic Press Inc., Orlando, FL (1978).

32 Mehl, Robert F., Metals Handbook Volume 7: Atlas of Microstructures of Industrial Alloys, 8th Edition, p. 342, American Society for Metals, Metals Park, OH (1972)

33 Mehl, Robert F., Metals Handbook Volume 7: Atlas of Microstructures of Industrial Alloys, 8th Edition, p. 249, American Society for Metals, Metals Park, OH (1972)

34 Alcoa Corporation, "Global Cold Finished Products Guide: Deltalloy® 4032",http://www.alcoa.com/gcfp/catalog/pdf/alcoa_deltalloy_4032.pdf, (Accessed October2007).

35 Prevey, P., S., "A Method of Determining the Elastic Constants of Alloys in Selected Crystallographic Directions for X-Ray Diffraction Residual Stress Analysis Measurement", *Advances in X-Ray Analysis*, vol 20, pp 345-354 (1977).

36 Cullity, B. D. and Stock, S. R., Elements of X-Ray Diffraction, 3rd Edition, pp 391, Prentice Hall, Upper Saddle River, NJ (2001).